



## **Smart Maintenance, Analysis and Remediation of Transport Infrastructure**

### **Deliverable 3.4 Validation of the model**



Project funded by the EU 7th Framework Programme under call SST.2011.5.2-6 Cost-effective improvement of rail transport infrastructure. Grant agreement no: 285683

## Project Information

Project Duration:

01/09/2011 – 31/08/2014

Project Coordinator:

Dr. Kenneth Gavin (kenneth.gavin@ucd.ie)

School of Civil, Structural and Environmental Engineering

University College Dublin

Newstead Building

Belfield,

Dublin 4

Ireland



## Document information

Version	Date	Action	Partners
01	18.12.2013	1 <sup>st</sup> draft	TUM, IGH, ZAG, HŽ, UT
02	20.03.2014	2 <sup>nd</sup> Draft	TUM, IGH, ZAG, HŽ, UT
03	20.05.2014	3 <sup>rd</sup> Draft	TUM, IGH, ZAG, HŽ, UT
04	15.07.2014	4 <sup>th</sup> draft	TUM, IGH, ZAG, HŽ, UT

Title: SMARTRAIL – DEL 3.4 Validation of the model

Authors: Duo Liu and Bernhard Lechner (TUM)

Reviewers: Irina Stipanovic Oslakovic (UT), Kenneth Gavin (UCD)

Copyright: © Copyright 2011 – 2014. The SMARTRAIL Consortium

This document and the information contained herein may not be copied, used or disclosed in whole or part except with the prior written permission of the partners of the SMARTRAIL Consortium. The copyright and foregoing restriction on copying, use and disclosure extend to all media in which this information may be embodied, including magnetic storage, computer print-out, visual display, etc.

The information included in this document is correct to the best of the authors' knowledge. However, the document is supplied without liability for errors and omissions.

All rights reserved.

---

## Executive Summary

In this deliverable, different field measurements and modelling were carried out for the evaluation of the constructed transitions for BUNA Bridge. Two measurements were carried out in the year 2013 and 2014.

One of the most important parameters providing guidelines for the quality of the structure would be the dynamic vehicle-track interaction. Running railway vehicles could excite the track through dynamic vehicle-track interaction by exerting dynamic wheel loads on track which could become critical for track quality. Those dynamic loads are controlled by overall track geometry and track elasticity.

Therefore the general track geometry and elasticity were measured for both transitions. Operational trains with normal speed were also recorded for understanding the track dynamics. Various numerical simulation models including FEM and MBS were constructed for a systematic co-simulation for both vehicle and track. A real-time illustration of the dynamic vehicle-track interaction was realized for the best view of the counterproductive effect from track side parameters to the vehicle, as well as the other way back.

Results of the measurement and simulations were documented and suggestions on inclusion of modern superstructure materials like sub-ballast-mat were also included. Comparisons with different scenario studies were made in the simulation environment providing guidelines for the future perspectives.

## Table of Contents

<b>1. INTRODUCTION .....</b>	<b>1</b>
1.1. Background of the research.....	1
1.2. Vehicle-track-substructure interaction.....	2
1.3. The advantage of modern numerical simulation tools.....	4
1.4. Scope and objectives.....	4
<b>2. STATE OF TECHNOLOGY .....</b>	<b>6</b>
2.1. Track elasticity (recoverable track deflections).....	6
2.1.1. Load distribution and elastic deflection line.....	6
2.1.2. The dynamic analytic model for the elastic components .....	7
2.2. Track irregularity (non-recoverable track settlement) .....	9
2.2.1. Track recording wagon (TRW) .....	9
2.2.2. Linear-Time-Invariant (LTI) analysis.....	10
2.3. Modeling approach for analyzing railway track dynamics.....	13
2.3.1. Background .....	13
2.3.2. Finite-Element-Method (FEM) .....	15
2.3.3. Multi-Body-Simulation (MBS) .....	16
2.3.4. Comparisons of both approaches.....	17
2.3.5. Modal analysis and co-simulation.....	20
<b>3. BRIDGE TRANSITION AND DESIGN OF FIELD MEASUREMENT.....</b>	<b>23</b>
3.1. Introduction .....	23
3.2. Bridge and transitions .....	23
3.3. Track design.....	25
3.3.1. Track superstructure .....	25
3.3.2. Substructure in open track.....	26
3.4. Design of field measurement.....	28
3.4.1. Selection of measurement section .....	28
3.4.2. Determination of track geometry (plastic track deformation, unloaded) ..	29

3.4.3.	Measurement of elastic rail deflection (quasi-static).....	30
3.4.4.	Recording the track dynamic behavior by strain gauges .....	33
3.5.	Test runs and train runs.....	35
3.5.1.	Test runs .....	35
3.5.2.	Train runs.....	35
3.6.	Boundary conditions (fish plated joints) .....	36
3.7.	Vehicle information.....	36
3.8.	Summary.....	39
3.8.1.	Review of the pilot section and design of the measurement.....	39
3.8.2.	Categorization of the measurement items and connections to numerical simulations.....	42
<b>4.</b>	<b>FIELD MEASUREMENT AND DATA ANALYSIS (OCTORBER, 2013) .....</b>	<b>43</b>
4.1.	Introduction .....	43
4.2.	Track geometry and irregularity (plastic settlement) .....	44
4.3.	Rail deflection under static loading .....	47
4.4.	Rail bending behavior under test runs .....	53
4.5.	Rail bending behavior under operational trains .....	59
4.5.1.	Train set 6111 .....	60
4.5.2.	Train set 6112 .....	62
<b>5.</b>	<b>FIELD MEASUREMENT AND DATA ANALYSIS (APRIL, 2014).....</b>	<b>63</b>
5.1.	Introduction .....	63
5.2.	Track geometry and irregularity (plastic settlement) .....	64
5.3.	Rail deflection under static loading .....	66
5.4.	Rail bending behavior under test runs .....	71
5.5.	Rail bending behavior under operational trains .....	78
5.5.1.	Train set 6111 .....	79
5.5.2.	Other types .....	82
<b>6.</b>	<b>COMPARISON OF BOTH MEASUREMENT RESULTS.....</b>	<b>84</b>
6.1.	Introduction .....	84

6.2.	Track geometry and irregularity (plastic settlement) .....	84
6.3.	Rail deflection under static loading .....	86
6.4.	Rail bending behavior under test runs .....	88
7.	THE NUMERICAL MODELING .....	90
7.1.	Introduction .....	90
7.2.	FEM analysis of the field side Benkelman measurement on behalf of substructure elasticity (Cell 21) .....	91
7.2.1.	Design of the model .....	91
7.2.2.	Model setup and boundary condition .....	94
7.2.3.	Iterative process – initial condition .....	96
7.2.4.	Iterative process – iteration procedure .....	99
7.2.5.	Iterative process – boundary conditions .....	99
7.2.6.	The exclusion of fish plated joints .....	101
7.2.7.	The results and other comments .....	103
7.2.8.	The adjustment to the new measurement results (April, 2014) .....	104
7.3.	FEM analysis on determination of the dynamic wheel load under running trains (Cell 22) .....	107
7.3.1.	Introduction and measurement result analysis .....	107
7.3.2.	Loading of the FEM model .....	107
7.3.3.	The modeling result and analysis – Test runs .....	108
7.3.4.	The modeling result and analysis – Train runs (train set 6111) .....	110
7.4.	MBS analysis on simulation of the dynamic wheel rail contact with pre-defined track excitations (Cell 31) .....	112
7.4.1.	Background and introduction .....	112
7.4.2.	Setup of track excitation .....	113
7.4.3.	Vehicle setup and parameters .....	114
7.4.4.	The simulation results .....	116
7.5.	MBS analysis on simulation of the dynamic wheel rail contact with modal represented FEM input (Cell 32) .....	118
7.5.1.	Background and introduction .....	118

---

7.5.2.	Input of track elasticity characteristic by FEM model.....	119
7.5.3.	Setup of model in Simpack and perform of simulation runs .....	122
7.5.4.	Simulation results – quasi-static runs.....	124
7.5.5.	Simulation results – dynamic runs .....	126
7.6.	Case study – Inclusion of sub-ballast-mat in the bridge section.....	130
7.6.1.	Background and introduction.....	130
7.6.2.	Determination of the bedding modulus of sub-ballast-mat .....	130
7.6.3.	Simulation of the dynamic vehicle-track interaction with built-in sub-ballast-mat .....	133
7.6.4.	Simulation result of the dynamic runs .....	134
<b>8.</b>	<b>Conclusion and recommendation .....</b>	<b>136</b>
8.1.	Overview of the research .....	136
8.2.	Conclusions .....	137
8.3.	Recommendations.....	141
	<b>SOURCE OF REFERENCE .....</b>	<b>143</b>
	<b>List of Figures.....</b>	<b>145</b>
	<b>List of Tables .....</b>	<b>148</b>



## 1. INTRODUCTION

### 1.1. Background of the research

*Smart Maintenance Analysis and Remediation of Rail Infrastructure* (SMART Rail) is international scientific research project started under FP7 program SST.2011.5.2-6. “Cost-effective improvement of rail transport infrastructure”. The SMART Rail vision is to provide a framework for infrastructure operators to ensure the safe, reliable and efficient operation of ageing European railway networks. This will be achieved through a holistic approach which will consider input from state of art inspection, assessment and remediation techniques and use this data to consider the adjusted stiffness scenarios using whole life cycle cost models. The output of the project will result in enhanced safety, reliability and capacity of these rail infrastructure networks.

A major maintenance issue for railway infrastructure is the track itself. Sufficient ballast needs to be maintained, of sufficient depth and quality, that the track is level and stiff. Maintenance operations may involve local repairs or major rehabilitation and /or replacement of ballast. A first step towards efficient and optimized maintenance is the modeling of the track settlement (plastic) and track foundation stiffness (elastic). In both cases, the models will be integrated with existing and new methods of monitoring current condition. Much can be learned from the current state-of-art in pavement deterioration, i.e. there are significant differences with railway track being much smoother and stiffer than the bituminous layer in the road and permanent deformation in roads that has no rail equivalent. Nevertheless, recent and emerging techniques from the road pavement sphere have greatly improved understanding of the evolution of damage and will be adapted in this project for use in rail track deterioration models.

The working package 3, *new rehabilitation technologies to extend service life of existing railway infrastructure*, oriented itself to develop and verify by on-site application, sustainable technologies for effective rehabilitation and strengthening of “older” existing railway infrastructure which were built in 19<sup>th</sup> and 20<sup>th</sup> century. The

---

main goal of the working package is the analysis of problems in transition zones between bridges, tunnels, artificial and earth structures.

Transition zones between bridges, tunnels, artificial and earth structures, including transitions between a ballast and non-ballast permanent way, are a part of the railway track structure where an abrupt change in the rigidity of track structure and track settlement occurs between individual transverse profiles, as a result of the change in the structural elements and the foundation. Variance in the rigidity of the rail structure is the basic parameter influencing the generation of new impulse mechanisms during interaction between the vehicle and the structure. This causes additional dynamic loads, resulting in further degradation of the track structure and indirectly, the decrease of safety level and riding comfort. Due to foregoing, the transition zones are defined as exceptionally problematic parts of railway track.

With that aim the case study is developed in Croatia by 2 Croatian partners in SMART Rail, Institut IGH d.d. and HŽ Infrastruktura d.o.o. In cooperation with colleagues from HŽ Infrastruktura d.o.o., the area before and after the bridge “Buna” on the railway line M104 Zagreb Main station- Sisak- Novska in the km 398+441 (near station Turopolje) has been chosen as the test area.

Two different transitions should be built at each end of the bridge, connecting the bridge and open track sections. A technical evaluation of the overall performance of the two transitions should be made by performing various kinds of field measurements and numerical modellings.

## **1.2.Vehicle-track-substructure interaction**

The source of the loading to all the railway structures is from train runs. Train runs could excite the track through the wheel - rail contact mechanisms. Under certain conditions of track, by uneven track settlement or change of elasticity, the load coming from the train could be significantly higher than the static value. Also the vehicle itself is contributing to dynamic loads e.g. by wheel flats (not focus of this

research). If the static load of a wheel is  $F_0$ , then the actual force of this wheel acting on the track ( $F_{\text{dyn}}$ ) could be calculated as follows:

$$F_{\text{dyn}} = F_0 + F_{\text{exc}}$$

where  $F_{\text{dyn}}$  – dynamic load

$F_0$  – static load

$F_{\text{exc}}$  – excitation load

This  $F_{\text{exc}}$  is the excitation load which is in the form of a time function, which makes the  $F_{\text{dyn}}$  also vary with time. It depends from the track side mostly on the elasticity and the geometrical excitation (track irregularity).

Normally, the most important factors determining the capacity of tracks to handle excitation loading is track elasticity and damping factors. For optimization of the track structural design, other solutions were developed such as implementing high elastic rail fastening systems, etc.

There is also connective effect between the track performance in terms of elasticity as well as track quality in terms of geometry. The appearance of microscopic track irregularity along the track shows highly stochastic distributions which are highly dependent on the initial condition and the traffic loading. But when certain track imperfections were spotted, the deterioration grade of the track quality (conventional, ballasted tracks) according to the traffic loads has a strong relationship with the overall track elasticity which is the most determinant factor from the track side on the level of the excitation load. It is intuitive to figure out, that higher track deterioration rate should appear in the location where higher vehicle excitation load is activated.

Higher excitation due to “spots” in track structure has counterproductive effect to the track quality itself, which increases the track deterioration rate. Therefore a deeper understanding of the train-track as well as track-substructure interaction by varies

kinds of field measurements and numerical simulations are the key for a systematic evaluation of the bridge transitions.

### **1.3.The advantage of modern numerical simulation tools**

In order to get a further view on the quasi-static and the dynamic behavior of the system, numerical models would be necessary not only for the validation of the experiments in lab and situ, but also for the prediction of the modification of the system behavior after years of operation. These numerical procedures focus on the quasi-static and dynamic performance of the track settlement as well as the track foundation. As wheel-rail interaction is a key element which can not be ignored, a complicated train-track interaction model should be generated. Possible numerical simulation models here would refer to the Finite-Element-Method (FEM) and Multi-Body-Simulation (MBS).

### **1.4.Scope and objectives**

In the current economic environment, it is important for railway organizations to be as competitive as possible. The major task for the railway track engineer is often that of analysis, determining the economic effect or allowable limit to increasing axle loads and vehicle speeds on existing tracks. By analyzing the railway track structure using realistic track simulation models, more informed design decisions could be made. The research presented in this report aims to find out the relationship between the track sided elasticity, irregularity parameters and the performance of the vehicle track interaction with modern numerical modeling strategies.

The overall scope of the research presented in this report includes:

- Orientation on the design of bridge transitions;

- 
- Understanding of the importance on track elasticity;
  - Stochastic distribution of track irregularities;
  - Study of test sensors and design of field measurement;
  - Identification and verification of railway dynamic analysis models (Finite Element Method and Multi-Body Simulation);
  - Analysis and evaluation of the test results;
  - Conclusions and perspectives for the future activities.

The overall work plan for the whole research work includes:

- Feasibility study (Literature review and methodologies);
- Development of suitable simulation tools based on Multi-Body-Simulation in combination with Finite Element Models;
- The field side measurements at given pilot sections;
- Verification of the model with measurement results;
- Analysis and conclusions on the whole research work.

## 2. STATE OF TECHNOLOGY

### 2.1.Track elasticity (recoverable track deflections)

Quality of rail transport has a strong relation to track quality. Wheel load distribution within rail track structure and wheel guidance is characterized by overall track design but especially by geometrical and elastic properties. The above mentioned elastic properties usually refer to Resilient Rail Pads, Under Sleeper Pads, Under Ballast Mat, etc. Figure 1 shows a normal railway superstructure together with the elastic elements.

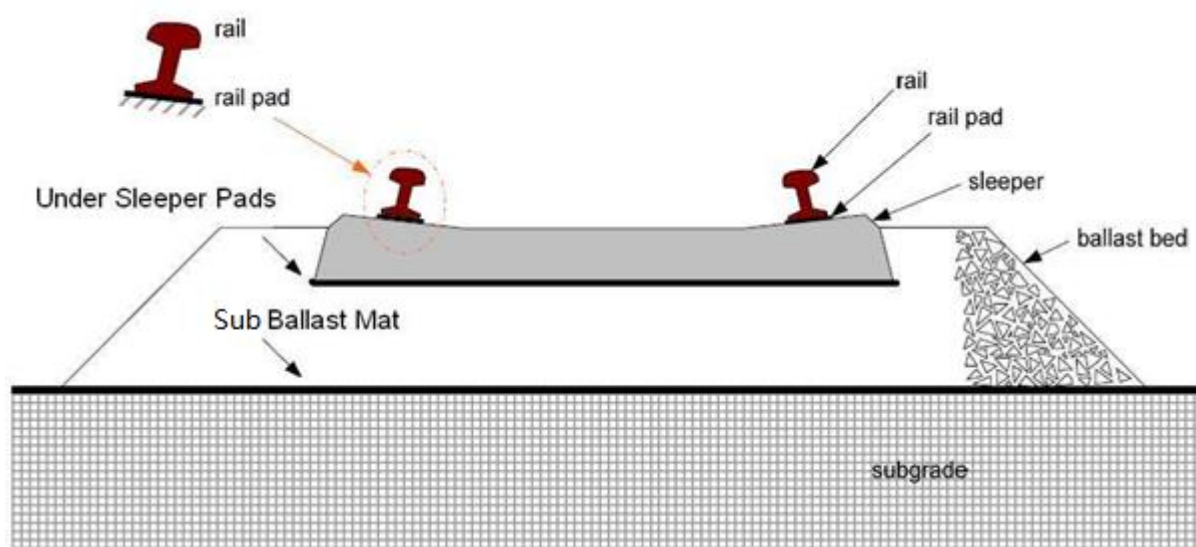


Figure 1 Typical railway superstructure and elastic elements <sup>[01]</sup>

#### 2.1.1. Load distribution and elastic deflection line

Determining the wheel load distribution within track superstructure under given train loads is always the first step in analyzing the overall performance of rail track.

The theory of Winkler and Zimmermann (Winkler, 1867; Zimmermann, 1888) is still frequently used because it allows a fairly good estimation of the essential parameters which are rail deflection and bending moment. It considers the rail as an infinitely long beam continuously supported by an elastic foundation. This is based on the assumption that the reaction forces of the foundation are proportional at every point to the deflection of the beam at that point. This assumption was first introduced by E. Winkler (WINKLER 1867) and formed the basis of H. Zimmermann's classical work on the railroad track in Berlin (ZIMMERMANN 1888).<sup>[02]</sup> Sample deflection line could be drawn as in Figure 2:

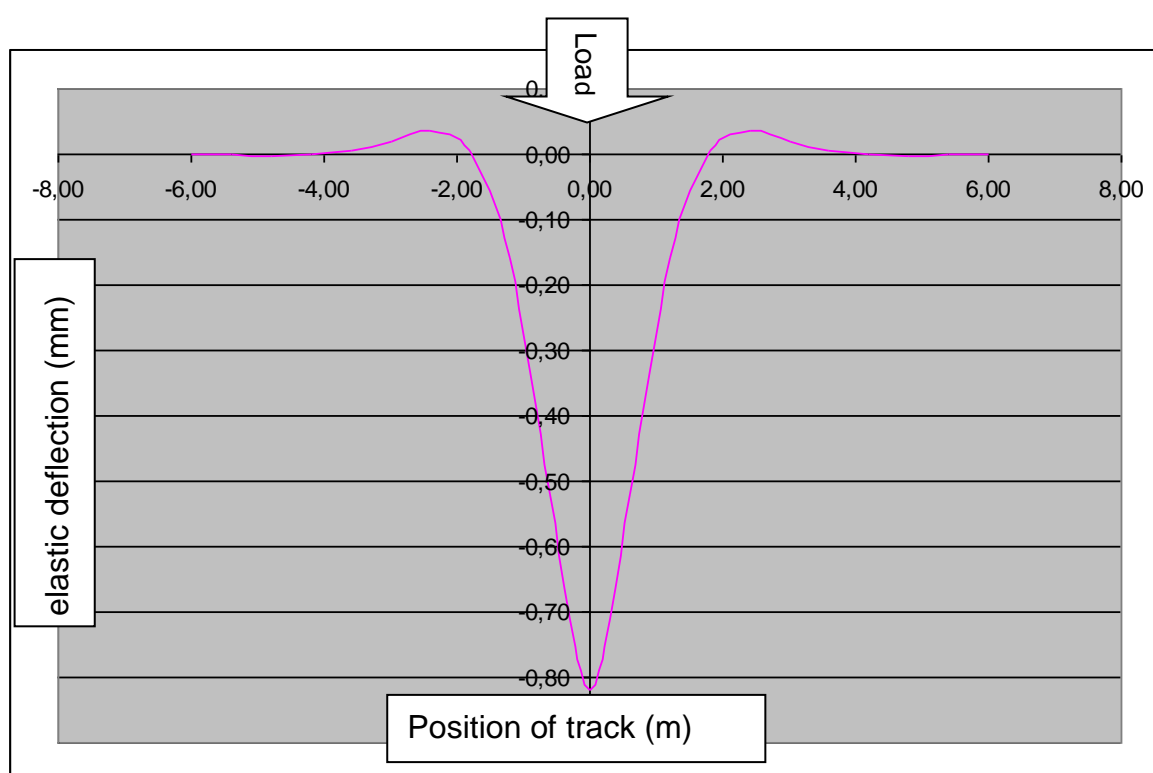


Figure 2 Typical deflection line calculated by Zimmermann Theory

### 2.1.2. The dynamic analytic model for the elastic components

The dynamic properties of the elastic elements in railway superstructure can be described in terms of the dynamic stiffness and damping. These parameters are dependent usually on the following properties: materials, design, temperature,

preload, loading frequency, thickness, unevenness, effective area and roughness of the contact surface. In practice the initial value of the dynamic stiffness and damping may change in time due to aging, weathering and fatigue. <sup>[03]</sup>

It was commented by Knothe and Grassie (1993) that the load/deflection behavior of the fastening system is non-linear; however since its behavior when loaded by one wheel is of greatest interest, some linearization of the load/deflection behavior can be justified. For vertical vibration an elastic element is usually modeled as a spring and viscous damper in parallel. Elements are mainly loaded in compression, permanently by the fastening system, the eigen load and/or repetitively by the traffic. Take elastic rail pad as examples, in two dimensional models a pad can be represented as acting at a point on the rail foot, however for three dimensional models a visco-elastic layer across the rail foot is often considered (Kumaran, 2003). <sup>[04] [05]</sup> It is then obvious to conclude that a systematic track model could be described as a multi-elastic system with different elasticity in each layer (see Figure 3).

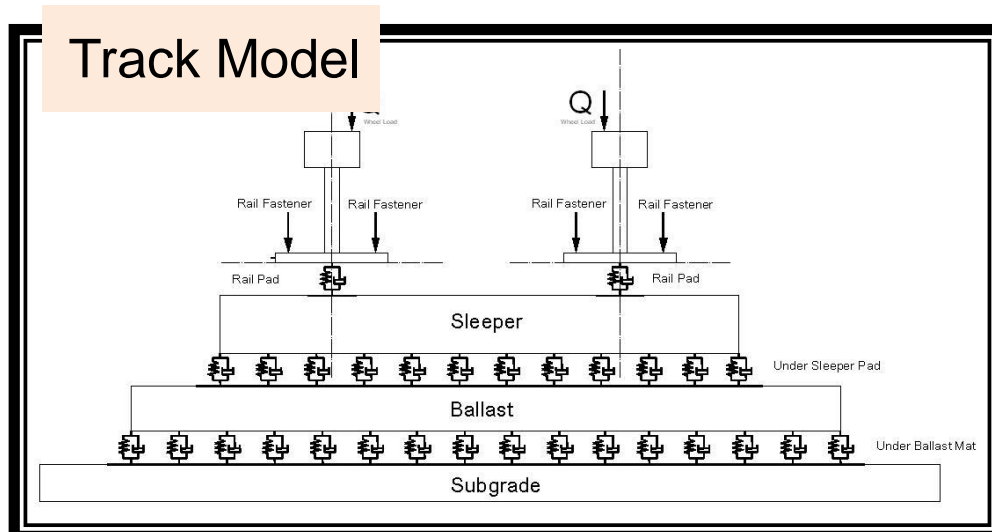


Figure 3 Multi-elastic track model in vertical direction



---

## **2.2.Track irregularity (non-recoverable track settlement)**

The appearance of track irregularity is quite decisive for track quality decline along the track. Such micro track imperfections could cause enormous consequences which degrade the quality of the wheel rail interaction and counteract on the track quality degradation again.

The characteristic of the track irregularity normally shows a wide banded spectral distribution which makes the rebuild and categorization quite complicated. Therefore, digital signal processing techniques are needed to provide the best ways of rebuilding the signal in an identical quality level. Many methodologies were studied and investigated on the representation of the track irregularity via Fast-Fourier-Transform (FFT) and Linear-Time-Invariant (LTI) analysis.

### **2.2.1. Track recording wagon (TRW)**

The measurement of the track irregularity was normally included by the track recording train. These measurements could be done under the travel of the train. Their recording (especially in vertical direction) of the track irregularity is under the loaded track.

Track recording wagon is found to be better for recording the track irregularity levels for this study. Those wagons were normally quite light which their eigen load could be neglected. By doing this, the measured track irregularity refers to the unloaded track condition and their measurement of vertical irregularity was then identical to the plastic track settlement. There were various products available in the market which could be easily operated by hand.

### 2.2.2. Linear-Time-Invariant (LTI) analysis

Due to the reason that the values measured by the TRW were normally indirect and need further processing, various methods of transferring those measured data into the realistic track irregularity distribution were developed. The following paragraphs focus on one of the best analysis method – Linear Time Invariant (LTI) analysis.

The LTI system theory could be applied to analyze the response of a linear and time-invariant system to an arbitrary signal <sup>[06] [07]</sup>. Recording of the raw data normally succeeds through time cursor, but in application of distance relevant measurements, the LTI system could also have trajectories in spatial dimensions.

The raw data for the application of the LTI analysis should fulfill the following two pre-requisites: Linearity and Time invariance. The general work flow of the LTI analysis is shown in Figure 4:

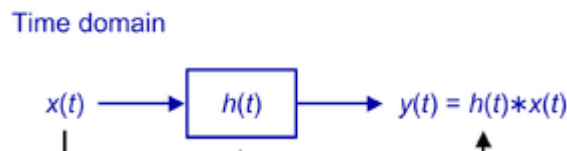


Figure 4 Principle of LTI system

$y(t)$  (output signal) is the convolution multiply of the  $x(t)$  (input signal) and  $h(t)$  (transfer function) which could be calculated using the following formula:

$$y(t) = x(t) * h(t) = \int_{-\infty}^{+\infty} x(\tau) \cdot h(t - \tau) d\tau$$

The calculation of the input or output signal from LTI analysis could be accomplished easier by transferring the time / distance signal into the frequency domain. This could be done by doing Fourier Transformation to the existing signals as follows:

$$x(t) \xrightarrow{\mathcal{F}} X(j\omega)$$

$$h(t) \xrightarrow{\mathcal{F}} H(j\omega)$$

$$y(t) \xrightarrow{\mathcal{F}} Y(j\omega)$$

According to the upper formula, the convolution multiply of the both signals becomes the normal multiplication in frequency domain:

$$Y(j\omega) = X(j\omega) \cdot H(j\omega)$$

The general process could then be visualized as shown in Figure 5:

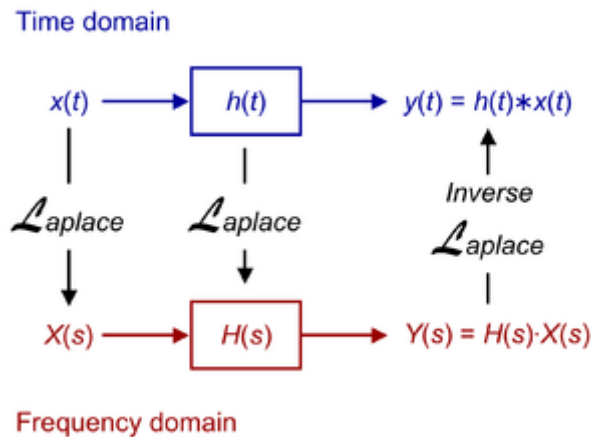


Figure 5 The calculation in frequency domain

After doing the Fourier transformation of the output signal  $y(t)$  into  $Y(j\omega)$ , the input signal in frequency domain could be calculated using the  $Y(j\omega)$  and  $H(j\omega)$  as shown

above. The calculated  $X(j\omega)$  could then be converted back to distance signal by doing the Inverse Fourier Transformation.

According to the measured raw data from the track recording car, it is obvious to figure out that the calculation of absolute track irregularities should only be applied in the vertical and horizontal direction (see Chapter 2.1.1 and 2.1.2).

The next important thing is then to understand the characteristic of the transfer function  $h(t)$ . This could be done by calculating the result  $y(t)$  under a Dirac delta function  $\delta(t)$  which has the following basic properties <sup>[08]</sup>:

$$\delta(t) = 1 \text{ (only when } t = 0 \text{; otherwise } \delta(t) = 0 \text{ )}$$

$$\int_a^b \delta(t - c) dt = 1 \text{ (} a < c < b \text{)}$$

The Dirac delta input at  $t = 0$  was shown in Figure 6:

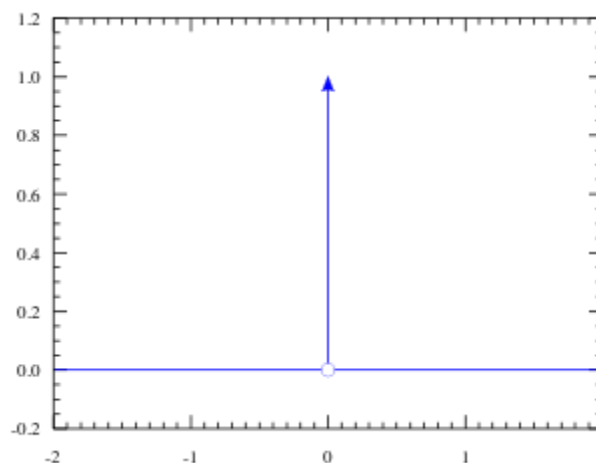


Figure 6 Dirac delta function

It is easy to figure out, that the output  $y(t)$  is the same as the transfer function  $h(t)$  under dirac input. This provides the calculation method for the transfer function. The

application of LTI with distance signals like data from track irregularity was fully identical to what had been illustrated above. It should only be pointed out, that the frequency in Hz was now changed to distance frequency ( $\text{m}^{-1}$ ) which is the reciprocal to the respective wave length in m.

## **2.3. Modeling approach for analyzing railway track dynamics**

Railway system components can be classified on the basis of their principal properties: either mass or elastic properties, or both. Together with the geometrical design (layout) of a track structure, a mechanical design or a model can be described. Such a model is basically formed by a set of relationships between all components with inertia properties. These relationships are influenced both by elastic properties and by dimensions of the components. The set of relationships gives a mechanical model of a track structure, suitable for the analysis of the structural behavior.

### **2.3.1. Background**

De Man (2002) comments that in order to combine properties and dimensions into models, two modeling methods may be used: analytical and numerical modeling <sup>[09]</sup>.

Analytical models are preferably based upon homogenous situations. For instance, continuous conditions applied with respect to support, a limited number of connections and a limited number of load positions. Examples for analytical models could be the mathematical solutions for an infinite beam on an elastic foundation by Zimmermann (1888), Euler, Bernoulli (1736) and Timoshenko (1926).

Numerical models are typically used for more refined stress analysis of track components and where retrieval of solutions in analytical models is difficult. Instead of finding a solution in a continuous input range, numerical methods search for the solution of a model, comprising of nodes, connecting elements and boundary

conditions. All component properties and model restrictions have to be embedded in the definition of this numerical model. Example for numerical models could be Finite Element Method (FEM) and Multi-Body Simulation (MBS).

Generally speaking, the working processes for either FEM or MBS could be split into six steps. <sup>[10]</sup> The six steps and the targets of them are as follows:

1, Problem Definition

Finding the exact specifications of the model

2, Development of a model

Dividing the mechanical structure into model specified bodies and elements  
(Structural analysis)

3, Provision of the physical parameters

Providing the physical information to the respective bodies and elements

4, Pre-Processing

Input of the pre-defined information in Step 1-3 into the software; Model setup

5, Problem solution

Calculation of the solution based on the given information using differential equations

6, Post-Processing

Numerical or graphical representation of the results

It has to be clarified that only the steps 4 to 6 could be handled by the respective simulation software. The steps 1 to 3 are related to the feasibility study and structural analysis of the system.

---

### 2.3.2. Finite-Element-Method (FEM)

As summarized from Madenci and Guven (2006); Suvo and Khemani (2010); Liu and Quek (2003); and Moaveni (1999) about Finite-Element-Method (FEM) or Finite-Element-Analysis (FEA): Courant (1943) has been credited with being as the first person who developed the FEM in his paper about investigation of torsion problems by using piecewise polynomial interpolation over triangular sub-regions. Nowadays, the FEM is known as a dominant discretization technique in structural mechanics, meaning the subdivision of the mathematical model into disjoint components with a predefined geometry called finite elements. Afterwards, each element would be given finite degrees of freedom characterized by special functions or expressions.<sup>[11]</sup>

The exact work which could be performed in FEM simulation software is as follows:

- Pre-processing: definition of geometry, materials, and element types; generation of finite-element grids (meshing)
- Problem solution: definition of analysis type, boundary conditions and constraints; application of loads; calculation of solution by intern defined calculation mechanisms.
- Post-processing: Visualization of the analysis results (usually time-independent)

The FEM software chosen for this research work is called ANSYS. It provides general solutions to the practical problems for universal purposes. The first version was released in 1971<sup>[12]</sup>.

With the help of Finite-Element-Method (FEM), a 3-D multi-elastic track model with fully elastic track settlement and track foundation could be generated. Unlike the track module in MBS, the FEM takes a deeper insight into the principle structure of the track itself, including material inputs and the elasticity of each key element. Summarized from the previous research works, the track could also be considered as

a multi-elastic system with 'quasi-rigid' elements like rail, sleeper and ballast as well as the elastic elements like resilient rail pad (RP), under sleeper pads (USP) and Sub Ballast Mat (SBM). Here the 'Quasi-rigid' means that these elements focus more on the distribution and support of the load and cause only minor influence to the system elasticity.

### **2.3.3. Multi-Body-Simulation (MBS)**

The Multi-Body-Simulation (MBS) procedure is the best solution for the modeling of train-track interaction as it is fully designed for the 3-D dynamic analysis between different bodies. The MBS could take a deep insight into the structure of the train itself which is composed of rigid elements like carriages, bogie frames and wheel sets and elastic elements like primary and secondary suspension springs and dampers, etc. All of these elements would be parameterized physically and such parameters would include the geometrical layouts, wheel set profiles, gravity, center of mass and inertia tensor for the rigid elements and 3-D linear or non-linear spring and damper coefficients as well as the combination strategy for the elastic elements. Furthermore, universal parameters like the speed, acceleration of train could also be taken into consideration for a possible spectrum analysis of the signal according to DIN or GM/RT standards.

The MBS could also provide an integrated track system as it would be essential for train runs. The generation of railway tracks would happen in two different extends namely the macroscopic view and microscopic view. The macroscopic view includes the alignment of the track in vertical, horizontal and lateral directions as well as the gauge and super elevation of the track itself. Rail surface profiles are also considered for a detailed modeling of wheel-rail interactions and both constraint contact and elastic contact could be determined based on different modeling strategies. As for the microscopic view, it is normally much smaller than the previous one but is actually one of the most determinant factors for railway dynamics. It could include the micro irregularity of the track in vertical, horizontal and lateral directions which is mostly resulted from the train runs. There is even a feedback mechanism where an irregular point along the track will cause an increase in the wheel-rail interaction and the



increase of the dynamic wheel load could again increase the grade of the irregularities.

Multi-Body Simulation is a newly developed modeling approach in railway engineering field. Such kinds of simulation software (e.g. SIMPACK) are already widely used in the design of automobiles or locomotives.<sup>[13]</sup> On MBS systems, the parts or bodies of the structure are often connected using complex joints (complex suspension joints, for example), with complicated force elements acting between these bodies. Often in systems such as these, the bodies themselves can be considered as rigid, as the relative deflection of the bodies is small in comparison to the 'Rigid body' motion. MBS software has allowed these types of dynamic systems to be modeled, where previously this was not possible. A sample model done by SIMPACK is shown in Figure 7:

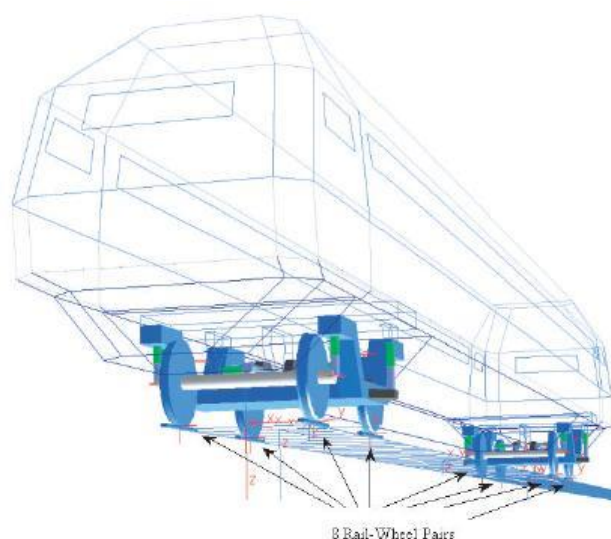


Figure 7 Sample SIMPACK Model for railway vehicle<sup>[13]</sup>

#### 2.3.4. Comparisons of both approaches

The challenge of the task is that none of the single method could fully handle the tasks. The MBS has a nice interface for the simulation of wheel-rail dynamics, but the

implementation of the track module is still not quite realistic at the moment. It is therefore also difficult to bring in the track plate also a multi-elastic system. The FEM could handle the difficulties by MBS easily as it is exactly designed for system elasticity analysis, but the disadvantages would be the unimaginable complexity of implementation of wheel-rail dynamic factors which would hardly lead to a converged result in the end.

Possible solutions are already encouraged and kinds of verification works have been performed. The target was achieved by an integrated simulation procedure called co-simulation, which both procedures were included for separate tasks and a feedback mechanism combining the both results. That is to say, that FEM gets calculation results of certain parameters from MBS for its own calculation, and returns its results back to MBS and so on. If an appropriate feedback mechanism has been defined, it will lead to a converged result which would represent the final result for calculation. Disadvantages for co-simulations are the parameters which are exchanged between two procedures must be defined manually and such definition is also determinant for the final results. As only a limited number of results would be exchanged and there is anyway still more than one system, the influence between different system like resonance effects and so on could not be fully considered.

The solution for the problems described above would be an integrated model for the whole system. An integrated FEM-MBS system would allow the dynamic analysis of the train-runs under an elastic track deflection as well as track foundation. The improvement is that the combined procedure could fully include the dynamic effects between train and track as they will interact with each other by every iteration point and the system convergence would also be checked parallelly. The output of the model would include both results from train and track and a better reshape of the reality could be expected.

The integrated FEM-MBS model would include an enough length of elastic track in order to gather information for the passage of the trains. Measurement sections would be carefully selected which would mostly stand on the most inconvenient side. Possible sections therefore would include bridges, tunnels, transition areas, etc. Parameters like the axle load, speed, suspension stiffness, track quality (evenness) and so on would be included as variables. The output therefore would include values

---

like the displacement of the track, the wheel-rail interaction force, the wheel load distribution, etc.

The verification of the model include on both sides of MBS and FEM. Specific measurement sections are selected and essential field and laboratory measurements should be made. For MBS simulations, suspension spring and damper coefficient as well as the physical parameters for the trains would be received and studied. Macroscopic data like track alignment in 3-D direction would be gathered from railway operators and microscopic data as 3-D track irregularity information would be concluded from track recording wagon (TRW).

For FEM models, Multi-elastic parameterized track system would be built and the above mentioned parameters would include the estimation of pad elasticity, subgrade modulus, ballast conditions and so on. Rail and sleeper would be generated according to the geometrical shape and respective materials while the elastic elements would rely on the linear or nonlinear spring and damper combinations.

As there are many elastic layers which are running into the problem, some analysis risks could happen like the calculation could hardly lead to a converged result. Therefore, minor model revision would be necessary but there is no need that the basic theory also has to be revised. Approximation on behavior of some elements would be necessary but the accuracy of the model would not be much disturbed by such kind of approximations.

When comparing MBS software to Finite Element (FE) software, it is quite clear to see the different concerning points between them. The FE software, which put emphasis on the elastic body itself, requires all bodies to be defined as elastic, whereas MBS software, requiring mostly only rigid bodies, focuses more on the complex interaction between them. Table 1 shows a comparison of modeling approaches.

Table 1: Comparison of FEM and MBS approach

	FEM Finite-Element-Method	MBS Multi-Body-Simulation
System characteristics	System with 2D/ 3D Elements	System with 3D bodies
Basic elements	Elastic elements (Material properties, Element types)	Rigid bodies (Mass, CoG, Inertia Tensor, etc.)
Formulation of the system	Elements are connected by nodes	Connection of bodies with idealistic joints
Type of analysis	Static analysis	Kinematic and dynamic analysis
Output results	Calculated Deflections, Strain, Stress	Calculated Force, Speed, Acceleration
Degrees of Freedoms	System with many Degrees of Freedoms	System with limited Degrees of Freedoms (Condensation)
Representative software	ANSYS, SoFisTiK ...	Simpack, Adams...

### 2.3.5. Modal analysis and co-simulation

It is easy to conclude from the table above that the FEM gains advantages in the representation of element elasticity whereas MBS could easily handle 4D systems with time-dependent dynamic analysis. Considering the complexity of the vehicle track dynamic system, both approaches have to be utilized in a most efficient way. The FEM allows the sufficiently accurate approximation of the track flexibility while the vehicles' motion including its complex wheel-rail interface is produced within the appropriate MBS system. Therefore a joint use of both called 'Co-simulation' is one of the best solutions to the challenge. <sup>[14]</sup> Co-simulation means that both FEM and MBS programs simulate their respective model separately on a superior artificial discretized time-scheme and interchange the 'conjunctive data' at the thus defined points of time. Especially for vehicle track interface, these 'conjunctive data' could refer to the wheel load from MBS as well as track deformation from FEM.

---

The MBS program Simpack provides a good possibility of doing integrated co-simulation for railway problems. This is the so called 'FlexTrack' module. The FlexTrack module was designed for considering the dynamic interaction between vehicle and elastic track. The consideration of track elastic properties was achieved through the modal approach which calculated a large number of eigenmodes to represent the track elasticity characteristics. This process was called model condensation.

The FEM model should be condensed since it originally contained too many variables. The way of condensing the FEM model is to specially define some nodes as so called "Master" nodes, whereas the other nodes would be controversially "Slave" nodes. By doing this, the master nodes would still hold independent equations, but the results of the slave nodes would be the linear combination of the results from neighboring master nodes, which in other words, slave nodes do not hold independent variables any longer. By carefully selection of master nodes, the number of independent variables could be significantly reduced without losing the general model characteristics. This calculation was called "Substructuring analysis" in ANSYS (see Figure 8).

The eigenmodes of the FEM system would provide the most important information for the FlexTrack, how the elasticity of the track should be simulated. The eigenmodes of the FEM system was calculated by the so called "Modal analysis" based on the condensed FEM model. The eigenmodes of the flexible track represent both its dynamic response and its local deformation due to the interface forces.

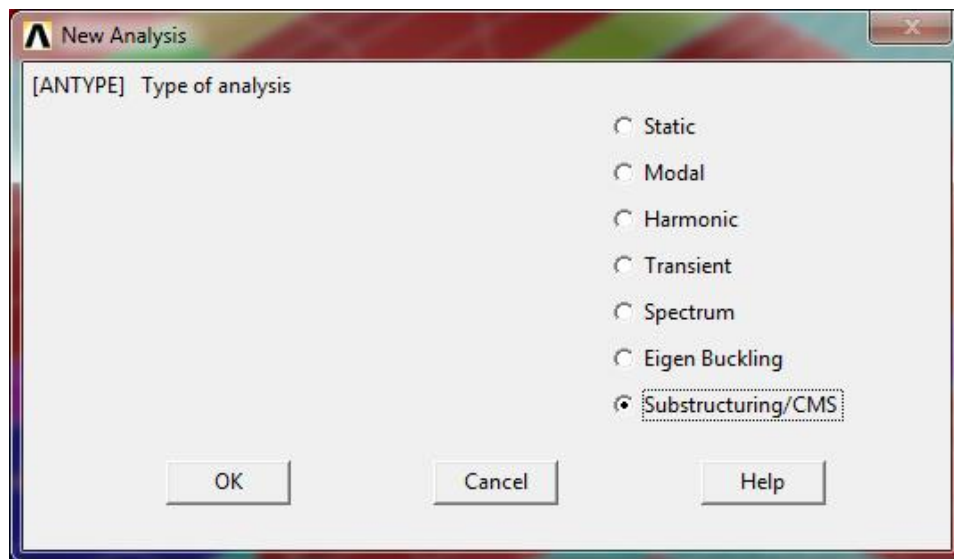
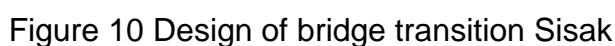


Figure 8: Type of analysis available in ANSYS







A large green steel beam, likely a railway component, is shown resting on wooden sleepers. The beam has 'APR' and a logo painted on it. The sleepers are laid on a bed of gravel ballast. The scene is outdoors, with other railway tracks visible in the background.

24 of 148



(Zagreb side)

Table 2: Location of the interruption point of construction

Transition	Distance to bridge (m)	Absolute location (m) <sup>*)</sup>
Zagreb	10	-10
Sisak	3	15

<sup>\*)</sup>: Bridge entrance at Zagreb set to be 0 m

### 3.3.Track design

#### 3.3.1. Track superstructure

The design of track superstructure was done by the local railway operators. It is a typical ballasted track structure containing rail, rail pad (fastenings), sleeper and ballast. Table 3 shows the general information on track superstructure design <sup>[16]</sup>:

Table 3: General information of track superstructure

<b>Rail</b>	
Profile	60E1
Slope	1:40
Gauge (mm)	1435
<b>Fastening</b>	
Pad density (g/cm <sup>3</sup> )	0.930 – 0.952
Pad stiffness (kN/mm)	≤ 200
Tensile strength – screws (N/mm <sup>2</sup> )	> 400
Longitudinal resistance – clamp (kN)	9
Clamping force (kN)	2 x 10
<b>Sleeper</b>	

Length (mm)	2600
Weight (kg)	300
Maximum allowable axle load (t)	25
Maximum allowable speed (km/h)	160
Sleeper spacing (mm)	600
<b>Ballast</b>	
Compressive strength, dry (N/mm <sup>2</sup> )	> 150
Thickness (cm)	> 30
<b>Substructure on open track</b>	
Subgrade modulus ( $E_{v2}$ , N/mm <sup>2</sup> )	> 90

It should be noticed that, extra elastic materials like under sleeper pad, sub-ballast mat were not built into the superstructure.

### 3.3.2. Substructure in open track

According to the information from the operator (HŽ Infrastruktura d.o.o, partner of the project), two different substructure models were used on both sides of the bridge (only for open track). General specifications were documented and shown in the following Figure 12 and Table 4 <sup>[17]</sup>.

Table 4: Design specifications

	Model 1	Model 3
Mile pot	km 396+900 – km 398+425	km 398+425 – km 398+800
Substructure	Geotextile	Geotextile + Geogrid
Protective layer thickness	30 cm	40 cm (2 x 20 cm)
Compression module (Surface substructure)	$E_{v2,min} = 35 \text{ MN/m}^2$	$E_{v2,min} = 15 \text{ MN/m}^2$
Compression module (Surface protective layer)	$E_{v2,min} = 90 \text{ MN/m}^2$	$E_{v2,min} = 90 \text{ MN/m}^2$
Bridge middle	km 398+441 in Model 3	

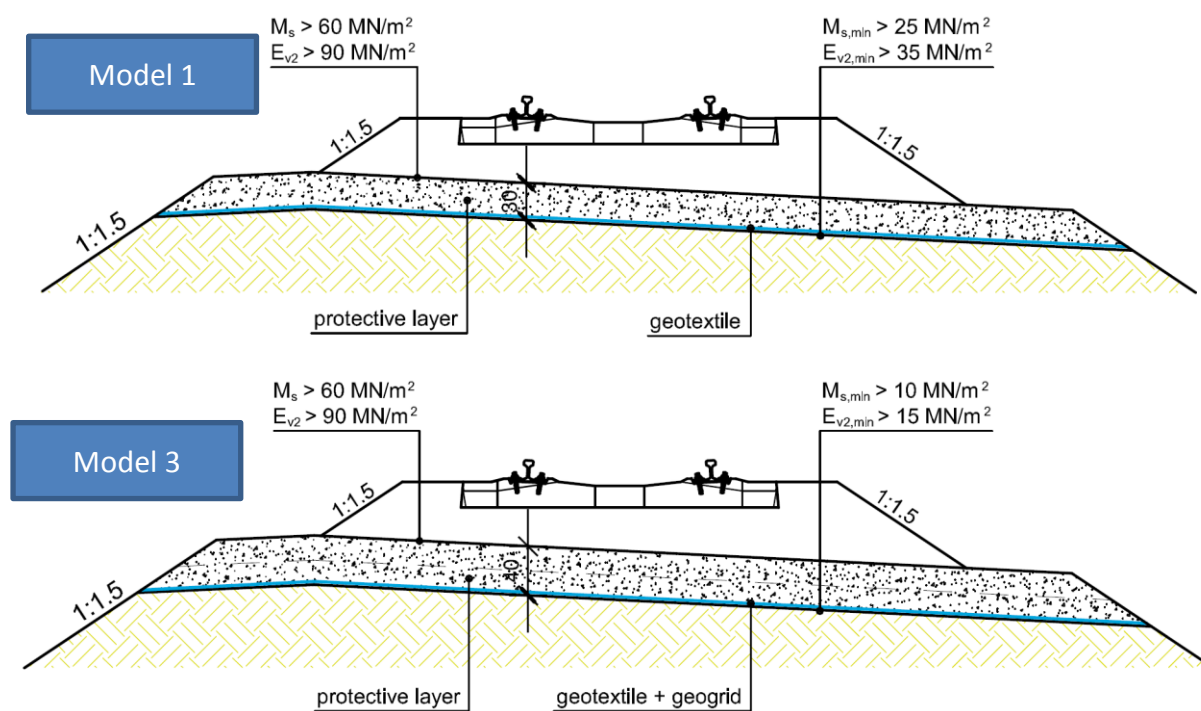


Figure 12: Structural design of the section (open track)

Due to different design specifications, different elasticity as well as different long-term impacts on track settlement should be expected. These aspects would be discussed in the following chapters.

---

### **3.4.Design of field measurement**

When talking about the research on vehicle-track interaction and the respective track quality, the necessary items for the measurements should include the measurement of elastic track deflection, the vertical geometry of the track and the dynamic track behavior. See Annexes 1 to 5 for performance of respective test items in field.

#### **3.4.1. Selection of measurement section**

Locations like bridge and bridge transitions are always the “spots”, where potential higher dynamic vehicle-track interaction should be expected. As introduced in Chapter 2, this kind of interaction always shows a time-dependent distribution covering the whole “spot” area and varies itself when the travel speed is different. Therefore, the measurement section should be able to cover the area from open track until the bridge itself. This is to say, that each measurement section should contain three areas shown as follows:

- Open track
- Transition
- Bridge

Each bridge transition has a construction length of around 17 m, covering approximately 29 sleepers. A total length of approximately 28 m is therefore selected, covering 5 m open track, 17 m bridge transition and 6 m bridge. The division of the two measurements sections is at the middle point of the bridge, with section 1 in direction Zagreb and section 2 in direction Sisak.

---

### **3.4.2. Determination of track geometry (plastic track deformation, unloaded)**

The determination of track geometry in representation of plastic track deformation was done previously only in vertical direction, but for a better understanding of the influence of track irregularity to the behavior of the wheel-rail interaction, there exists the necessity to record the track geometry continuously in 3 dimensions.

Track geometry in representation of plastic track settlement is the direct source influencing the vehicle-track interactions. By increasing the travel speed, a longer influence section could be expected.

The design of modern passenger coach always follows the principle, that an eigenfrequency of approximately 1 Hz should be achieved <sup>[18]</sup>, which means the calm down time for single impulse could be up to 1 s long. This defines the minimum wave length which should be included in the calculation of track geometry. Due to the reason that the maximum measured speed level of train passage was around 55 km/h (around 15 m/s), the maximum wave length should be at least 15 m. From the previous experiences of the institute, this wave length must have at least 8 repeats in each measurement, meaning a total length of more than 120 m should be measured with the transitions and bridge located in the middle of the measurement area.

New track recording wagon was introduced and applied in this research work. The wagon was manufactured by the company Vogel & Plötscher with a type series called 'MessReg CLS' <sup>[19]</sup>. It could record the respective track parameters continuously along the line by just pulling the wagon with walking speed. See Figure 13 and Table 5 for the handled parameters as well as accuracies.

Table 5: Performance data of movable track geometry recording tool  
(Type CLS from company V&P) <sup>[19]</sup>

Measured parameters	Range from (mm)	Range to (mm)	Accuracy (mm)
Gauge	1415	1500	0.005
Versed sine	-230	+230	0.005
Gradient	-100	+100	0.3
Cant	$\pm 170$		0.001°
Distance	Continuous		2



Figure 13 Movable track recording wagon (Type CLS from company V&P) <sup>[19]</sup>

It is especially important to mention that the Under-sleeper-gap is actually another phenomenon of track plastic deformation in vertical direction. These deformations could only be detected by loaded track, therefore the gaps would be measured by other measurement methods.

### 3.4.3. Measurement of elastic rail deflection (quasi-static)

To check the uniformity of vertical load distribution of the track by rail deflection, it is needed to perform static rail deflection measurements on certain amount of rail seats (sleepers) within each test section. Rail deflection is influenced by all the elastic components within the railway sub- and superstructure as well as by potential gaps between sleepers and ballast.

---

For achieving a systematic view of the track elasticity, both rails along the measurement section should be measured. Considering the limited length of the bridge, this measurement covers all the rail seats on the bridge. A total number of 75 rail seats (continuous) were calculated based on the following considerations:

- Length of transition is 17 m for each
- Length of bridge is around 12 m
- This comes to a total length of 46 m
- This covers 75 rail seats

This is to say, that the selection of 75 rail seats could be able to cover the both transitions and the whole bridge. Extra 20 points on both rails near the transitions are also randomly selected for gathering the elasticity behavior on open track. Those measurements could be judged as the guideline for symbolizing the overall track elasticity.

Rail deflection measurements on successive rail seats could be performed using the track movable, modified Benkelman-beam which gives the overall rail deflection under a given quasi-static axle load as well as the shape of the deflection bowl of one rail during the approach of the loaded wheel. The quasi-static loading was given by a ballast bulk wagon with a single axle load. A loco was used to push and pull the wagon by walking speed regularly within a stop to stop distance of about 10 m. See Figure 14 for the design of the Benkelman measurement wagon:



Figure 14 Benkelman beam for the measurement of track elastic deflection (photo from previous measurement event)

For analysis purposes, the deflection line should be calculated based on the measured influence line. The values of the deflection line for each rail seat could not directly be given from the measurement data, because the specification for the deflection line requires stable load (in the Benkelman measurement, the load train was moving while the data were measured). Therefore an interpolation should be carried out which functions as follows:

- Choose the rail seat  $i$  where the deflection line would be drawn
- The deflection at load point (max. deflection) is read from the measurement  $i$  under the position of  $s = 0$  m
- The deflection at  $x = x_0$  m ( $x_0$  is sleeper spacing) is read from the measurement  $i-1$  under the position of  $s = x_0$  m (this is exactly the deflection of  $x = x_0$  m when the load is on rail seat  $i$ )
- The deflection at  $x = 2 \cdot x_0, 3 \cdot x_0, 4 \cdot x_0, \dots$  could be equally calculated



### 3.4.4. Recording the track dynamic behavior by strain gauges

Strain gauges could be installed in one rail in a length of sleeper spacing. The strain gauges were located at the rail foot center between sleepers and could record the strain changes caused by wheel load from the vehicle. Type of strain gauges was 6/120 LY 61 of HBM (Hottinger-Baldwin-Messtechnik). For data recording, the QuantumX MX840A was used which could measure 8 channels at the same time. Through fire-wire connection, more units could be connected and measured with synchronized time axis (See Figure 15 for hardware information).

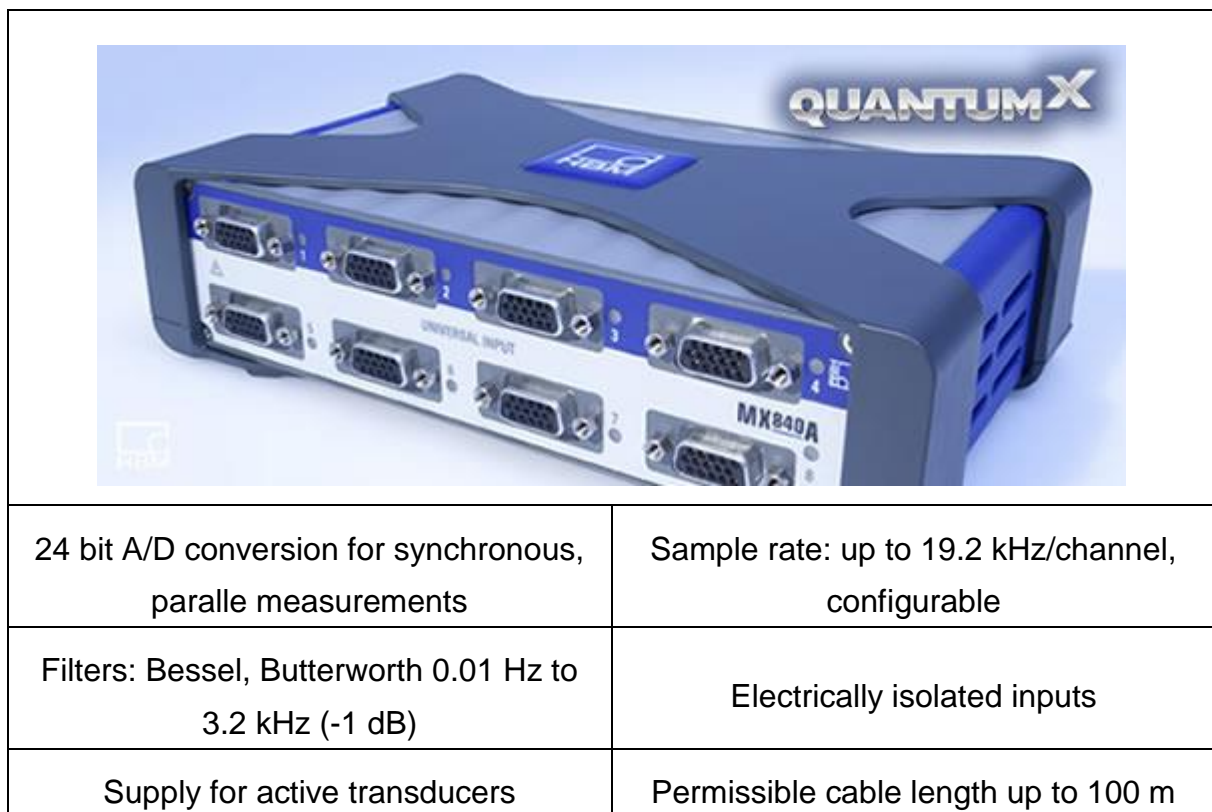


Figure 15 Data amplifier QuantumX MX840A <sup>[20]</sup>

It supports a maximal measurement frequency up to 19 kHz, meaning that for a train running with 300 km/h, within a distance of 4 mm of train movement one set of data had been recorded. This was needed to clearly identify the peak values of rail foot strain influence lines. For evaluation strain values had been used to determine the respective rail foot stress using the formula  $\sigma = \epsilon \cdot E$ , whereas the Young's modulus  $E$  was set to  $2.1 \cdot 10^5$  N/mm<sup>2</sup>.

There were in total 6 pieces of data amplifier, meaning that the maximum allowable channels for a synchronized measurement are 48, meaning that when the rail foot stress between every two rail seats were measured, the installed strain gauges could not cover the whole bridge transition. Since strain gauges should be distributed in all the open track, bridge transition and bridge, a split of channels on all the areas should be made.

Two measurement sections divided at the middle of the bridge were defined, with section 1 in direction Zagreb and section 2 in direction Sisak. It is clear that the bridge transition is the most important area. Therefore the most numbers of strain gauges should be installed in the transition with special concentration on the side connecting the bridge. Following this principle, the allocation of the sensors was finally decided as follows (see Table 6):

Table 6: Allocation of strain gauges

	Section 1 – transition Zagreb	Section 2 – transition Sisak
Number of strain gauges in open track	6	6
Number of strain gauges on bridge	4	6
Number of strain gauges in transition	36	35
Total installed strain gauges	46	47
Max allowable channels	48	

The test should be done under test runs and normal operational train runs. It must be taken into account that measurement data for analysis and evaluation could be therefore affected by respective train speed (fixed according to operational or actual, random conditions) and train type (axle loads and axle spacing, suspension system) as well as by load deviations and conditions of individual axles (potential wheel flats) even if the type of train was identical.

---

## 3.5. Test runs and train runs

### 3.5.1. Test runs

The strain Test runs with predefined train sets are very essential for the understanding of the real-time vehicle-track interaction parameters. Speed could be set as the variation parameter, which enables the vision of change of dynamic impact according to speed. The test run should be better performed by the same vehicle used in the Benkelman beam test in 3.4.2.

The design of the test runs including speed of passage should follow the criteria shown below:

- Inclusion of quasi-static runs ( $V < 10$  km/h);
- Inclusion of the maximum allowable speed of the line (or maximum speed of the train when below the speed limit of line);
- Speed level between 10 km/h and the maximum speed should also include 40 km/h, 60 km/h and so on;
- A forward and backward travel should be performed for each speed level.

A joint measurement with other partners in the project (IGH and ZAG) would be preferred in order to gather the synchronized measurement results of substructure reactions. The design of the test sensors and allocation were already described in the deliverable 3.2 <sup>[15]</sup>.

### 3.5.2. Train runs

The test should be performed under normal operational train runs. The aim of the test is a statistical summary of the train sets or locomotive with the same type according to their measured speed levels. Another concentration would be the examination of the maximum measured dynamic strain and the potential risk of overload or failures. Following criteria should be set:

- Measurement should include all the normal train sets and locomotives which frequently use the track;
- For each type of train, enough measurement samples should be gathered;
- There should be measured train runs with the maximum allowable speed level of the track;

### 3.6. Boundary conditions (fish plated joints)

It should be specially noticed, that due to the need of construction work, rail at this location was connected using the fish plated joint (see Figure 16), which would have numerous effect on track geometry and track elasticity. Since these joints (in total 6 covering both measurement sections, not presence in measurement 2014) were only temporary solutions during the construction work, measurement values at these locations might not be representative for the actual track condition.



Figure 16 Installation of fish plated joint


### 3.7. Vehicle information

Different types of vehicles were measured during the train run tests. As the evaluation of the measurement data is highly dependent on the design of the vehicles (axle load,

suspension design, etc.), an overview of the measured locomotive and multiple units were collected and shown in the following sections.

The general information of the locomotive and multiple units which were recorded on field could be seen in the following Table 7 to Table 10 <sup>[25]</sup>:


Table 7: EMU series 6111, (HR- HŽ)

	
HŽ series 6111	
Type of vehicle	EMU
Formation	2'2'+Bo'Bo'+2'2'
Max. speed (km/h)	120
Weight (t)	145
Max. axle load (t)	17.0
Axle spacing (mm)	2650

<sup>\*)</sup> Pic source: Wikipedia




Table 8: EMU series 6112, (HR- HŽ)

	
HŽ series 6112	
Type of vehicle	EMU
Formation	Bo'2'2'2'Bo
Max. speed (km/h)	160
Weight (t)	172
Max. axle load (t)	17.5
Axle spacing (mm)	2700


\*) Pic source: Wikipedia

Table 9: Locomotive series 1141, (HR- HŽ)

	
HŽ series 1141	
Type of vehicle	Locomotive
Formation	Bo'Bo'
Max. speed (km/h)	140
Weight (t)	82
Max. axle load (t)	20.5
Axle spacing (mm)	2700

\*) Pic source: Wikipedia

Table 10: Locomotive series 2062, (HR- HŽ)

	
HŽ series 2062	
Type of vehicle	Locomotive
Formation	Co'Co'
Max. speed (km/h)	124
Weight (t)	103
Max. axle load (t)	20.5
Axle spacing (mm)	2700

\*) Pic source: Wikipedia

### 3.8.Summary

In this chapter, the design of the bridge as well as the bridge transition was reviewed. Important points from the design were discussed and necessary track superstructure data were gathered.

#### 3.8.1. Review of the pilot section and design of the measurement

Generally, two measurement sections were formulated which should cover the bridge, bridge transition and open track. Type of measurement as well as their boundary conditions was defined. The following Table 11 and Table 12 show the information for

measurement sections and the design of measurement items. For values like '46 / 47', the first value refers to the number for section 1 and the second value for section 2.

Table 11: Summary of the general information along the bridge

Item	Description
<b>Transition issue</b>	
Construction work interrupted at	-10 / 15 m (bridge entrance of Zagreb at 0m)
<b>Design of track superstructure</b>	
Art of Superstructure	Ballasted
Stiffness of rail pad (kN/mm)	$\leq 200$
Design speed (km/h)	160
Design axle load (t)	25.0
Thickness of ballast (cm)	$> 30$



Table 12: Summary of the design of measurement

Item	Description
<b>Split of measurement sections</b>	
Location of bridge (middle point)	km 398+441
Length of bridge transition (m)	17 for each
Length of the measurement section (m)	ca. 28.0 for each
Measurement section includes	open track 5 m bridge transition 17 m bridge 6 m
Measurement section 1	From bridge middle in direction Zagreb (including transition Zagreb)
Measurement section 2	From bridge middle in direction Sisak (including transition Sisak)
<b>Measurement of track elasticity</b>	
Number of measurement points in transition and bridge	75 on each rail
Number of measurement points in open track	18
<b>Measurement of track geometry</b>	
Length of measurement (m)	> 120
Location of the measurement	Bridge and bridge transition in the middle of the measurement
<b>Installation of strain gauges</b>	
Installed number of strain gauges	46 / 47
Number of strain gauges in transition	36 / 35
<b>Test runs and train runs</b>	
speed level of test runs(km/h)	<10, 40, 60, ..., max speed

### 3.8.2. Categorization of the measurement items and connections to numerical simulations

According to the effective track measurement methodologies, it could be categorized referring to its functionality as follows (see Table 13). The data transfer for the further numerical simulation models were also shown to illustrate how the measurement data could be used in the models:

Table 13: The measurement items and their functionalities for the numerical models

Item	Location	Parameters measured	Data provision for numerical models	
Geometry	rail head	plastic track deformation	MBS (Input)	Track irregularity input
Displacement (quasi-static)	rail absolute	Elastic track deformation	FEM (Input)	Track elasticity input
Strain / stress	rail foot	Dynamic wheel load	FEM + MBS (Output)	Dynamic wheel rail interaction

It is clear to see that for a systematic understanding of the track behavior under running trains, both FEM and MBS methodologies would be necessary. The written 'Input' was referring the parameters which were needed for model calibrations while the written 'Output' to those parameters which were seen as the results of the simulations.

It should be mentioned that for FEM and MBS, more parameters including the profiles and design parameters should be also given. Since these are not any parameters from the measurements, they were not listed in the table above.

A detailed application of the modeling strategies would be introduced in Chapter 7.

## 4. FIELD MEASUREMENT AND DATA ANALYSIS (OCTORBER, 2013)

### 4.1. Introduction

The field measurement on site was carried out by the team of chair and institute of road, railway and airfield construction from Technische Universitaet Muenchen between October 22<sup>th</sup> and 28<sup>th</sup>, 2013. All the above mentioned measurements were accomplished and the following chapters would show those results as well as the analysis of those values. The sortation of the discussion of the recorded measurement data would be according to different measurement items.

Figures showing the status of the measurement section are attached in Annexes 1. Various figures and tables showing the data acquisition as well as data evaluation would be listed below. The x-axis in the figures would always show the distance [m] between beginning of the test section and actual point of interest within the section. Direction of X-axis is equivalent to the direction in Sisak. It was manually defined, that the bridge end at Zagreb side is 0 m and the rail on the left side in direction Sisak is called 'Left rail'. This definition would be used through all the following figures and tables in this chapter. The arrangement of the sensors in each section would be shown in Figure 17:

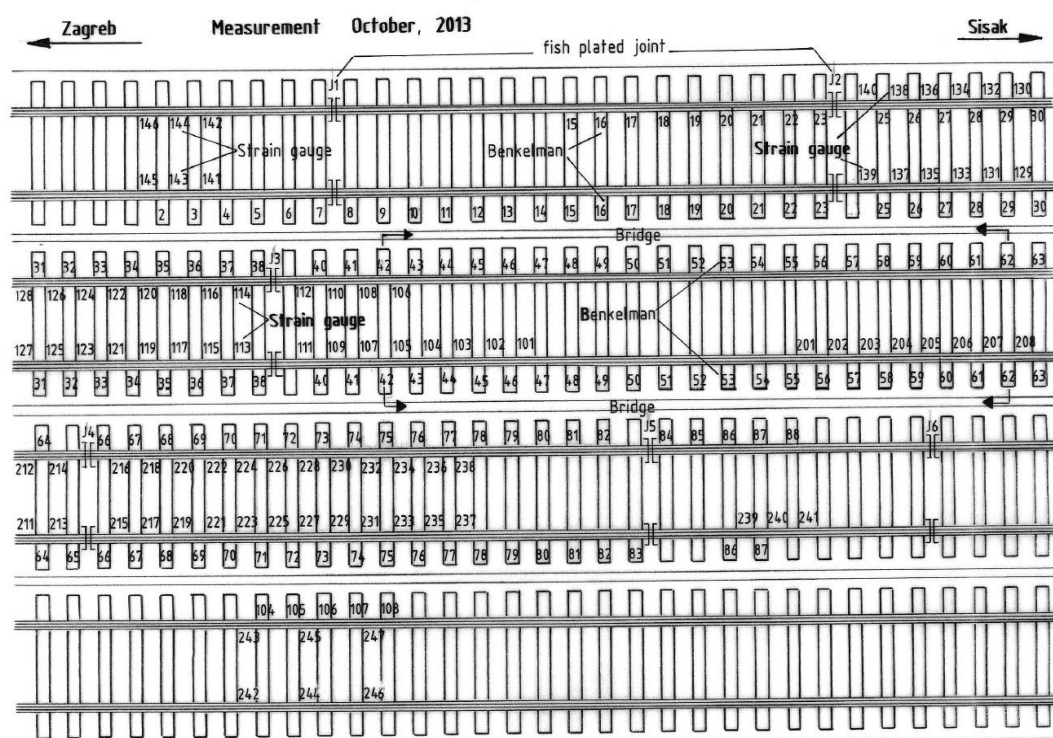


Figure 17 Section plan and installation of test sensors (October, 2013)

## 4.2. Track geometry and irregularity (plastic settlement)

The geometry measurement recorded the track parameters in a length of 133 m for the both measurement sections with the in 3.4.2 introduced track recording wagon. See Figure 18 for a sample three dimensional track geometry on vertical, gauge and cant. For processing of data, a maximum wave length of 15 m was used.

The location of fish plated joint (in total 6 pieces) was marked in line (with the abbreviation “J”) in the Figure. It is clear to see that the location of fish plated joint could have a big influence on the overall track geometry. A maximum settlement of 6.5 mm could be found by passage of one joint.

The through line in red with the abbreviation of “M” symbolizes the middle of the bridge. It could be therefore concluded as in the following Table 14 about the location of interest points.

Table 14: Location of the interest points along the measurement of track geometry

item	Location
Bridge middle at (m)	6.0
Bridge entrance – transition Zagreb (m)	0.0
Open track – transition Zagreb (m)	-17.0
Bridge entrance – transition Sisak (m)	12.0
Transition Sisak – open track (m)	29.0

It is therefore reasonable to see, that the track geometry inside the transition (between 44.8 and 61.8 m as well as between 73.8 and 90.8 m) could not be evaluated due to the presence of fish plate joints. This is for the reason, that one fish plated joint could have an impact area of more than  $\pm 5.0$  m.

An evaluation of the vertical track geometry in open track and bridge could be done by ways of statistical analysis and the result was shown in Table 15:

Table 15: statistical analysis of vertical track geometry – open track and bridge

Item	Open track	Bridge
Length of measurement (m)	67	8
highest (mm)	0.83	0.73
lowest (mm)	-1.14	-0.58
Standard deviation (mm)	0.50	0.37

Generally the track geometry is smoother in bridge than in open track, due to the smaller value of standard deviation in bridge section. Reasons for this effect could be considered as follows:

- Track in the bridge is newly constructed;
- Track in the bridge has different overall elasticity than in open track.

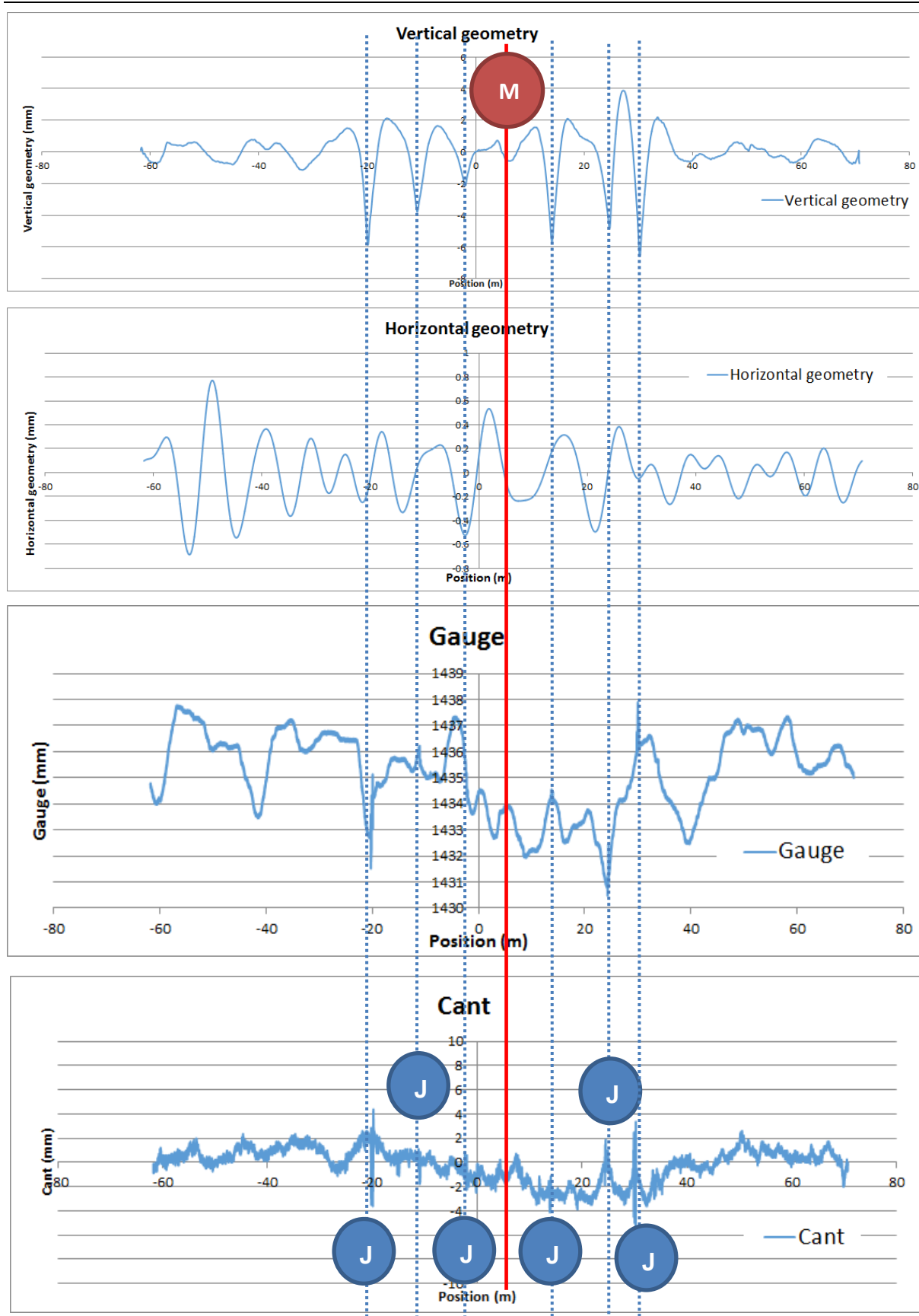


Figure 18 three dimensional track geometry

### 4.3.Rail deflection under static loading

The load wagon numbered Hz 21 78 3329 072-9 with totally 2 axles was used. A total weight after loading of approximate 38.5 t was measured (specified by Croatian railway). It is figured out that the axle load of both axles could be fixed to 192 kN (Wheel load around 96.0 kN). The axle spacing of the wagon is 8 meters, which means no influence from the neighboring axle as well as other axles should be taken into consideration. The ballast wagon was driven by a construction locomotive. Elastic deflections on both left and right rail were recorded which means both axles of the ballast wagon would be recorded for the measurement (left and right rail specified on behalf of the milepost direction from Zagreb to Sisak; locomotive was turned around between different measurement). Totally 150 measurements were performed on both bridge transitions and the bridge and 18 measurements on open track.

For reference reasons, extra points on open track were also measured. See Table 16 for the measured rail seats as well as the served axle load from the load wagon. The served wheel load for all the measurements was always 96 kN. The rail seats on both sides of open track were randomly selected. The result of the measurement was shown in Figure 19. The location of the 5 rail joints along the measurement area was written in the figure as “Joint”.

Table 16: Benkelman beam test – bridge and transition

Test of track elasticity (totally recorded 168 rail seats)		
Location	Measured rail	Interval between (m)
Open track – Zagreb	Right rail	-24 and -16.8
Transition Zagreb	Left / Right rail	-16.2 and -0.6
Bridge	Left / Right rail	0.0 and 12.0
Transition Sisak	Left / Right rail	12.6 and 28.2
Open track – Sisak	Left rail	37.2 and 39.6

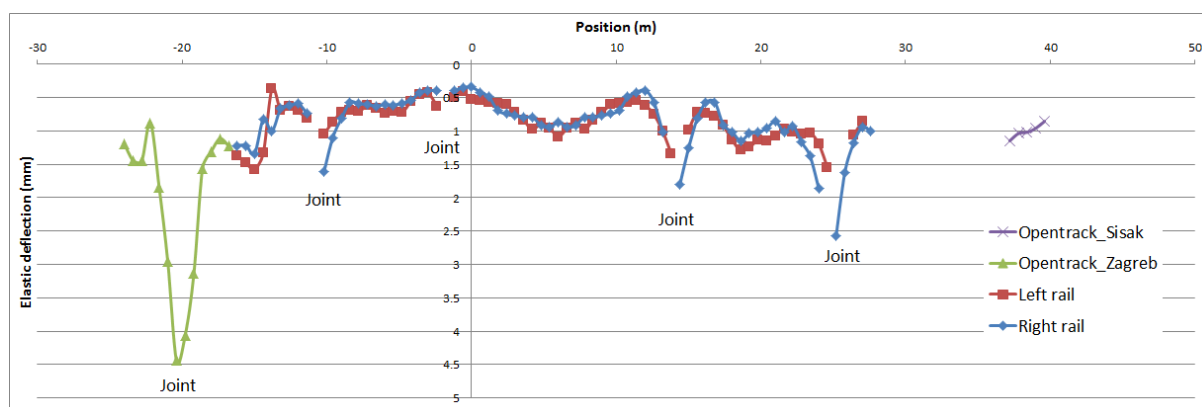


Figure 19 Measured maximum rail deflection

The measured maximum deflection of 4.5 mm is due to the location of fish plated joint, which should be seen only as a temporary solution. For evaluation of the track elasticity, those locations would not be included.

Furthermore, it should be realized, that the measured points next to the joints could also be influenced as well. Since the influence area of one joint is dependent on the deflection of the track next to this location, this influence area should be determined by checking the measured influence line. Taking an example for the determination of the influence area of the joint at location  $x = -20.1$  m (max. rail seat deflection of 4.5 mm), the measured influence line was shown in Figure 20:

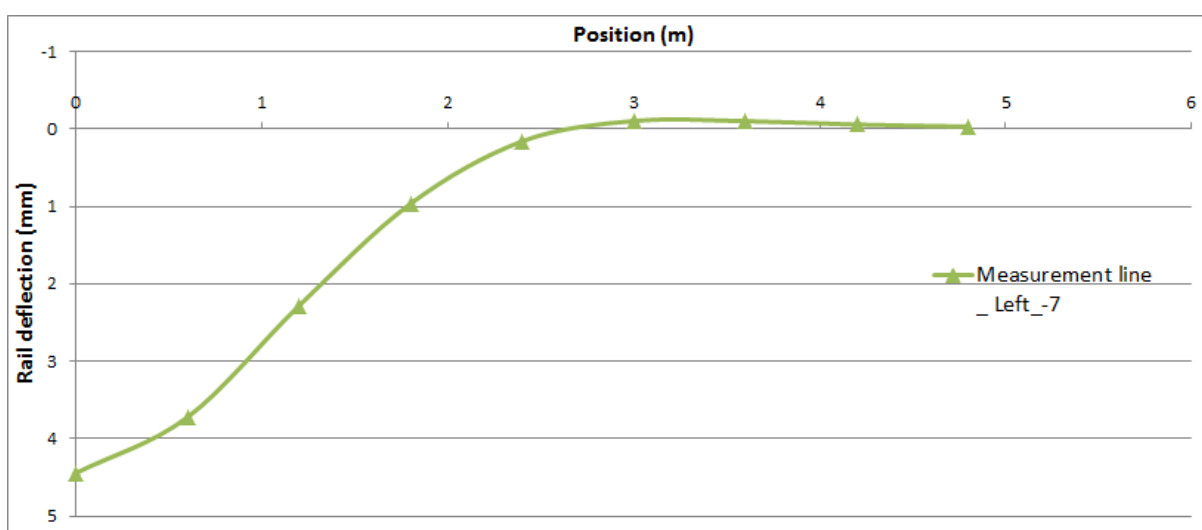


Figure 20 Measured influence line (left rail seat -7)



The above figure shows the measured deflection of the rail seat No. -7 when the wheel was approaching ( $x = 0$  m meaning the wheel was exactly above the measurement point). It could be found out the average value at those locations was around 1.0 mm, therefore the values at 0, 0.6 and 1.2 m should be considered to be inside the influence area of the joint. This is to say, that besides rail seat No. -7, the rail seats -5 until -9 should all be considered influenced due to the fish plated joint.

By this way, the points next to the fish plated joint could be taken out and Table 17 shows the number of measurements on different locations. It should be noticed that the analysis is now based on the division of different track structures. The deflection of left and right rail for identical section could be collected together due to unique wheel load of 96 kN.

Table 17: Information on selection of measurement points

	Number of measurements	Number of measurements not disturbed by fish plated joint
Open track_Left_ZG	13	7
Transition_ZG	54	46
Bridge	42	42
Transition_Left_SI	52	34
Open track_Right_SI	5	5

A rough analysis was performed on all the values WITHOUT the rail seats next to fish plated joints. It should be noticed that the values for bridge and transition were only made for comparison with the values from open track area. Table 18 shows the results of the analysis:

Table 18: statistical analysis of rail seat deflection<sup>\*)</sup>

	Open track _ Zagreb	Transition Zagreb	Bridge	Transition Sisak	Open track _ Sisak
Number of points	7	46	42	34	5
Minimum (mm)	1.12	0.35	0.34	0.57	0.85
Maximum (mm)	1.56	1.57	1.08	1.29	1.14
Average (mm)	1.33	0.73	0.72	0.96	1.00
Standard deviation (mm)	0.16	0.31	0.19	0.19	0.11
Coefficient of variation (%)	12.1	42.4	26.1	19.3	10.7

<sup>\*)</sup>: deflected rail shows positive value

The utilization of statistical analysis (especially the term “coefficient of variation”) is a typical way of understanding the track quality. Therefore, if the values from different sections have similar number in coefficient of variation, it could be concluded, that the overall quality of the track in those sections is also similar. This should be considered as a fact which could bring potential risks of interpreting the data, which means that the analysis method has its limitations. These imitations could be concluded as follows:

- Special structures like bridge and tunnel could have different characteristics on behalf of track quality;
- The variation of the mean value could be significant;
- Sections like transitions have different design proposals which makes the calculation of statistical values meaningless;
- Special locations of single defects should not be included.

Therefore, a more systematic methodology should be developed which could improve the evaluation of the measurement values especially for sensible structures like bridge or transitions.

A transition is generally used to smooth the difference between two different sections, which is bridge and open track in this study. An idealistic transition should be able to achieve the similar elastic deflections of both sections at both ends. Therefore, the new methodology could be concluded as follows:

- Calculate the mean value of the deflection on open track. Give it a symbol ' $D_{ot}$ ';
- Calculate the average value with data from both ends of the bridge and take the measurement value of bridge middle;
- Calculate the deflection line of the bridge according to in (b) calculated values (polynomial function, second power). Give it the symbol  $D_{bg}(i)$  ('i' is the location of the bridge);
- Connecting the value of  $D_{ot}$  and  $D_{bg}(0)$  with a line, which is considered to be the reference line of the transition;
- Draw the reference line according to position;
- Calculate the difference between every measured deflection and the reference value from the reference line;
- Make statistical analysis of the from (f) calculated values according to section (including mean value and standard deviation).

By doing this, the calculated standard deviation is the factor symbolizing the variation of the track deflection. A unique value of standard deviation for each section should then be judged as the real parameter about the track quality.

The Figure 21 shows the reference line (after step (e), marked in red) and the surrounded measurement data:

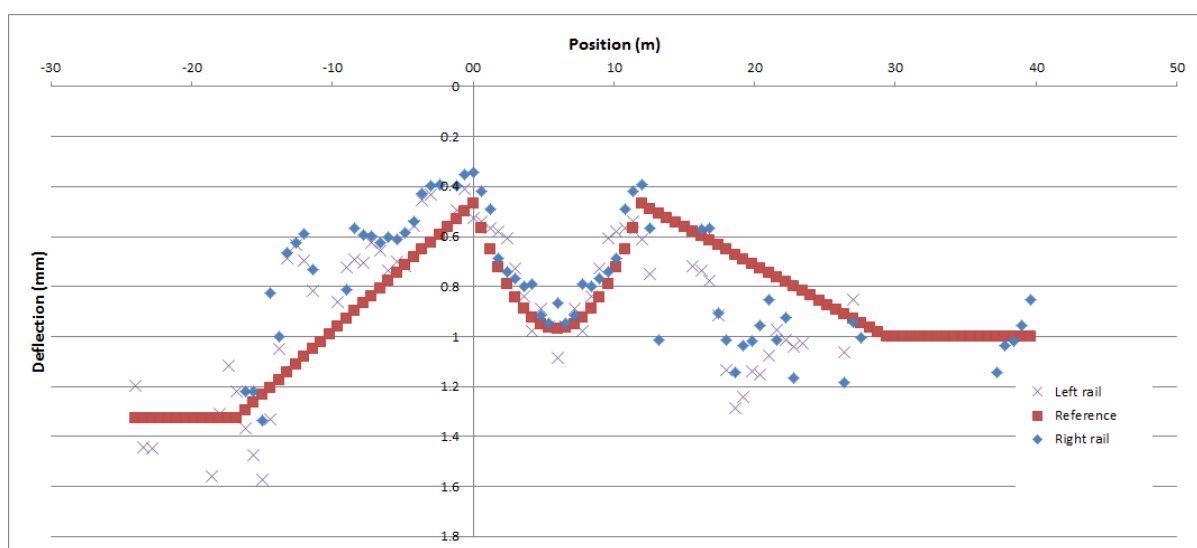


Figure 21 Difference of measurement data and reference line

The Figure 22 shows the results after step (f). Different sections were already marked with different colors for better distinguishing them from each other. Table 19 shows the results of statistical analysis (after step (g)) according to the new method:

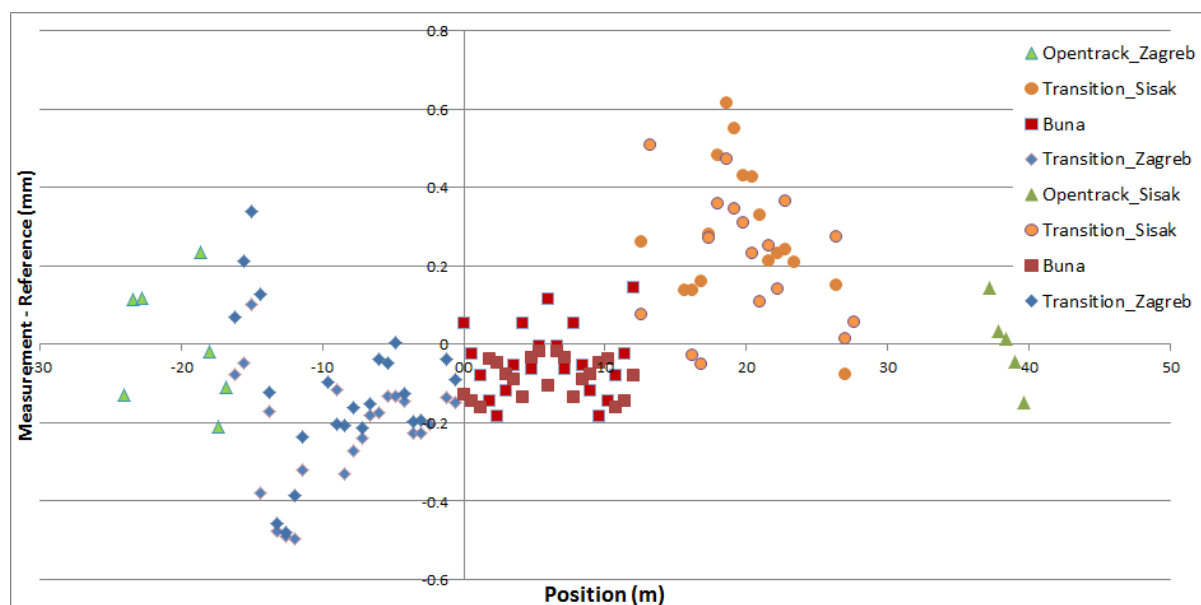


Figure 22 Difference of measurement data and reference line

Table 19: Statistical analysis according to new method

	Open track _ Zagreb	Transition Zagreb	Bridge	Transition Sisak	Open track _ Sisak
Number of points	7	46	42	34	5
Average (mm) <sup>*)</sup>	0.00	-0.17	-0.07	0.25	0.00
Standard deviation (mm)	0.16	0.16	0.08	0.17	0.11

<sup>\*)</sup>: Measurement - Reference

It is clear that the average value in open track should be zero. The average value for transition at Zagreb side is 0.17 mm, smaller than the values from transition at Sisak side which is 0.25 mm. This difference points out the fact that the actual situation of the transition at Sisak side is farther than the ideal situation. The standard deviation at both transitions is quite similar, meaning that the quality of the transitions is comparable.

The standard deviation at section “bridge” has the smallest value. This is easy to be understood due to the fact that the bridge structure is prefabricated and the quality could be better controlled.

It is good to see, that the standard deviation of the transitions and open tracks are similar, meaning that the track quality at both transitions are not significant different than the situation in open track. This fulfills the design requirement of the transitions on the first line.

#### 4.4.Rail bending behavior under test runs

According to the design of the test described in section 3.5.1, the same load train for the test of track elasticity was used. According to the capacity of the locomotive, a maximum speed level of 60 km/h could be reached.

Sections 1 and 2 were measured separately on different days. A slight difference in travel speed could be seen. The following Table 20 shows the recorded speed and the travel direction. Term ‘1F4’ refers to the 4<sup>th</sup> measurement at section 1.

Table 20: Information on test runs – section 1

Run number	Speed (km/h)	Direction	Run number	Speed (km/h)	Direction
1F1	11.1	ZG	2F1	7.1	SI
1F2	56.3	SI	2F2	49.1	ZG
1F3	56.3	SI	2F3	7.7	SI
1F4	10.3	ZG	2F4	32.3	ZG
1F5	35.1	SI	2F5	12.0	SI
1F6	9.3	ZG	2F6	56.3	ZG
1F7	44.6	SI			
1F8	10.6	ZG			

The test with 10 km/h could be understood as the quasi-static runs. It is clear to see from the Figure 23 below that the maximum strain is higher for the first two axles due to different axle loads.

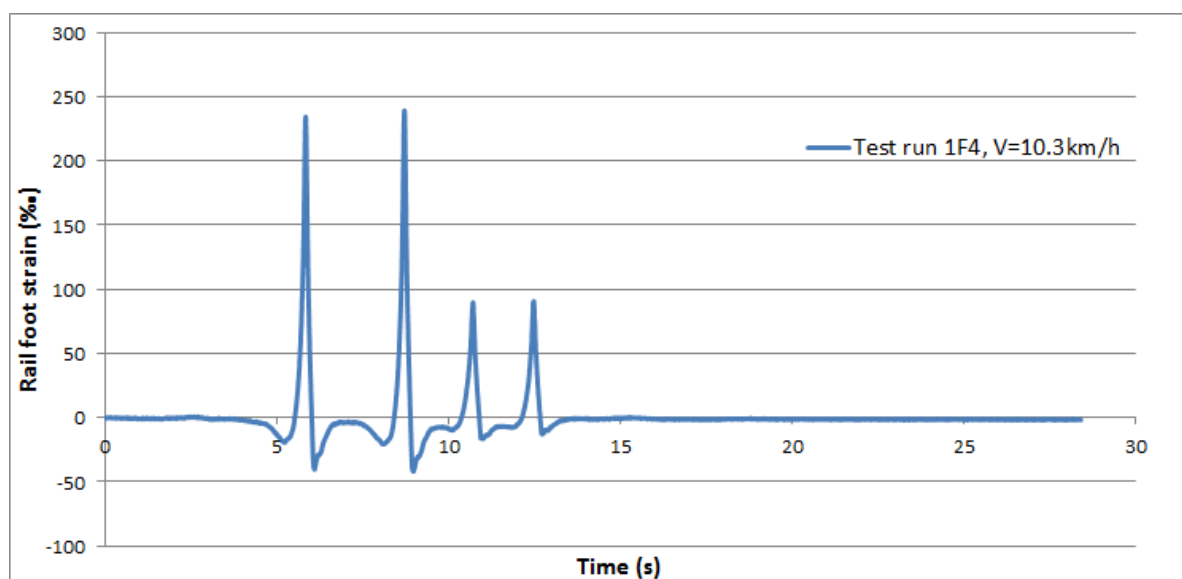


Figure 23 Sample strain gauge measurement result  
(4 axles, max. axle load around 19.0 t)

Table 21 and Table 22 list the typical distribution of the stresses at rail foot during passage of the 4 axles for both transitions. Statistical analysis is also performed for further analysis needs. (Tab '1W2 (96 kN)' represents the 1st measurement section (transition Zagreb) from the second axle of the wagon with a static wheel load of 96 kN). Strain gauges which are inside 1 sleeper spacing of the fish plated joint were considered to be not reliable and would be excluded for analysis. Figure 24 and Figure 25 summarize the average stress of the both wagon axles and shows the overlapped results of quasi-static run (in continuous line) and dynamic run (in points).

Table 21: Sample evaluation of the rail foot stress  
(sensors on right rail, Transition Zagreb)

Run 1:	Sisak - Zagreb	Speed: 11.1 km/h			
		Rail foot stress [N/mm <sup>2</sup> ]			
Sleeper No.	Position [m]	1W2(96kN)	1W1(96kN)	1L2(40kN)	1L1(35kN)
133	-9.9	52.11	53.29	23.98	21.91
131	-9.3	48.21	49.23	20.16	18.95
129	-8.7	46.63	47.02	19.99	17.51
127	-8.1	36.03	36.24	15.96	12.58
125	-7.5	42.62	43.91	18.59	15.76
123	-6.9	45.56	47.82	19.10	17.05
121	-6.3	30.85	32.00	13.14	11.07
119	-5.7	48.71	51.12	22.81	18.52
117	-5.1	47.29	49.35	20.94	18.13
115	-4.5	46.99	48.16	18.25	18.10
113	-3.9	45.25	46.18	17.99	16.99
111	-3.3	42.65	43.07	16.80	14.67
105	-0.9	46.57	45.97	18.90	15.63
103	-0.3	46.22	45.99	18.32	15.13

Table 22: Sample evaluation of the rail foot stress  
(sensors on right rail, Transition Sisak)

Run 3:	Zagreb - Sisak	Speed: 7.1 km/h			
		Rail foot stress [N/mm <sup>2</sup> ]			
Sleeper No.	Position [m]	2W1(96kN)	2W2(96kN)	2L1(35kN)	2L2(40kN)
211	14.7	46.34	44.29	14.38	17.27
213	15.3	42.36	42.08	12.58	15.87
215	15.9	44.41	43.55	13.62	15.76
217	16.5	46.23	46.30	15.75	17.33
219	17.1	55.33	54.80	19.19	23.60
221	17.7	54.41	53.25	19.93	24.86
223	18.3	51.98	51.71	19.56	23.31
225	18.9	48.99	48.13	18.85	20.93
227	19.5	48.20	47.07	16.63	19.76
229	20.1	48.13	47.07	15.08	19.63
231	20.7	48.83	48.30	15.05	18.53
233	26.1	48.05	48.54	16.58	16.98
234	26.7	48.93	48.49	17.48	17.34

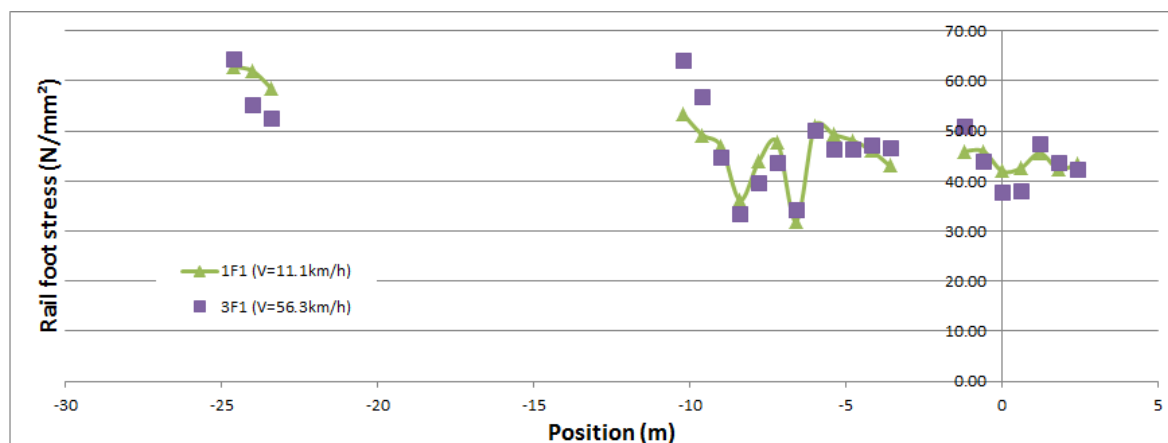


Figure 24: Test section 1 – runs 1F1 and 1F3

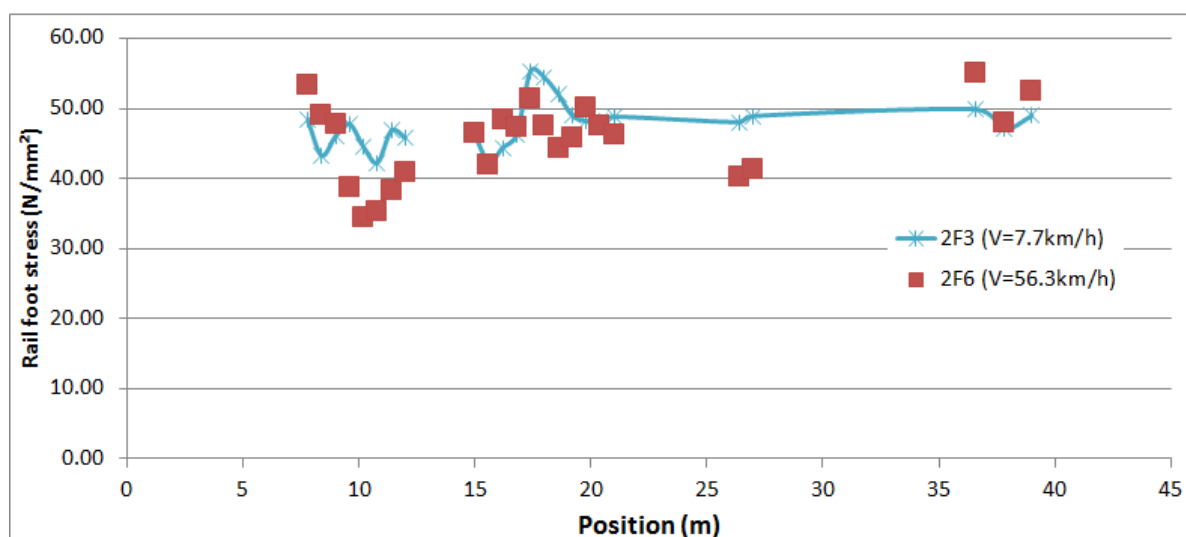


Figure 25: Test section 2 – runs 2F3 and 2F6

It could be easily figured out, that the distribution of the rail foot stress is not very close to each other even under a limited passage speed of 10 km/h. This should be explained by looking back to the distribution of elasticity at this location. The measurement under a higher running speed with higher variation of single values should be understood by the increasing influence due to track dynamics.

Due to the variation of track elasticity at different rail seats, higher stress does not principally identical to higher load. The actual wheel load along the passage of the measurement section would be calculated from the Finite-Element models.



Table 23 and Table 24 show the analysis of the rail foot stress only for the load wagon according to the speed level (only including strain gauges inside the transition area). The distribution of the rail foot stress according to travel speed is therefore clear to be seen.

Table 23: Statistical analysis of load wagon according to speed level (transition Zagreb)

Average speed (km/h)	10	40	56
Number of measurements	4	2	2
Number of measured points	120	60	60
Average rail foot stress (N/m <sup>2</sup> )	45.0	42.2	45.2
Max. rail foot stress (N/m <sup>2</sup> )	50.3	50.0	56.6
Standard deviation (N/m <sup>2</sup> )	3.88	4.47	5.98
Dynamic factor (%)	11.6	18.6	25.2

Table 24: Statistical analysis of load wagon according to speed level (transition Sisak)

Average speed (km/h)	9	41	56
Number of measurements	3	2	1
Number of measured points	69	46	23
Average rail foot stress (N/m <sup>2</sup> )	47.7	48.7	47.5
Max. rail foot stress (N/m <sup>2</sup> )	55.2	55.9	59.7
Standard deviation (N/m <sup>2</sup> )	3.69	4.46	5.99
Dynamic factor (%)	15.72	14.77	25.59

A term called “dynamic factor” was calculated by dividing the maximum stress into the average one. A clear increase of this value according to the increase of speed could be seen which explains the fact that the dynamic wheel rail interaction is stronger when the speed of the train is faster. The average rail foot stresses for all speed categories are similar but the maximum values for higher speed are higher which symbolizes a higher impact load under higher speed level.

An evaluation of the design of the transition on behalf of the measured test run data could be done. It should be mentioned, that this evaluation is focused on the aspect of dynamic wheel-rail interaction. A better transition design should be able to control the dynamic wheel-rail interaction in a reasonable way, especially by trains running under high speed levels. The effects due to fish plated joints were already excluded for the analysis.

The evaluation is done by overlapping important parameters from both test sections together which could be seen in Table 25. Furthermore, the distribution of standard deviation according to speed level was shown in Figure 26. Evaluation was done based on the data from the both axles of the load wagon.

Table 25: Comparison of both transitions

	V = 10 km/h		V = 60 km/h	
	Transition Zagreb	Transition Sisak	Transition Zagreb	Transition Sisak
Average rail foot stress (N/mm <sup>2</sup> )	45.0	47.7	45.2	47.5
Maximum rail foot stress (N/mm <sup>2</sup> )	50.3	55.2	56.5	59.7
Standard deviation (N/mm <sup>2</sup> )	3.88	3.69	5.98	5.99
Coefficient of variation (%)	8.6	7.7	13.2	12.6
Dynamic factor (%)	11.6	15.7	25.2	25.6

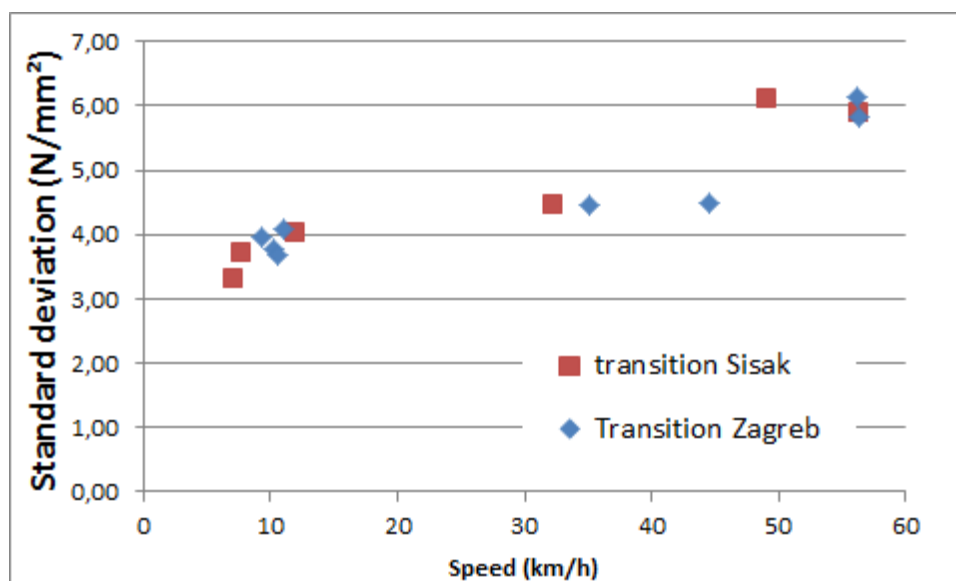


Figure 26: standard deviation according to speed (both transitions)

It could be seen that the value of standard deviation increases with the speed level. Nonlinearity could be seen, but this should not be considered as a general tendency due to the reason that the values at higher speed level were till now not included. The quality of the both transitions on behalf of dynamic wheel-rail interaction is similar, referring to a similar quality of both transitions.

It should be noticed that for normal operation, a maximum speed of 160 km/h was allowed which was much faster than the measured speed level of 60 km/h. Therefore, the behavior of wheel-rail interactions under higher speed levels should also be checked.

#### 4.5. Rail bending behavior under operational trains

Due to the speed limit of 20 km/h by the time of measurement, no obvious dynamic effect should be expected. Therefore, those values were only used for understanding of general behavior of the track due to frequent and common loadings.

Measurement points were selected which were equally distributed in both transitions. Therefore, it could be ensured, that the measured values for both transitions were under the passage of the same train.

In total 17 train runs are recorded and the evaluation is done using the passage of the first bogie of the locomotive or multiple units. Travel speed is as well evaluated. Table 26 lists the type of trains according to the measurement time point. Please refer to section 3.7 for the respective information of the trains.

Table 26: Recorded train runs and time of passage

Direction Zagreb - Sisak			Direction Sisak - Zagreb		
Time	Train / Locomotive	Speed (km/h)	Time	Train / Locomotive	Speed (km/h)
11:26	6111	21.7	11:41	6112	20.1
12:05	2041 + Freight	20.9	12:17	6111	20.8
14:23	6111	21.4	13:05	6111	19.1
15:16	6111	19.9	13:30	1141 + Freight	22.8
16:06	6112	19.6	14:39	6111	16.0
16:29	6111	16.5	14:55	1141 + Freight	21.2
17:02	6111	20.3	15:33	6111	17.2
			16:00	2041 + Freight	18.6
			16:56	6111	22.6

#### 4.5.1. Train set 6111

It is clearly to see, that the train set type 6111 was the most frequent user of the track. Since the middle wagon of train set 6111 has higher axle load (static axle load 17.0 t) than the other wagons, Figure 27 shows a sample measurement of the passage of the middle wagon (4 axles) along the test section ( $x = 0$  m refers to bridge entrance at Zagreb side). Strain gauges inside 1 sleeper spacing of the fish plated joint were excluded for all the analysis.

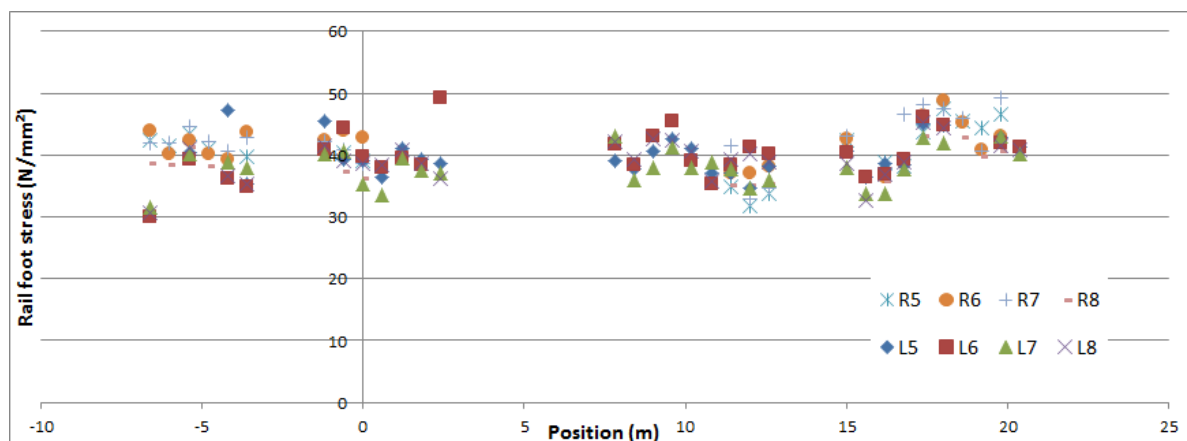


Figure 27 Sample measurement of train set 6111 (middle car,  $V = 21.4$  km/h)

Since the middle wagon of the train set 6111 has the heaviest axle load, a summary of all the recorded train runs from this wagon was made. Figure 28 shows the distribution of the average rail foot strain (all the included train runs have a passage speed of around 20 km/h).

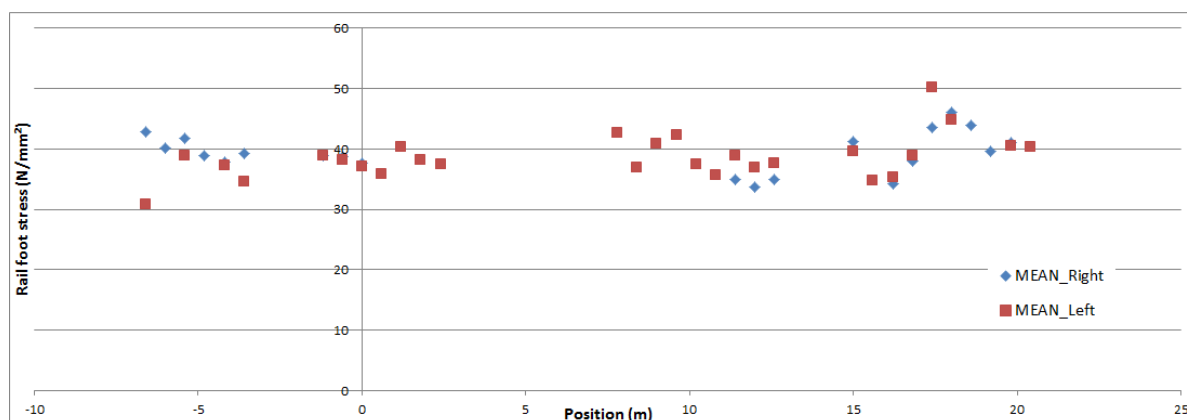


Figure 28 Summary of all the passage of train set 6111 (middle wagon)

It is easy to see that the distribution of the measurement points is highly identical to the measured values from test runs under low speed level, which is provable for the fact that no significant dynamic factors due to travel speed could be expected and this distribution is mainly dependent on the actual track elasticity variation.

#### 4.5.2. Train set 6112

The train set 6112 was released to be the modern passenger train set. Since the train set 6112 would probably replace the older train set 6111 in the future, this train runs were also evaluated.

The maximum induced rail foot stress for train set 6112 was quite similar as for 6111, meaning that the maximum wheel loads for both train sets were similar. The average rail foot stress according to axle number was shown in Figure 29:

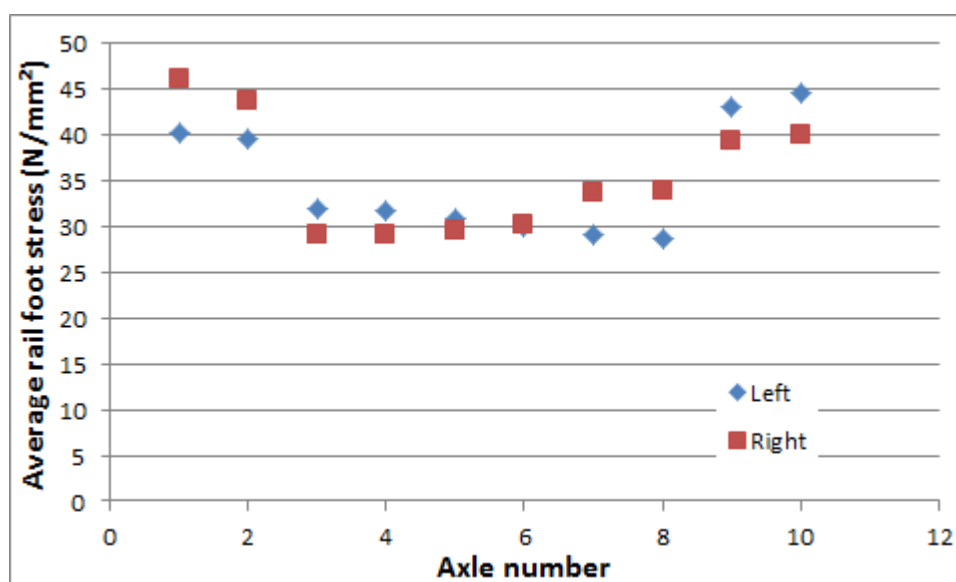


Figure 29: Distribution of the rail foot stress according to axle number

It could be firstly found out, that the first and the last two axles of the train set are generally heavier than the middle ones, due to higher induced rail foot stress levels. The measured rail foot stress of the train set 6112 is generally smaller than the values for train set 6111. Notice that the design axle load of train set 6112 was heavier than 6111, this symbolizes a better vehicle design and travel behaviour of the new train set.

## 5. FIELD MEASUREMENT AND DATA ANALYSIS (APRIL, 2014)

### 5.1. Introduction

The second field measurement on site was carried out by the team of chair and institute of road, railway and airfield construction from Technische Universitaet Muenchen between April 24<sup>th</sup> and 30<sup>th</sup>, 2014. The measured items were the same as in 2013 and the following chapters would show the results as well as the analysis of the values.

Various figures and tables showing the data acquisition as well as data evaluation would be listed below. The x-axis in the figures would always show the distance [m] between beginning of the test section and actual point of interest within the section. Direction of X-axis is equivalent to the direction in Sisak. It was manually defined, that the bridge end at Zagreb side is 0 m and the rail on the left side in direction Sisak is called 'Left rail'. This definition would be used through all the following figures and tables in this chapter. The arrangement of the sensors in each section would be shown in Figure 30:

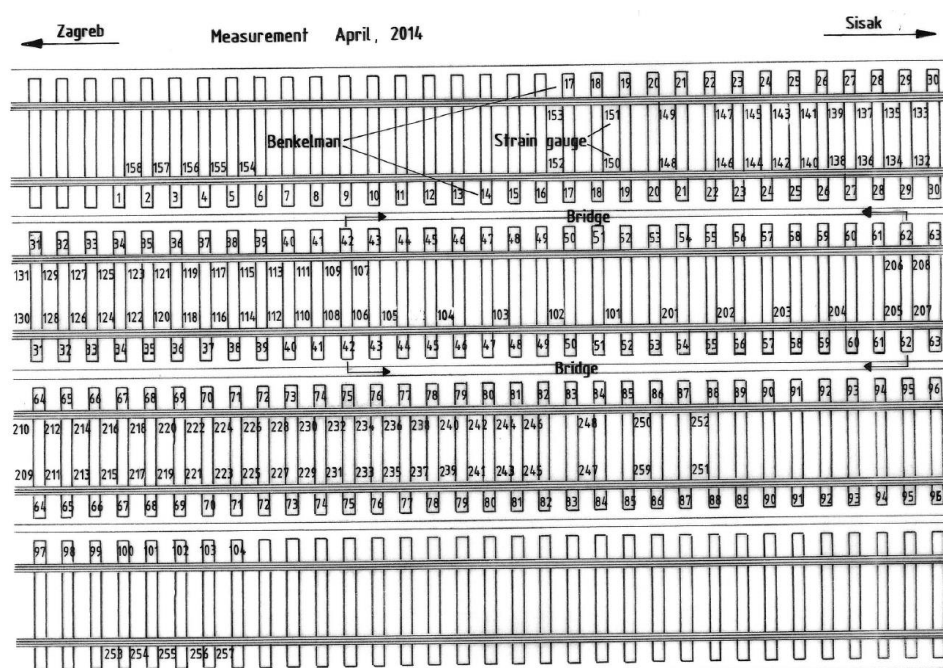


Figure 30 Section plan and installation of test sensors (April, 2014)

## 5.2. Track geometry and irregularity (plastic settlement)

The geometry measurement recorded the track parameters in a length of 500 m for the both measurement sections with the in 3.4.2 introduced track recording wagon. See Figure 31 for a sample three dimensional track geometry on vertical, gauge and cant. For processing of data, a maximum wave length of 15 m was used. After replacing the fish plated joint, no significant settlement could be seen.

The through line in red with the abbreviation of “M” symbolizes the middle of the bridge. It could be therefore concluded as in the following Table 27 about the location of interest points.

Table 27: Location of the interest points along the measurement of track geometry

item	Location
Bridge middle at (m)	6.0
Bridge entrance – transition Zagreb (m)	0.0
Open track – transition Zagreb (m)	-17.0
Bridge entrance – transition Sisak (m)	12.0
Transition Sisak – open track (m)	29.0

An evaluation of the vertical track geometry in open tack, bridge transition and bridge could be done by ways of statistical analysis and the result was shown in Table 28:

Table 28: statistical analysis of vertical track geometry – open track and bridge

Item	Open track Zagreb	Transition and bridge	Open track Sisak
Length of measurement (m)	218	50	230
highest (mm)	1.63	1.44	2.68
lowest (mm)	-1.69	-1.32	-3.14
Standard deviation (mm)	0.56	0.54	0.89



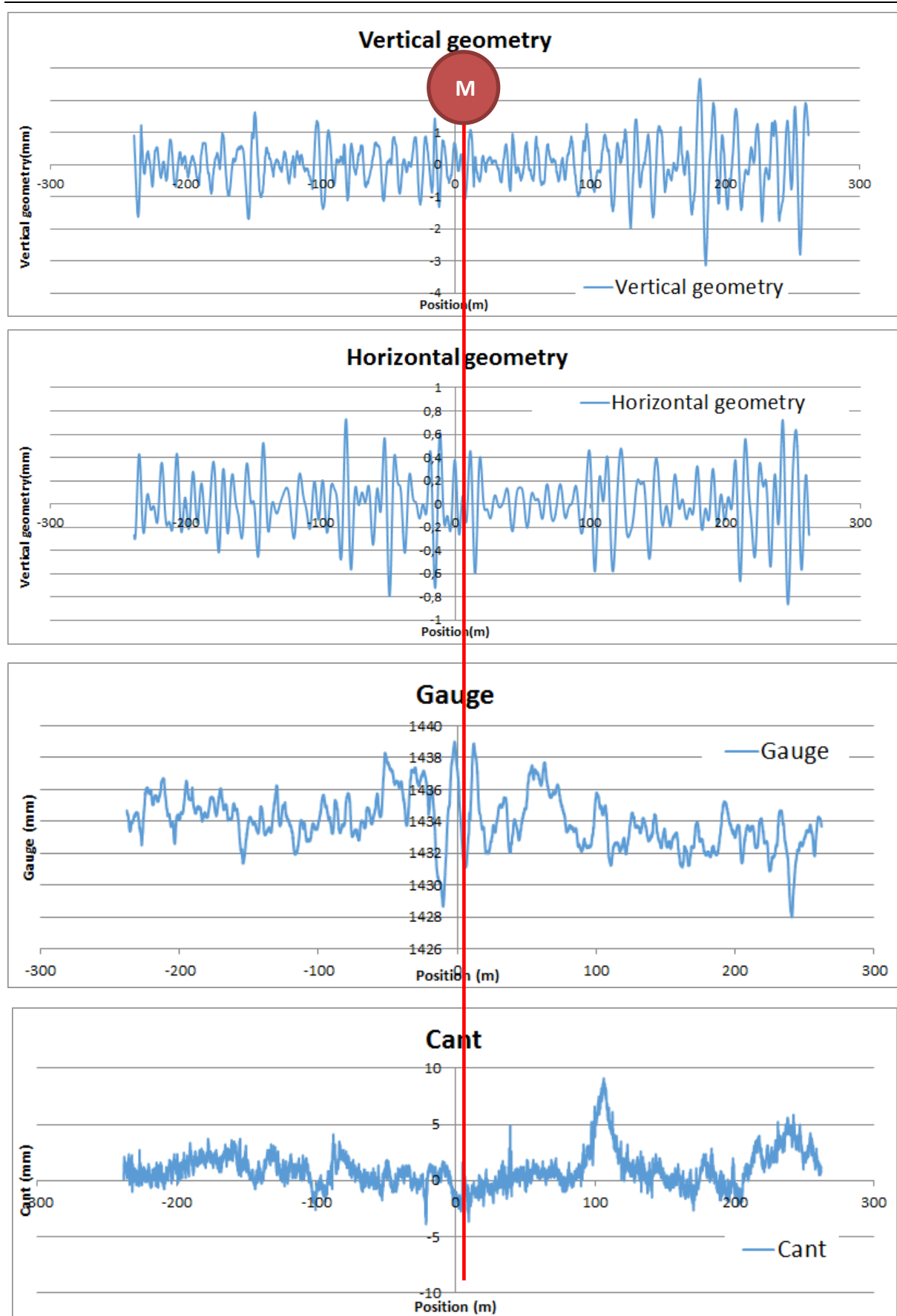


Figure 31 three dimensional track geometry (state 2014)

Generally the track geometry is smoother in bridge and transitions than in open track, due to the smaller value of standard deviation. Reasons for this effect could be considered as follows:

- Track in the bridge and transition is newly constructed;
- Track in the bridge and transition has different overall elasticity than in open track.

### **5.3.Rail deflection under static loading**

The load wagon numbered Hz 21 78 3329 082-8 with totally 2 axles was used. A total weight after loading of approximate 36.0 t was measured (measured by strain gauges). It is figured out that the axle load of both axles could be fixed to 167 and 192 kN (Wheel load around 80.0 and 96.0 kN). The axle spacing of the wagon is 8 meters, which means no influence from the neighboring axle as well as other axles should be taken into consideration. The ballast wagon was driven by a construction locomotive. Elastic deflections on both left and right rail were recorded which means both axles of the ballast wagon would be recorded for the measurement (left and right rail specified on behalf of the milepost direction from Zagreb to Sisak; locomotive was turned around between different measurement). Totally 150 measurements were performed on both bridge transitions and the bridge and 18 measurements on open track.

For reference reasons, extra points on open track were also measured. See Table 29 for the measured rail seats as well as the served axle load from the load wagon. It was manually defined, that the bridge end at Zagreb side is 0 m. This definition would be used through all the following figures in this section.

Table 29: Benkelman beam test – bridge and transition

Test of track elasticity (totally recorded 168 rail seats)		
Location	Measured rail	Interval between (m)
Open track – Zagreb	Right rail	-24 and -16.8
Transition Zagreb	Left / Right rail	-16.2 and -0.6
Bridge	Left / Right rail	0.0 and 12.0
Transition Sisak	Left / Right rail	12.6 and 28.8
Open track – Sisak	Left rail	29.4 and 37.2

It should be noticed that the numbering of the rail seats is exactly the number of sleeper spacing in reference to the rail seat connecting open track and transition in Zagreb side. The rail seats on both sides of open track were randomly selected. The result of the measurement was shown in Figure 32.

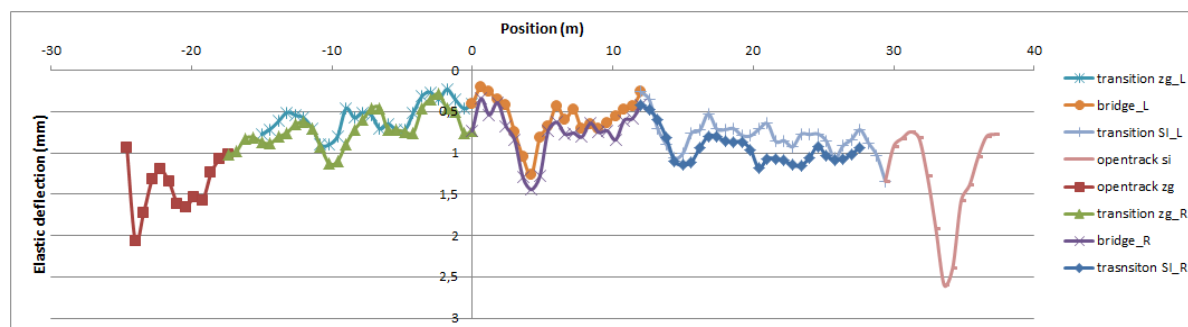


Figure 32 Measured maximum rail deflection

For analysis reasons, the maximum deflection measured on left rail would be multiplied by a factor of 1.2 (equal to 96/80) in order to roughly calculate the deflection under the axle load of 96 kN. This was done in order to exclude the influence factor of axle load to the overall elastic deflections. A rough analysis was performed on all the values. It should be noticed that the values for bridge and transition were only made for comparison with the values from open track area. Certain values from both open track sections were taken out since those locations were considered to be single failures which would not be representative for the general track quality. Table 30 shows the results of the analysis:

Table 30: statistical analysis of rail seat deflection<sup>\*)</sup>

	Open track _ Zagreb	Transition Zagreb	Bridge	Transition Sisak	Open track _ Sisak
Number of points	7	56	42	56	7
Minimum (mm)	0.94	0.27	0.24	0.42	0.89
Maximum (mm)	1.35	1.12	1.51	1.27	1.26
Average (mm)	1.16	0.70	0.72	0.96	1.02
Standard deviation (mm)	0.15	0.21	0.30	0.18	0.13
Coefficient of variation (%)	13.4	30.5	40.9	18.5	12.5

<sup>\*)</sup>: deflected rail shows positive value

The utilization of statistical analysis (especially the term “coefficient of variation”) is a typical way of understanding the track quality. Therefore, if the values from different sections have similar number in coefficient of variation, it could be concluded, that the overall quality of the track in those sections is also similar. This should be considered as a fact which could bring potential risks of interpreting the data, which means that the analysis method has its limitations. These imitations could be concluded as follows:

- Special structures like bridge and tunnel could have different characteristics on behalf of track quality;
- The variation of the mean value could be significant;
- Sections like transitions have different design proposals which makes the calculation of statistical values meaningless;
- Special locations of single defects should not be included.

Therefore, a more systematic methodology should be developed which could improve the reliability of the existing values especially for sensible structures like bridge or transitions.

A transition is generally used to smooth the difference between two different sections, which is bridge and open track in this study. An idealistic transition should be able to achieve the similar elastic deflections of both sections at both ends. Therefore, the new methodology could be concluded as follows:

- Calculate the mean value of the deflection on open track. Give it a symbol ' $D_{ot}$ ';
- Calculate the average value with data from both ends of the bridge and take the measurement value of bridge middle;
- Calculate the deflection line of the bridge according to in (b) calculated values (polynomial function, second power). Give it the symbol  $D_{bg}(i)$  ('i' is the location of the bridge);
- Connecting the value of  $D_{ot}$  and  $D_{bg}(0)$  with a line, which is considered to be the reference line of the transition;
- Draw the reference line according to position;
- Calculate the difference between every measured deflection and the reference value from the reference line;
- Make statistical analysis of the from (f) calculated values according to section (including mean value and standard deviation).

By doing this, the calculated standard deviation is the factor symbolizing the variation of the track deflection. A unique value of standard deviation for each section should then be judged as the real parameter about the track quality.

The Figure 33 shows the reference line (after step (e), marked in red) and the surrounded measurement data:

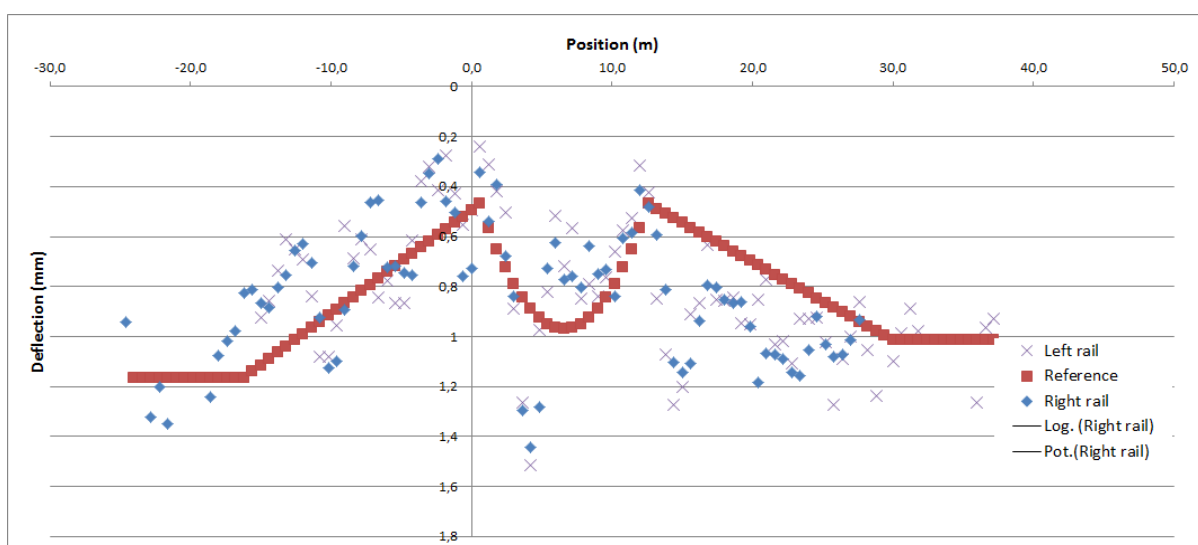


Figure 33 Difference of measurement data and reference line

The Figure 34 shows the results after step (f). Different sections were already marked with different colors for better distinguishing them from each other. Table 31 shows the results of statistical analysis (after step (g)) according to the new method:

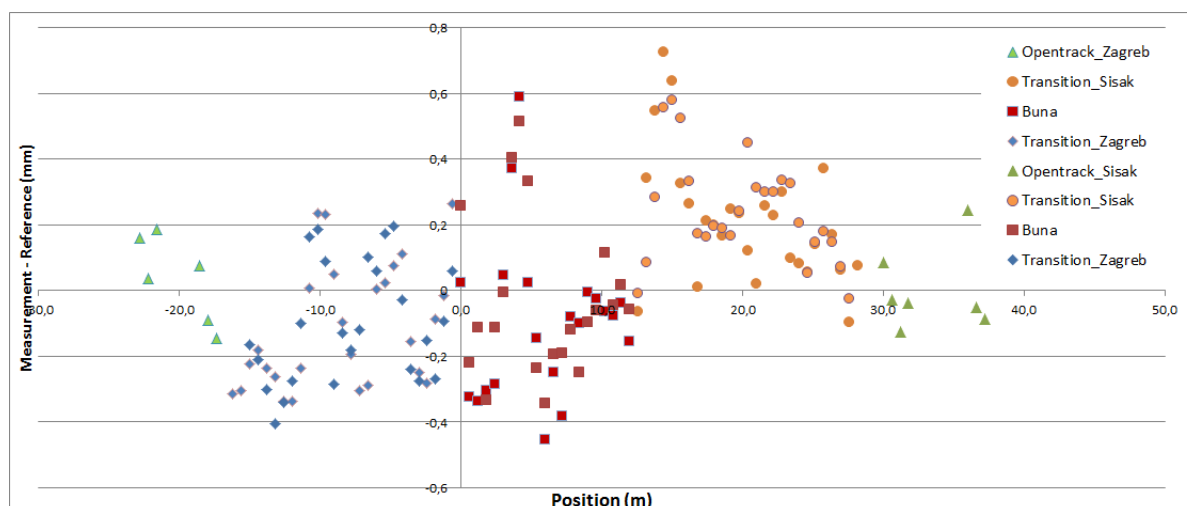


Figure 34 Difference of measurement data and reference line

Table 31: Statistical analysis according to new method

	Open track _ Zagreb	Transition Zagreb	Bridge	Transition Sisak	Open track _ Sisak
Number of points	7	56	42	56	7
Average (mm) <sup>*)</sup>	0.00	-0.11	-0.07	0.23	0.00
Standard deviation (mm)	0.16	0.18	0.24	0.18	0.13

<sup>\*)</sup>: Measurement - Reference

It is clear that the average value in open track should be zero. The value for transition at Zagreb side is 0.11 mm, smaller than the values from transition at Sisak side which is 0.23 mm. This difference points out the fact that the actual situation of the transition at Sisak side is farther than the ideal situation. The standard deviation at both transitions is the same, meaning that the quality of the transitions is comparable.

The standard deviation at section “bridge” has the largest value. This is due to the appearance of spot in the bridge area. The reason for this single spot would be discussed in following chapters.

It is good to see, that the standard deviation of the transitions and open tracks are similar, meaning that the track quality at both transitions are not significant different than the situation in open track. This fulfills the design requirement of the transitions on the first line.

## 5.4.Rail bending behavior under test runs

According to the design of the test described in section 3.5.1, the same load train for the test of track elasticity was used. According to the capacity of the locomotive, a maximum speed level of 80 km/h could be reached.

Sections 1 and 2 were measured separated on different days. A slight difference in travel speed could be seen. The following Table 32 shows the recorded speed and the travel direction. Term '1F4' refers to the 4<sup>th</sup> measurement at section 1.

Table 32: Information on test runs – section 1

Run number	Speed (km/h)	Direction	Run number	Speed (km/h)	Direction
1F1	13.4	ZG	2F1	10.1	SI
1F2	18.5	ZG	2F2	9.2	SI
1F3	13.6	ZG	2F3	10.4	SI
1F4	12.7	ZG	2F4	9.1	SI
1F5	13.2	ZG	2F5	6.0	SI
1F6	13.0	ZG	2F6	7.5	SI
1F7	35.1	SI	2F7	10.0	SI
1F8	39.9	SI	2F8	8.7	ZG
1F9	40.3	SI	2F9	26.7	ZG
1F10	37.1	ZG	2F10	37.1	ZG
1F11	61.2	SI	2F11	39.3	ZG
1F12	63.4	SI	2F12	38.9	ZG
1F13	68.5	SI	2F13	73.2	ZG
			2F14	74.2	ZG
			2F15	77.8	ZG

It is easy to see that the travel speed for both sections 1 and 2 includes value groups from 10 km/h to 80 km/h, where the test with 10 km/h being the quasi-static runs. It is clear to see from the Figure 35 below that the maximum strain is higher for the first two axles due to different axle loads.

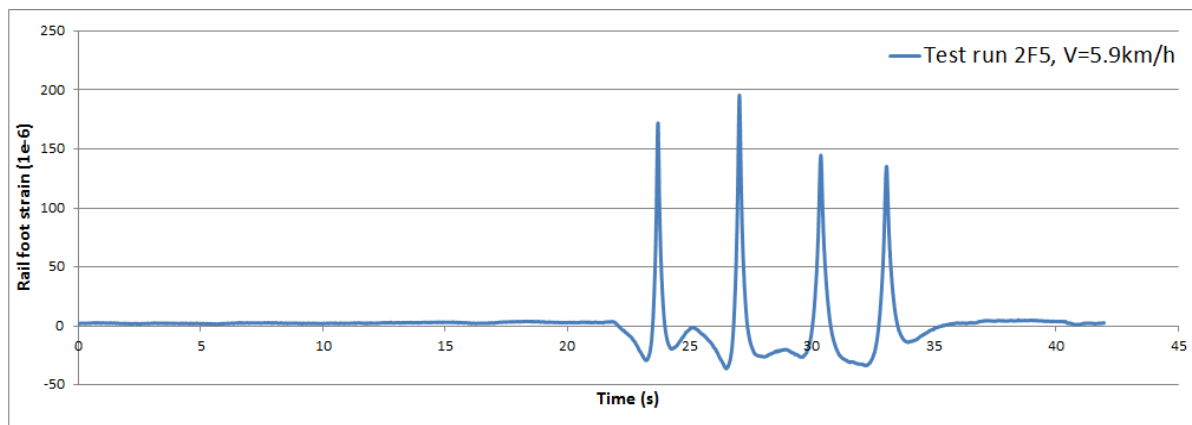


Figure 35 Sample strain gauge measurement result  
(4 axles, max. axle load around 19.0 t)

Table 33 and Table 34 list a typical analysis of the stresses at rail foot during passage of the 4 axles according to the series number when they were measured. Tab “1W2 (92 kN)” represents the 1st measurement section (transition Zagreb) from the second axle of the wagon with a static wheel load of 92 kN. Figure 36 and Figure 37 summarize the average stress of the both wagon axles and shows the overlapped results of quasi-static run (in continuous line) and dynamic run (in points).



Table 33: Sample evaluation of the rail foot stress (sensors on left rail, Section 1)

Run 4: Direction Zagreb	Speed: 13.2 km/h			
	Rail foot stress [N/mm <sup>2</sup> ]			
Position [m]	1L1(62kN)	1L2(65kN)	1W1(80kN)	1W2(92kN)
-15.3	27.44	27.22	33.74	42.46
-14.1	33.34	33.27	40.03	48.31
-12.9	27.81	28.46	34.66	41.01
-11.7	25.19	26.39	32.45	38.55
-11.1	30.32	32.01	38.92	45.04
-10.5	37.79	39.71	47.57	54.33
-9.9	32.21	33.98	40.01	46.75
-9.3	27.63	28.47	36.79	42.71
-8.7	24.22	25.39	32.99	37.70
-8.1	24.77	25.68	32.18	40.38
-7.5	26.95	28.42	35.16	42.61
-6.9	27.54	28.25	36.14	43.72
-6.3	26.43	27.51	33.89	40.78
-5.7	27.51	28.05	34.48	41.93
-5.1	32.70	34.01	41.18	47.01
-4.5	32.25	32.91	40.24	47.15
-3.9	23.66	24.59	31.30	36.83
-3.3	23.53	23.40	30.90	36.61
-2.7	25.32	25.68	33.26	39.21
-2.1	24.70	24.87	31.29	37.67
-1.5	26.78	26.26	33.45	39.00
-0.9	31.79	31.65	38.20	43.36
0.3	27.70	26.61	32.53	37.56

Table 34: Sample evaluation of the rail foot stress (sensors on right rail, Section 2)

Run 3: Direction Sisak	Speed: 9.4 km/h			
	Rail foot stress [N/mm <sup>2</sup> ]			
Position [m]	2L2(65kN)	2L1(62kN)	2W2(92kN)	2W1(80kN)
11.7	23.87	24.55	35.65	31.11
12.3	24.98	26.38	38.52	33.86
12.9	24.05	25.70	38.06	32.52
13.5	27.09	28.55	40.45	35.98
14.1	37.48	38.48	53.38	47.09
14.7	40.07	40.35	54.11	49.14
15.3	30.47	31.20	43.09	37.54
15.9	29.31	30.38	43.46	37.47
16.5	29.08	30.91	44.14	38.04
17.1	27.45	29.18	41.66	35.90
17.7	28.01	29.44	42.82	36.17
18.3	29.06	30.95	43.92	38.36
18.9	30.65	32.68	46.08	40.09
19.5	29.66	31.05	44.10	37.90
20.1	30.82	31.86	44.41	39.81
20.7	28.71	30.14	42.05	37.11
21.3	29.39	29.79	44.21	38.08
21.9	30.40	30.88	45.14	39.45
23.1	30.85	32.43	45.86	40.31
23.7	29.07	30.18	43.46	37.36
24.9	30.68	31.72	46.42	39.44
26.1	28.20	30.32	41.16	36.22
27.3	26.81	29.25	42.15	35.54

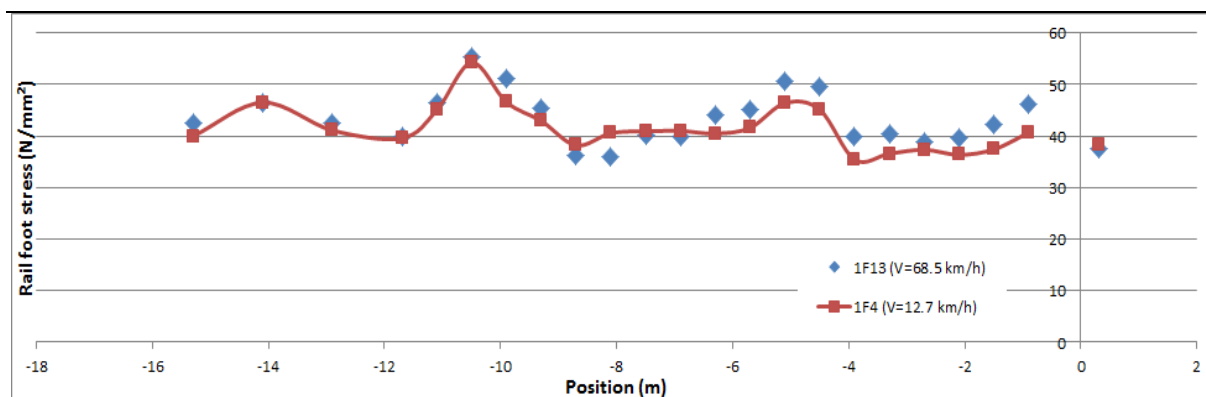


Figure 36: Test section 1 – runs 1F4 and 1F13

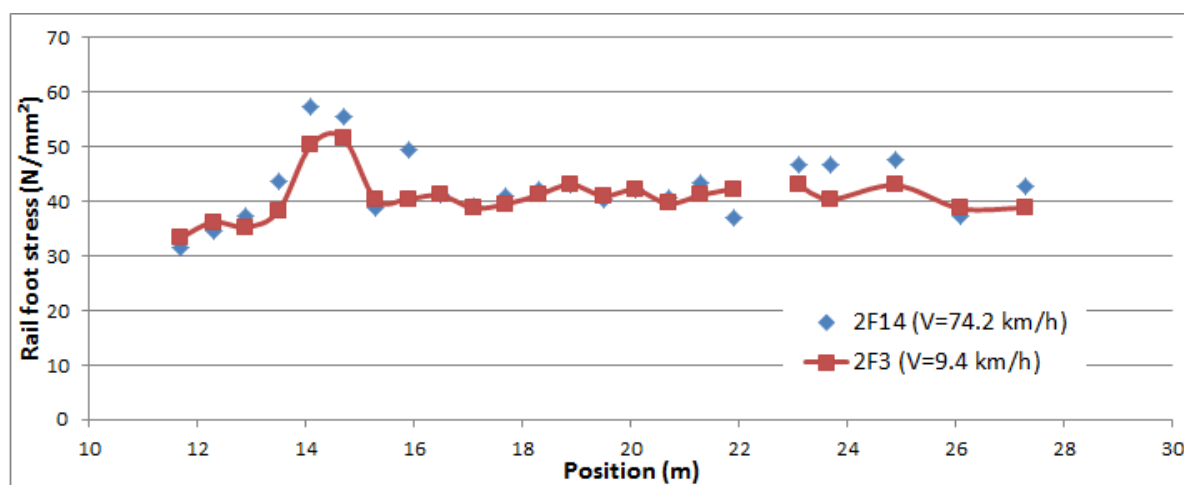


Figure 37: Test section 2 – runs 2F3 and 2F14

It could be easily figured out, that the distribution of the rail foot stress is not very close to each other even under a limited passage speed of 10 km/h. This should be explained by looking back to the distribution of elasticity at this location. Notice that the 1F13 and 2F14 were measured under a higher running speed with higher variation of single values; this should be understood by the increasing influence due to track dynamics.

Due to the variation of track elasticity at different rail seats, higher stress does not principally identical to higher load. The actual wheel load along the passage of the measurement section would be calculated from the Finite-Element models.

Table 35 and Table 36 show the analysis of the rail foot stress only for the load wagon according to the speed level (only including strain gauges inside the transition area).

The distribution of the rail foot stress according to travel speed is therefore clear to be seen.

Table 35: Statistical analysis of load wagon according to speed level  
(transition Zagreb)

Average speed (km/h)	14	38	65
Number of measurements	6	4	3
Average rail foot stress (N/m <sup>2</sup> )	41.3	41.0	44.6
Max. rail foot stress (N/m <sup>2</sup> )	53.5	54.8	60.3
Standard deviation (N/m <sup>2</sup> )	5.02	5.23	6.48
Dynamic factor (%)	29.6	33.8	35.3

Table 36: Statistical analysis of load wagon according to speed level  
(transition Sisak)

Average speed (km/h)	9	36	75
Number of measurements	8	4	3
Average rail foot stress (N/m <sup>2</sup> )	42.6	43.6	44.3
Max. rail foot stress (N/m <sup>2</sup> )	56.4	58.0	61.6
Standard deviation (N/m <sup>2</sup> )	4.93	4.75	7.19
Dynamic factor (%)	32.8	33.0	38.9

A term called “dynamic factor” was calculated by dividing the maximum stress into the average one. A clear increase of this value according to the increase of speed could be seen which explains the fact that the dynamic wheel rail interaction is stronger when the speed of the train is faster. The average rail foot stresses for all speed categories are similar but the maximum values for higher speed are higher which symbolizes a higher impact load under higher speed level.

An evaluation of the design of the transition on behalf of the measured test run data could be done. It should be mentioned, that this evaluation is focused on the aspect of dynamic wheel-rail interaction. A better transition design should be able to control the dynamic wheel-rail interaction in a reasonable way, especially by trains running under high speed levels.

The evaluation is done by overlapping important parameters from both test sections together which could be seen in Table 37. Furthermore, the distribution of standard deviation according to speed level was shown in Figure 38. Evaluation was done based on the data from the both axles of the load wagon.

Table 37: Comparison of both transitions

	Transition Zagreb	Transition Sisak	Transition Zagreb	Transition Sisak
Average speed	V=14 km/h	V=9 km/h	V=64 km/h	V=75 km/h
Average rail foot stress (N/mm <sup>2</sup> )	41.3	42.6	44.6	44.3
Maximum rail foot stress (N/mm <sup>2</sup> )	53.5	56.4	60.3	61.6
Standard deviation (N/mm <sup>2</sup> )	5.02	4.93	6.48	7.19
Dynamic factor (%)	29.6	32.8	35.3	38.9

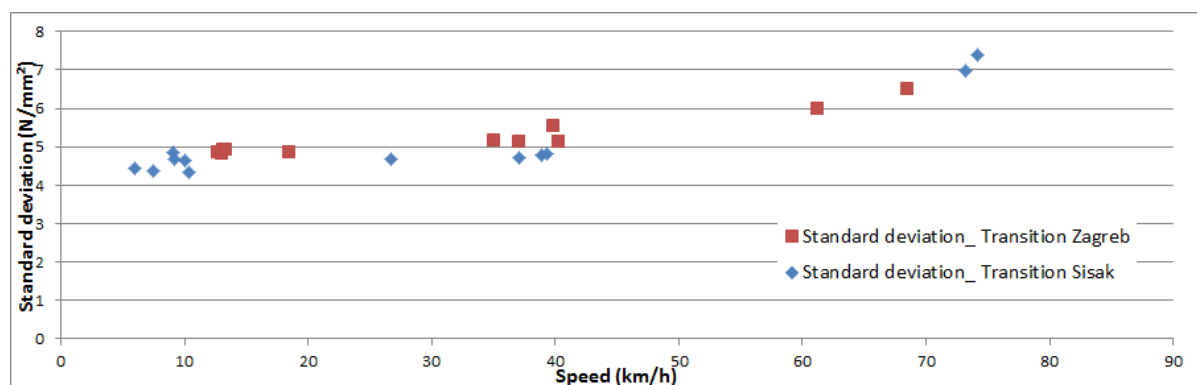


Figure 38: standard deviation according to speed (both transitions)

The value of standard deviation increases with the speed level. Nonlinearity could be seen, but this should not be considered as a general tendency due to the reason that the values at higher speed level were till now not included. The quality of the both transitions on behalf of dynamic wheel-rail interaction is similar. The rail foot stress for the transition Sisak is slightly higher than the values for the transition Zagreb.

It should be noticed that for normal operation, a maximum speed of 160 km/h was allowed which was much faster than the measured speed level of 80 km/h. Therefore, the behavior of wheel-rail interactions under higher speed levels should also be checked.

## 5.5. Rail bending behavior under operational trains

Measurement points were selected which were equally distributed in both transitions. Therefore, it could be ensured, that the measured values for both transitions were under the passage of the same train.

In total 19 train runs are recorded and the evaluation is done using the passage of the bogies of the locomotive or multiple units. Travel speed is as well evaluated. Table 38 lists the type of trains according to the measurement time point. Please refer to section 3.7 for the respective information of the trains.

Table 38: Recorded train runs and time of passage

Direction Zagreb - Sisak			Direction Sisak - Zagreb		
Time	Train / Locomotive	Speed (km/h)	Time	Train / Locomotive	Speed (km/h)
11:25	6111	124.2	11:05	6112	120.6
12:22	6112	121.9	12:12	2062+Freight	79.3
14:24	6111	115.7	12:49	6111	116.8
15:21	6111	98.2	14:40	6112	122.7
15:55	2062	83.7	15:51	6111	119.5
16:16	6111	121.2	16:11	2062	79.6
17:14	6111	128.5	16:44	6111	95.2
18:09	2062+Freight	83.7	17:40	6111	118.8
18:21	6111	109.0	18:46	6111	117.8
19:30	6111	116.5			

### 5.5.1. Train set 6111

It is clearly to see, that the train set type 6111 was the most frequent user of the track. This train set normally has a passage speed of 120 km/h. Therefore the first attention should be drawn to it. Since the middle wagon of train set 6111 has higher axle load than the other wagons, Figure 39 shows a sample measurement of the passage of the middle wagon (4 axles) along the test section (x = 0 m refers to bridge entrance at Zagreb side).

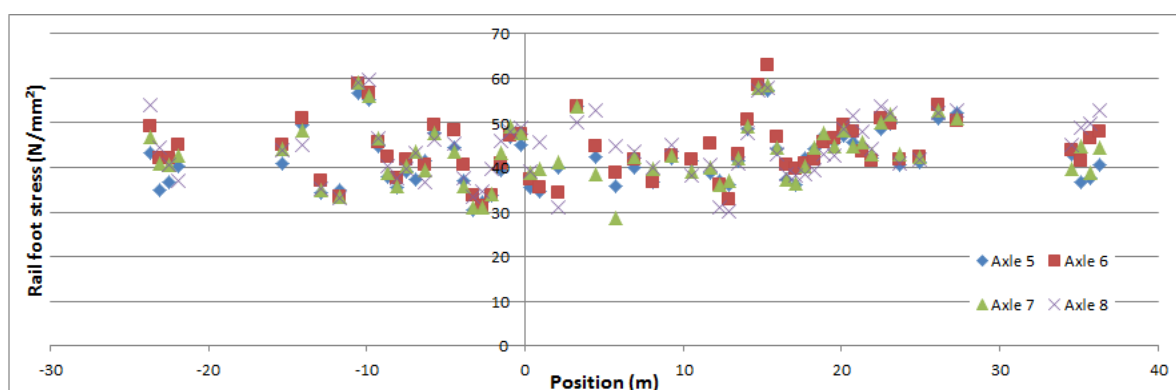


Figure 39 Sample measurement of train set 6111 (Right rail, V = 121 km/h)

Since the middle wagon of the train set 6111 has the heaviest axle load (static load of 17.0 t), a summary of all the recorded train runs from this wagon was made. Figure 40 shows the distribution of the average, maximum and minimum rail foot strains (All included runs have the passage speed of  $120 \pm 10$  km/h). For better understanding, the average value would be illustrated with a line and the maximum and minimum values only in points.

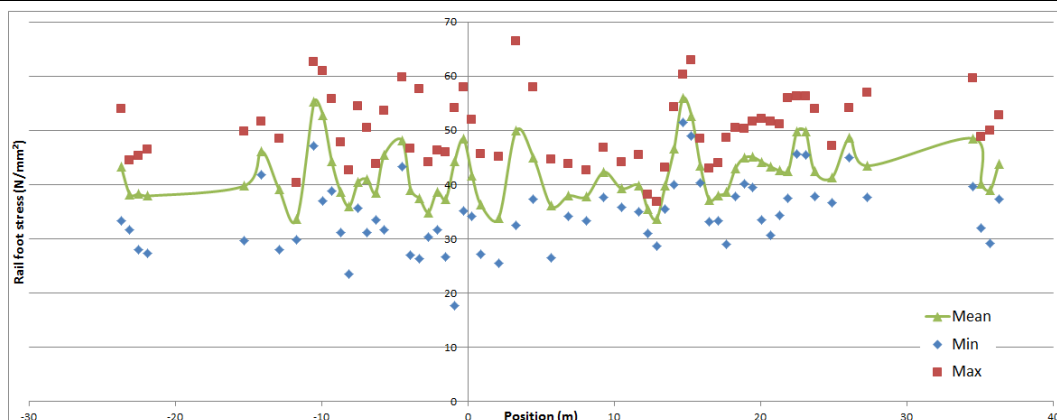


Figure 40 Summary of all the passage of train set 6111 (middle wagon)

It could be seen that the dynamic rail foot stress showed a cyclic distribution with similar shape as a sinus curve. This symbolizes a very significant dynamic vehicle-track interaction inside the measurement area. When looking back to the distribution of elasticity at this area, higher rail foot stress would appear at those locations where higher elastic deflections occur. Therefore, those peaks in dynamic rail foot stress should be explained by discontinuity in track elasticity.

There exist also other peaks from the figure where no significant elasticity changes were spotted. The appearance of those peaks should then be because of the repeated loading effect of the wagon and would have counterproductive influence to the track quality at those locations. Therefore, those locations should be considered as high risk of causing new single failures.

The maximum measured rail foot stress of 66.5 N/mm<sup>2</sup> at  $x = 3.3$  m symbolizes the highest dynamic impact at this location, taking into the consideration that this point inside the bridge also holds a very significant change of elasticity. The reason of this higher rail foot stress would be due to the appearance of track under sleeper gap at this location. The effect of the dynamic vehicle-track interaction would be taken a closer look in the simulation models.

For better visualization of the effect of dynamic wheel rail interaction, an analysis of coefficient of variation according to location was made. The following Figure 41 shows the distribution of the points. It is obvious to find out, that in the area of the under sleeper gap discussed in the last paragraph ( $x = 3.3$  m), the coefficient of variation on



the measured dynamic rail foot strain is significantly higher than the other locations. It is also to point out, that the effect due to the appearance of track under sleeper gap could have an influencing area more than 10 m (in this case from -5 m to 5 m) under a speed level of 120 km/h. For trains running with higher speed, a longer influencing area could be expected.

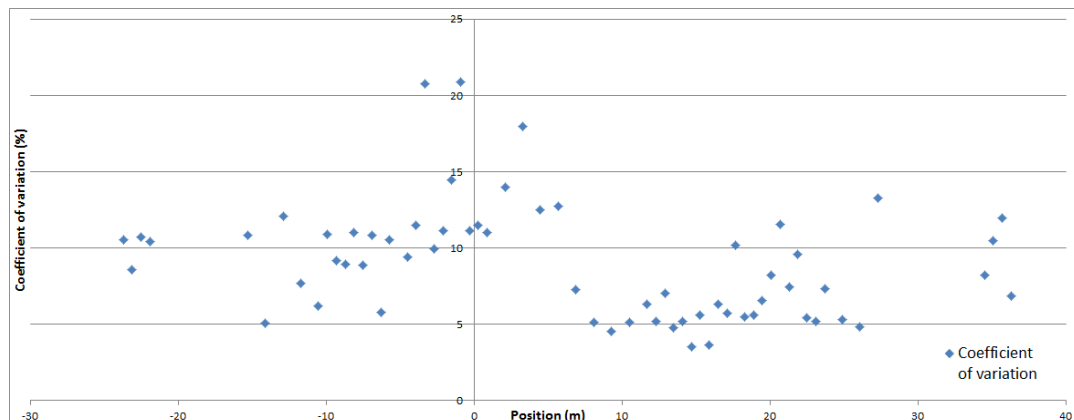


Figure 41: Coefficient of variation of train set 6111

The values in the transition on Zagreb side of around 10% are generally twice higher than those in the transition on Sisak side (around 5%). But when referring to the values for open track which holds the value of around 10%, the transitions do not cause higher dynamic vehicle track interaction at this moment.

It is therefore clear to see the effect of track under sleeper gap to the overall dynamic impacts between vehicle and track. The four axles caused similar rail foot bending stresses by locations of  $x < -5.0$  m and  $x > 5$  m and caused quite different stresses between  $x = -5.0$  m and  $x = 5.0$  m. Looking back to the formula

$$F_{\text{dyn}} = F_0 + F_{\text{exc}}$$

where  $F_{\text{dyn}}$  – dynamic load

$F_0$  – static load

$F_{\text{exc}}$  – excitation load

This statement supports the assumption, that the coefficient of variation for  $F_{exc}$  would be much higher in the area of discontinuities, which symbolizes a more extreme load distribution at this location, meaning a faster deterioration and higher safety risks.

### 5.5.2. Other types

Besides the frequent passage of the train set 6111, the train set 6112 and locomotive 2062 were also recorded. Since the method was already illustrated in 5.5.1, the following Figure 42 to Figure 45 show the distribution of the rail foot stress and coefficient of variation. For illustration, the middle axles of the train set 6112 (axle 3 to 8 with similar axle loads) were used.

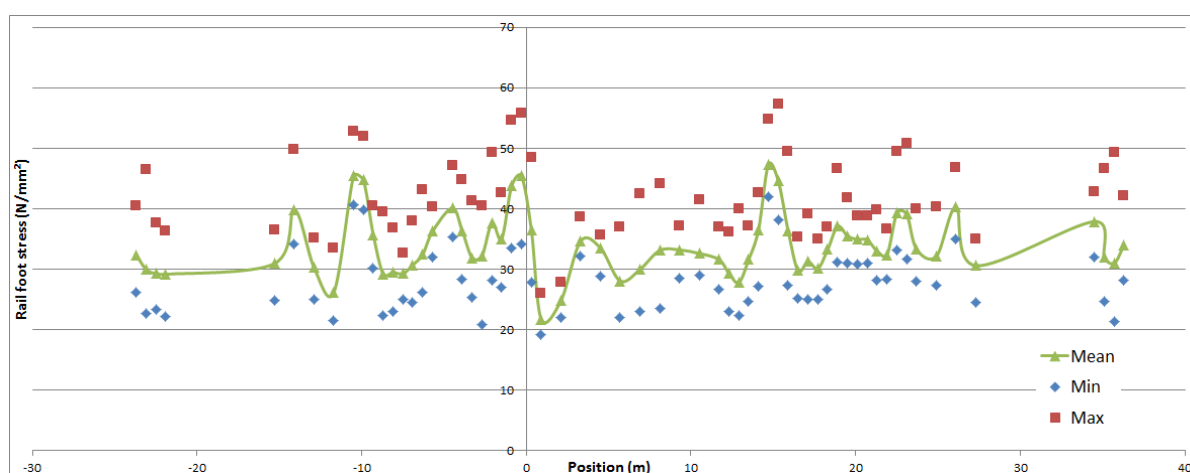


Figure 42: Summary of all the passage of train set 6112 (middle axles)

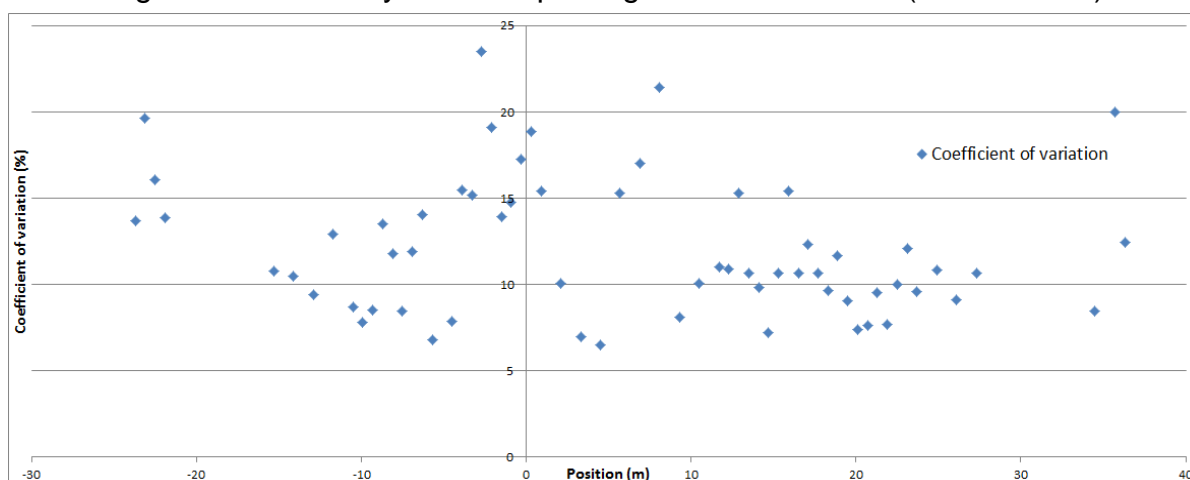


Figure 43: Coefficient of variation of train set 6112 (middle axles)

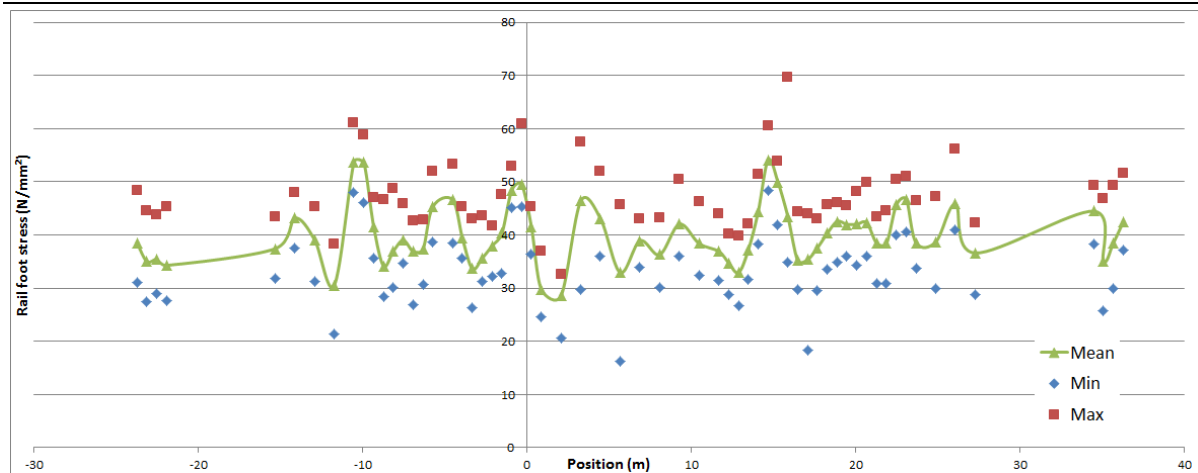


Figure 44: Summary of all the passage of locomotive 2062

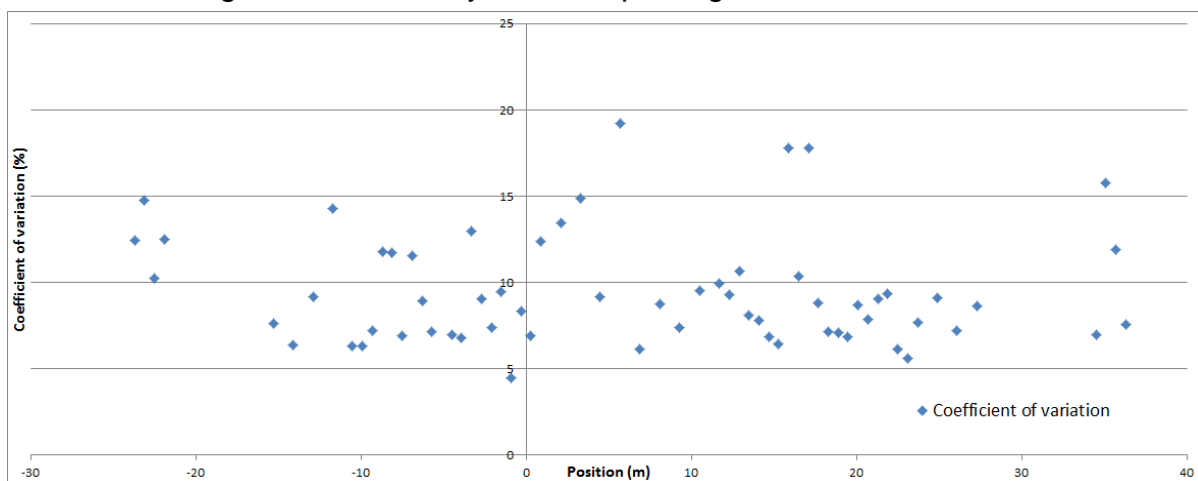


Figure 45: Coefficient of variation of locomotive 2062

A maximum rail foot stress of around 70 N/mm<sup>2</sup> was recorded under the passage of the locomotive 2062, due to its higher axle load. According to the distribution of coefficient of variation, it could be seen that the values in transitions were generally smaller or similar as the values in open track. It should not be neglected that due to reduced track elasticity in the transitions, the dynamic load in the section could be higher than in open track.

The analysis also shows that the middle wagon of the train set 6111 could be considered as the highest potential source of dynamic loading. This is due to the better vehicle design of the passenger train set 6112 and the slower allowable speed of the freight locomotive. Therefore, the middle wagon of the train set 6111 would be selected for the simulation phase.

---

## 6. COMPARISON OF BOTH MEASUREMENT RESULTS

### 6.1. Introduction

A comparison between both measurement results is necessary for understanding of the long-term track behavior according to traffic loads. It should not be neglected, that the appearance of fish plated joints would also be considered as an important parameter between the both measurements.

For all the evaluations below, the x-axis in the figures would always show the distance [m] between beginning of the test section and actual point of interest within the section. Direction of X-axis is equivalent to the direction in Sisak. It was manually defined, that the bridge end at Zagreb side is 0 m and the rail on the left side in direction Sisak is called 'Left rail'. This definition would be used through all the following figures and tables in this chapter.

### 6.2. Track geometry and irregularity (plastic settlement)

For the aspect of dynamic vehicle-track interaction, the vertical track geometry would be the most important parameter. Therefore a comparison between the both measurements was only done for the vertical track geometry. The following Figure 46 and Figure 47 show the graphical illustration of the comparison.

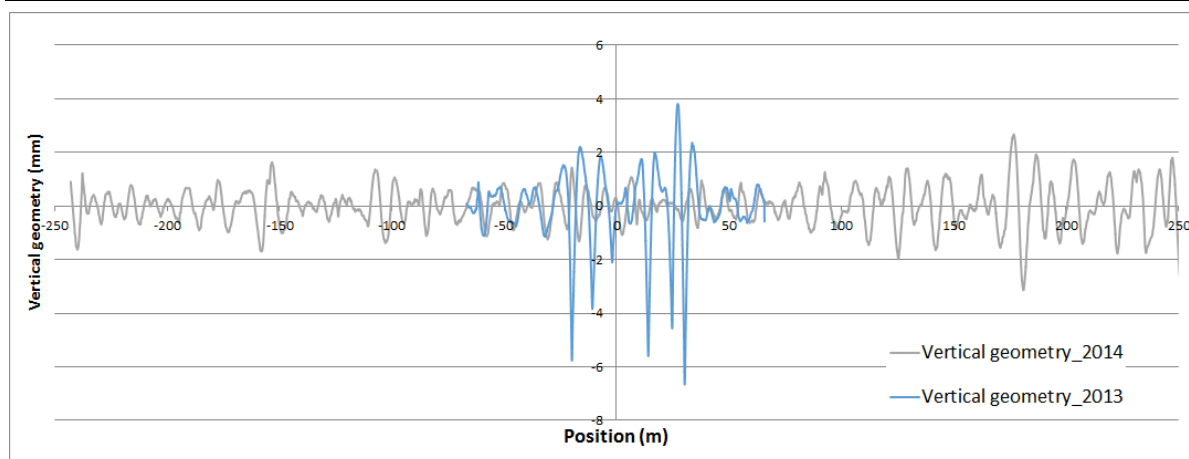


Figure 46 Comparison of track geometry (all area)

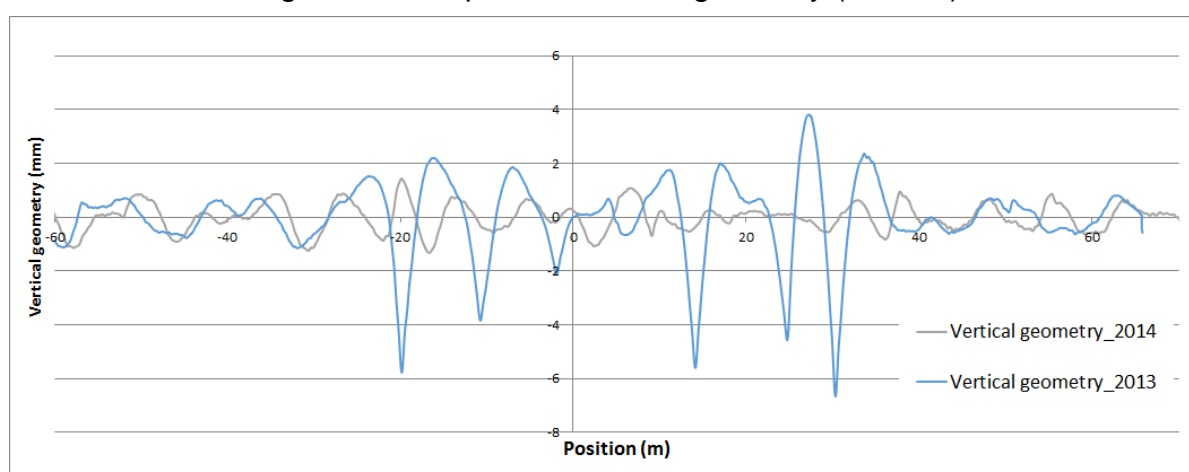


Figure 47 Comparison of track geometry (bridge and transition)

It could be seen that the track geometry was significantly changed due to removing of the fish plated joint in 2014. Due to the installation of continuous welded rail (CWR), the track geometry inside the transition area was even better than in open track. It is clear to see that the section outside the influence area of the fish plated joint did not show any change in both measurements. It should be understood due to the limited time period and traffic volume that the track geometry would not change a lot.

The section of the bridge should be taken a closer look. It could be seen that the track geometry in the bridge (between  $x = 0$  and 12 m) shows different distributions. This difference could be associated to the following activities in track:

- The track in the bridge was newly tamped;

- The obvious change of elasticity leads to higher dynamic impact between vehicle and track in the bridge.

The bridge section was measured in both measurements and the Table 39 shows the comparison of the both.

Table 39: statistical analysis of vertical track geometry – bridge

	Bridge	
Measured in	October, 2013	April, 2014
Length of measurement (m)	8	12
highest (mm)	0.73	1.03
lowest (mm)	-0.58	-0.69
Standard deviation (mm)	0.37	0.32

It should be noticed that the standard deviation measured in October, 2013 could be inaccurate since the fish plated joints were installed just 1.5 m away from both ends of the bridge. A slight increase in the high and low altitude of the bridge could be seen.

### 6.3.Rail deflection under static loading

Due to removing of the fish plated joint, the track elastic deflection under static loading showed significant difference distribution in the area of bridge and transition. For analysis reasons, the maximum deflection measured on left rail in 2014 would be multiplied by a factor of 1.2 (equal to 96/80) in order to roughly calculate the deflection under the axle load of 96 kN. Figure 48 showed the overlapped results from 2013 and 2014 for both left and right rails.

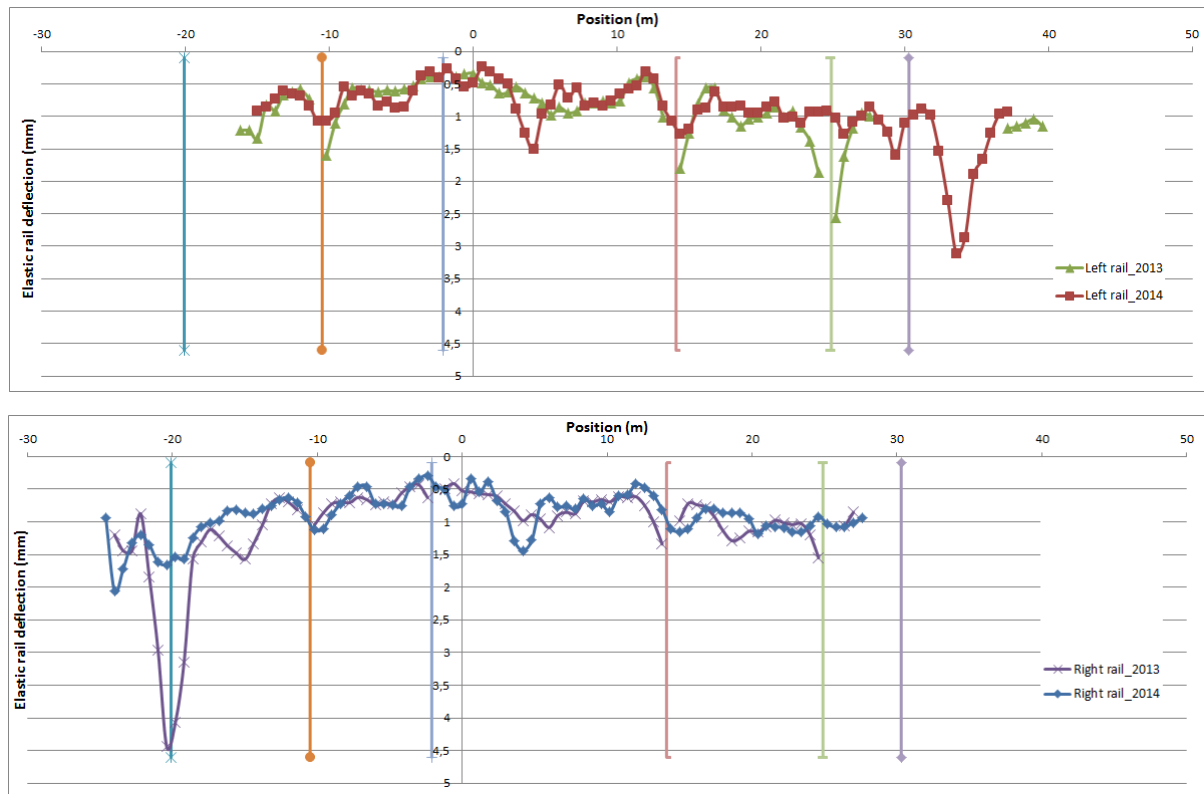


Figure 48 Measured maximum rail deflection

The included 6 lines in the figure symbolize the location where fish plated joints were installed during the measurement in 2013. It could be therefore seen that most of the single failures due to the joints were already eliminated. Furthermore, when comparing the both curves, it could be found out that there still exist some spots in the area of bridge and transition, two of which in the area of formal joints ( $x = -10.5$  m and  $14.1$  m). Referring to the information provided in chapter 3.2, those spots were exactly located at the points where constructions were interrupted. Therefore, it was reasonable to conclude, that the presence of the spot in 2014 should be due to the discontinuous substructure behavior.

By comparing, a new failure in the bridge area ( $x = 4.2$  m) could be spotted where no significant failure could be seen in 2013. The appearance of this failure could then only be explained by the increased dynamic vehicle-track interaction under higher speed. The other failure in the left rail at  $x = 33.6$  m could be similarly explained. The appearance of those failures would be later on explained by the numerical simulation models.

## 6.4. Rail bending behavior under test runs

Test runs with load wagon were done in both 2013 and 2014. The load wagon was lighter in 2014 than in 2013, meaning that the values in 2014 could be smaller than usual.

The term “standard deviation” of all the strain gauges inside the transitions provides useful information on the extend of variation of dynamic load according to speed level. Therefore a direct comparison between all the measurements could be done. A graphical illustration of it is shown in Figure 49.

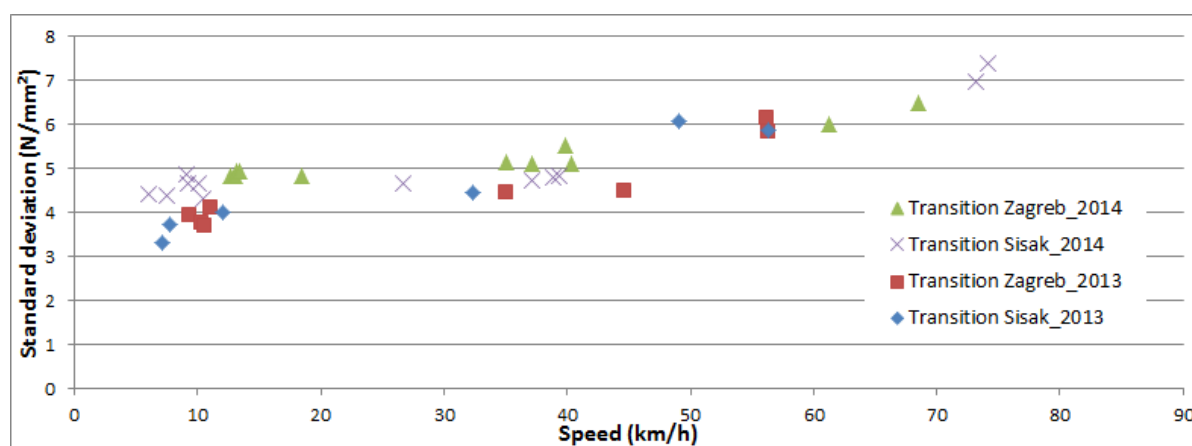


Figure 49: Transition Zagreb – standard deviation according to speed

It should be noticed, that the amount of values for measurements in 2013 is less than for 2014, due to the reason of elimination of those strain gauges which were inside the influence area of the fish plated joint. Therefore, the influence of the joints was not included for the data in 2013.

It could be found that the distribution of standard variation of the load wagon did not show any changes between the measurements in 2013 and 2014. The following Table 40 and Table 41 collect the important data for both measurements. Due to change of boundary conditions, a direct comparison with values in 2013 and 2014 was not made.



Table 40: Comparison of the test runs (transition Zagreb)

	2013			2014		
Average speed (km/h)	10	40	56	14	38	65
Average rail foot stress (N/m <sup>2</sup> )	45.0	42.2	45.2	41.3	41.0	44.6
Max. rail foot stress (N/m <sup>2</sup> )	50.3	50.0	56.6	53.5	54.8	60.3
Standard deviation (N/m <sup>2</sup> )	3.88	4.47	5.98	5.02	5.23	6.48
Dynamic factor (%)	11.6	18.6	25.2	29.6	33.8	35.3

Table 41: Comparison of the test runs (transition Sisak)

	2013			2014		
Average speed (km/h)	9	41	56	9	36	75
Average rail foot stress (N/m <sup>2</sup> )	47.7	48.7	47.5	42.6	43.6	44.3
Max. rail foot stress (N/m <sup>2</sup> )	55.2	55.9	59.7	56.4	58.0	61.6
Standard deviation (N/m <sup>2</sup> )	3.69	4.46	5.99	4.93	4.75	7.19
Dynamic factor (%)	15.72	14.77	25.59	32.8	33.0	38.9

## 7. THE NUMERICAL MODELING

### 7.1.Introduction

As revealed from Chapter 2, a more detailed understanding of the track behavior in concerning of vehicle-track interaction could be achieved through numerical models. Various modeling approaches should be applied in order better to accomplish the requirement. The two approaches which will be applied in this research work would be the FEM (Finite-Element-Method) and MBS (Multi-Body-Simulation).

A numerical model concentrates itself on part of the object from reality and simplifies the others. In this chapter, various kinds of models based on the field measurement would be introduced. These models were developed with different objectives. Imaginary data as well as experience data were also used for some parameters inside the models. These models utilize FEM and MBS approaches to solve the problems.

The general structural tree of utilizing measurement data for different modeling strategies was shown in Figure 50. The arrows on top symbolized the general process of modeling which in principle contained three layers. The cell 21, which FEM modeling on behalf of track elasticity was firstly made in order to calculate the dynamic wheel load in cell 22 together with the measurement data from test runs and train runs. Afterwards, the FEM model was condensed by modal representation of the model itself which could be imported into the MBS system. By doing this, the dynamic response of elastic track due to stochastic train loads was able to be calculated. The final step – cell 32 – was the result of MBS calculation, which included the wheel-rail contact, the track irregularity and track elasticity (coming from the condensed FEM model).

In the following sections, different models were built according to this process. The cell number would be written for each model in order to categorize the input and output values. The cell pictures provided general impressions of the process.

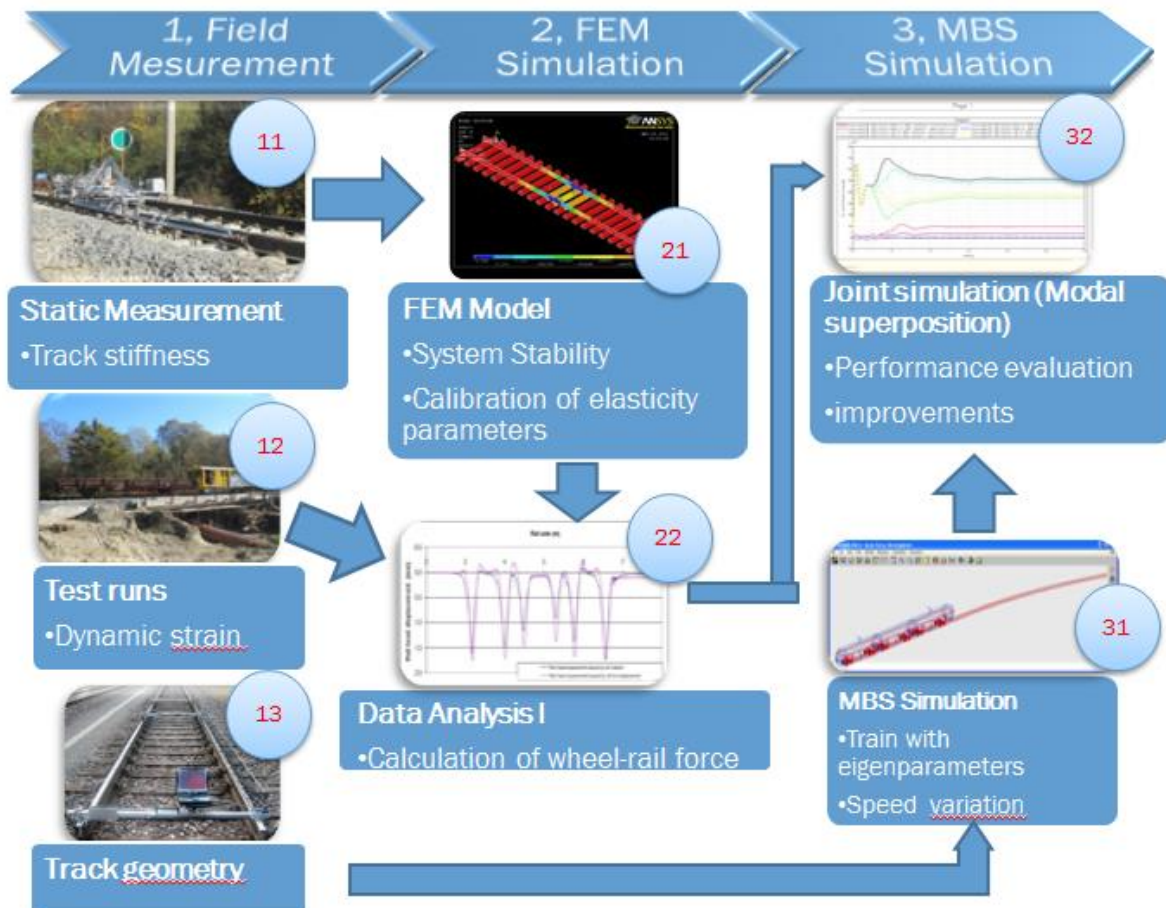


Figure 50 General modeling process

## 7.2. FEM analysis of the field side Benkelman measurement on behalf of substructure elasticity (Cell 21)

### 7.2.1. Design of the model

Simplified rail profile was used with the same physical parameters as from the original profile needed for calculation. <sup>[21]</sup> Figure 51 and Table 42 showed the geometry and the parameters of the simplified model.

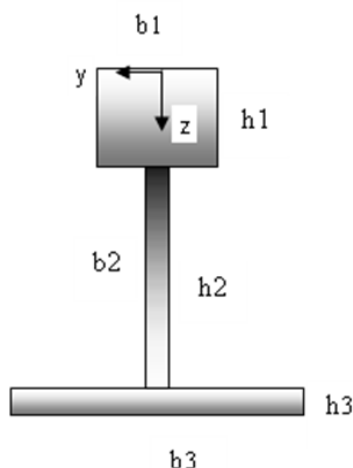


Figure 51 Simplified rail model UIC60<sup>[21]</sup>

Table 42: Parameters of the simplified rail model<sup>[21]</sup>

	$h_i$ (mm)	$b_i$ (mm)	$A_i$ (mm <sup>2</sup> )	$Z_i$ (mm)	$Z_s$ (mm)
1	48.3	73.5	3550.05	24.15	83.5
2	114	19	2166	105.3	
3	12.8	150	1920	168.7	

With  $A_i$  – Area of the body  $i$   
 $Z_i$  – Center of gravity of body  $i$   
 $Z_s$  – Center of gravity of the whole system

According to section 4.3, the bridge and both transitions include in total 75 rail seats on each rail and totally 150 rail seats were covered by the measurement. Therefore it is good to define the model firstly with 150 rail seats (75 on each rail) which cover all the rail seats in bridge and transitions. Another 40 rail seats (20 on each end) would be also defined which represent for the rail seats in open track.

The mechanism of the FEM model was shown in Figure 52. Three elastic layers naming 'Pad', 'Ballast' and 'Substructure' were given with predefined unique values for each rail seat.

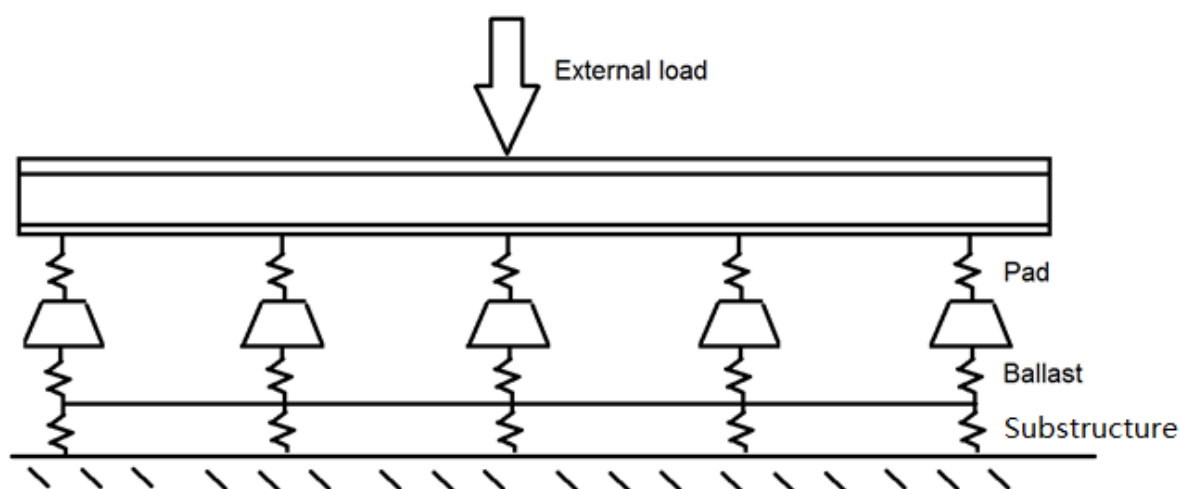


Figure 52 Principle of the FEM model

It should be noticed, that the elastic layer “Pad” and “Ballast” would be given a constant factor for all the rail seats. These constant values were defined according to the design specifications (see section 3.4.3).

The modeling of pad, ballast and substructure relies on the volume element input from the FE code. It requires the Young’s Modulus and Poisson number as material input and length, width and thickness as geometrical input. Ballast is modeled as a volume element for simplification because the elasticity of the ballast not the single ballast stone is the most important factor for this model. A value of 30 cm thickness for ballast was given. The Young’s modulus of the ballast layer would be defined according to standard design specifications.

Although the substructure performance is very much different under each rail seat, the layer “substructure” was still modeled as volume element with unique thickness of 30 cm. Reasons for this design is again for simplification without losing the elasticity characteristics of the layer. The Young’s modulus of the substructure layer on bridge and transitions would be set as variables and the modulus would be calculated based on the measurement data.

The Young's modulus of the substructure for open track would be calculated by building up the average value of the measurement results on open track from the respective side. A unique value for substructure elasticity at each end of the substructure would be given. This should be seen as the starting point of the calculations.

### 7.2.2. Model setup and boundary condition

The FEM program ANSYS was used for building up the model. The Figure 53 below shows the modeled rail, pad, sleeper, ballast and substructure etc. Different colors for substructure layer symbolized the border of different materials. Irregular meshing was used for achieving higher efficiency as well as higher accuracy in model calculation.

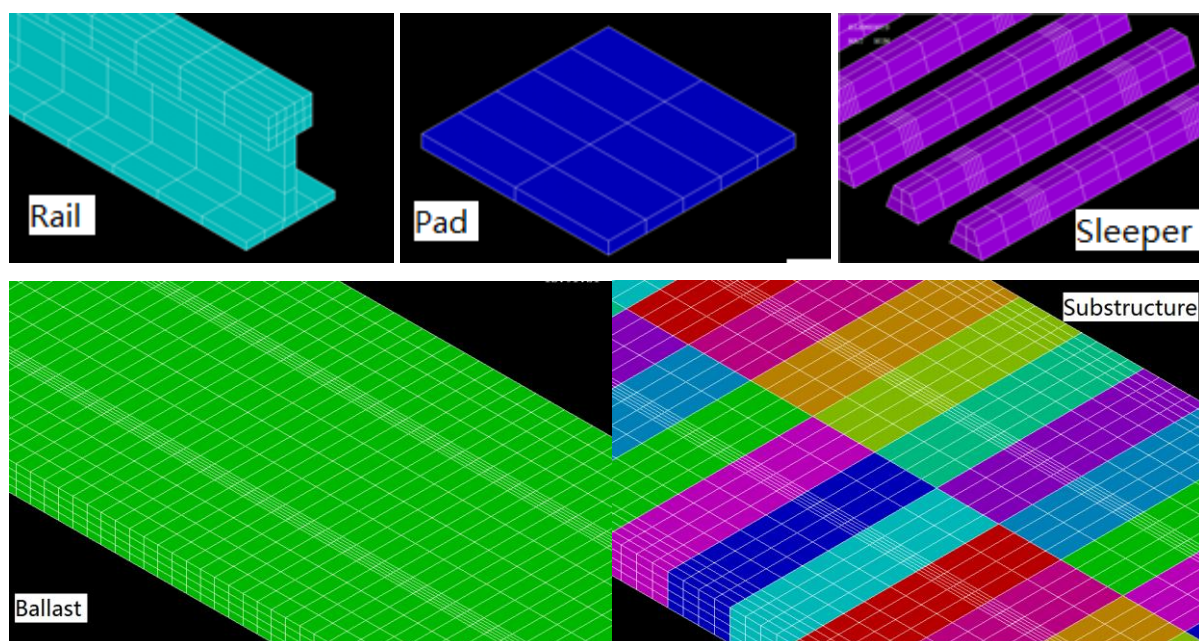


Figure 53 Graphical representation of different elements in FEM model

Although there were a lot of elements and materials with different characteristics in this model, the whole system was built only by linear materials without damping input for the following reason:

- Linear elastic approach already provides very good accuracy level for standard ballasted track;
- Significant saving of calculation time in comparison with nonlinear models;
- For further needs of other calculation programs (like modal analysis);
- Damping could be neglected under quasi-static runs.

The application of boundary conditions was mainly according to the actual situation. The nodes from bottom side of the substructure layer on open track and transition would be given 0 degrees of freedom (0 DoF). But those nodes on bridge would be kept free. The substructure on bridge was therefore representative for the concrete bridge structure itself.

Table 43: Characteristic E and  $\mu$  value for each section

	Young's modulus (MPa)	Poisson number ( $\mu$ )
Rail	2.1e5	0.3
Pad	50	0.45
Ballast	150	0.45
Substructure	Variable	0.4

The above Table 43 showed the material parameters. The equivalent stiffness of the pad and ballast was around 200 and 125 kN/mm. (values from design specifications)

The calibration of the model utilized an iterative approach, which would be described in the following sections 5.2.3 to 5.2.5. Design of the approach was according to the general process: Initial condition, iteration procedure and boundary condition. The completed ANSYS model was shown in Figure 54:



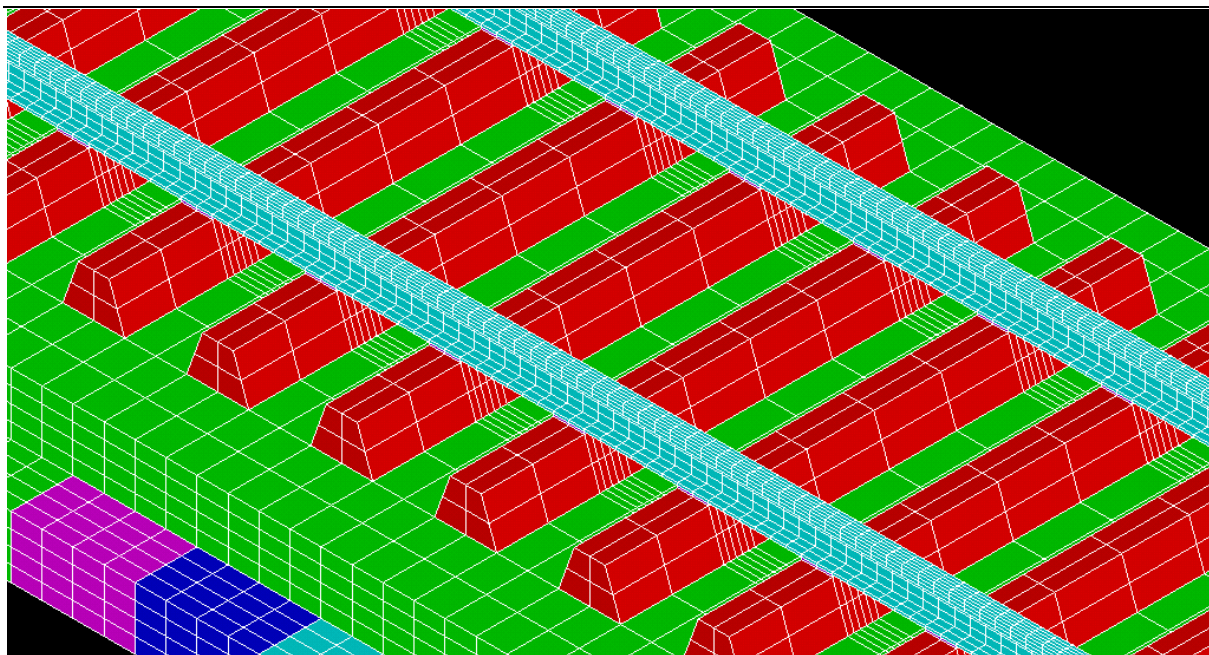


Figure 54 The ANSYS model with 95 rail seats

### 7.2.3. Iterative process – initial condition

The initial condition was firstly defined in order to find the starting point by setting up a unique value for all Young's modulus for substructure (symbolized as  $E_0$ ). A static wheel load of 96 kN was extracted to one rail seat which was identical to the wheel load from the Benkelman beam measurement. The deflection at the loading rail seat and 6 rail seats next to the loaded rail seat was recorded. At first, a table was made by varying the Young's modulus of substructure with different values and recorded the maximum rail deflection, which could be seen in Table 44. It should be noticed, that those Young's modulus was randomly selected which enabled a wide variation of rail deflection.



Table 44: Characteristic E and  $\mu$  value for open track and transition

Young's modulus – substructure (N/mm <sup>2</sup> )	Maximum rail deflection (mm)	Young's modulus – substructure (N/mm <sup>2</sup> )	Maximum rail deflection (mm)
0.7	2.84	10	0.71
1	2.29	30	0.49
2	1.54	100	0.38
3	1.24	500	0.32
5	0.96		

An exponential regression of the above data points was made which could be described as the following formula:

$$E = 4.8 * B * S^{-2} \quad 1)$$

Where E – Young's modulus

B – Bridge factor (B = 1.0 for open track and transition)

S – max. rail deflection

The initial parameter for Young's modulus for the substructure under each rail seat ( $E_{x,0}$ ) could be calculated by inputting the measured maximum deflection at the rail seat  $S_{x,0}$  into the formula 1.

For rail seats on bridge, due to different boundary conditions, the bridge factor "B" would be multiplied to the calculated  $E_{x,0}$ , because the concrete bridge structure is much stiffer than the substructure on open track and transition.

Simulation was done in ANSYS with the initial value of Young's modulus. Deflection line of each rail seat was calculated and compared with the measured values.

It is clear to understand, that there must exist a small variation (called "error") between the measured deflection line and the simulated deflection line under certain rail seat.

Reasons for that were because of the Young's modulus of neighboring rail seats had slight different values. Sample results from error analysis were shown in Table 45 ( $A_{x,0}$ ). All errors which were bigger than 0.1 mm were marked in yellow and the maximum and minimum values were marked in red. Sample measurement and calculation curves were shown in Figure 55. The line with legend "Z5" marked in red collected the deflection line of the rail seat number 5 (measured value). The number "0A5" represented for the results after 0<sup>th</sup> iteration (initial condition) and rail seat number 5 (3<sup>rd</sup> rail seat on left rail).

Table 45: Error analysis after initial condition \*)

	RS i-8	RS i-7	RS i-6	RS i-5	RS i-4	RS i-3	RS i-2	RS i-1	RS i
	-4.8	-4.2	-3.6	-3	-2.4	-1.8	-1.2	-0.6	0
0A1	0.00	-0.03	0.01	0.03	0.07	0.08	0.00	-0.03	0.08
0A3	-0.02	0.02	0.03	0.03	0.08	0.04	0.04	0.13	0.13
0A5	0.02	0.02	0.01	0.07	0.06	0.10	0.20	0.21	0.24
0A7	0.01	0.00	0.05	0.06	0.13	0.26	0.30	0.31	0.30
0A9	-0.01	0.03	0.04	0.11	0.24	0.32	0.38	0.28	0.19
0A11	0.01	0.02	0.05	0.13	0.16	0.24	0.18	0.07	0.02
0A13	0.01	0.01	0.04	0.02	0.09	0.09	0.10	-0.03	-0.07
0A15	0.00	0.02	0.01	0.03	0.03	0.15	0.02	-0.11	-0.04
0A17	0.01	0.00	0.03	0.03	0.09	0.08	-0.05	-0.14	-0.01
0A19	0.00	0.01	0.00	0.05	0.08	0.01	-0.02	-0.02	0.02

\*) : calculated by "Measurement – Simulation"

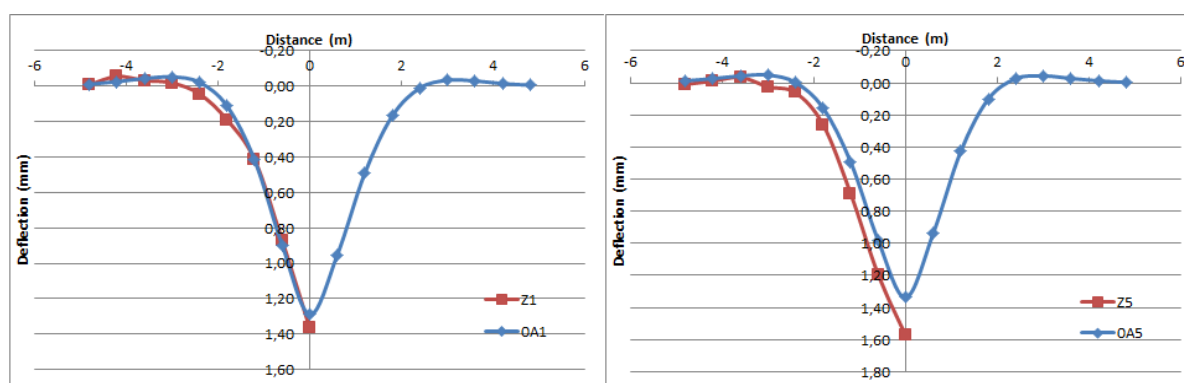


Figure 55 Sample measurement and calculation result  
(Rail seats 1 and 3 on left rail)

---

#### 7.2.4. Iterative process – iteration procedure

A recalculation of the Young's modulus of the substructure was needed for all rail seats. This recalculation was done by the so called "iteration procedure". It utilized the results from the last calculation and set them as the pre-conditions for the next calculation. The recalculation of the Young's modulus was based on the results of the error analysis from the last calculation. The new maximum deflection of the rail seat ( $S_{x,n}$ ) was calculated by the following formula:

$$S_{x,n} = S_{x,n-1} + A_{x,n-1} \quad 2)$$

Where  $S_x$  – max. rail deflection at rail seat  $x$

$A_x$  – Error between measurement and simulation at rail seat  $x$

$n$  – Iteration number ( $n \geq 1$ )

The  $S_{x,n}$  would again be used for calculating  $E_{x,n}$  according to formula 1. Then the model would be calculated again for the  $n+1^{\text{th}}$  iteration.

#### 7.2.5. Iterative process – boundary conditions

It was important to setup the boundary conditions to end the iteration process. Principally the iteration should stop when the results from the  $n^{\text{th}}$  and  $n-1^{\text{th}}$  iteration returns similar results (Difference < 0.01 mm). This held the meaning, that the  $n+1^{\text{th}}$  iteration would not make any sense. The boundary condition could be concluded in the following formula:

$$S_{x,n} - S_{x,n-1} < 0.01 \quad 3)$$

Following this principle, the result after 5<sup>th</sup> iteration could already fulfill the criterion (see Table 46):

Table 46: Boudary condition; Diff. Deflection [mm], Iteration 5 - 4

	RS i-8	RS i-7	RS i-6	RS i-5	RS i-4	RS i-3	RS i-2	RS i-1	RS i
	-4.8	-4.2	-3.6	-3	-2.4	-1.8	-1.2	-0.6	0
Z1	0.00	0.00	0.00	0.00	0.00	0.00	0.00	-0.01	0.00
Z3	0.00	0.00	0.00	0.00	0.00	0.00	0.00	0.00	0.00
Z5	0.00	0.00	0.00	0.00	0.00	0.00	0.00	0.01	0.01
Z7	0.00	0.00	0.00	0.00	0.00	0.00	0.01	0.01	0.01
Z9	0.00	0.00	0.00	0.00	0.00	0.01	0.01	0.01	0.01
Z11	0.00	0.00	0.00	0.00	0.00	0.01	0.01	0.01	0.00
Z13	0.00	0.00	0.00	0.00	0.00	0.00	0.00	0.00	0.00
Z15	0.00	0.00	0.00	0.00	0.00	0.00	0.00	0.00	0.00
Z17	0.00	0.00	0.00	0.00	0.00	0.00	0.00	0.00	0.00
Z19	0.00	0.00	0.00	0.00	0.00	0.00	0.00	0.00	0.00

Table 47 showed the number of differences bigger than the limitation (0.01 mm) after each calculation. It could be concluded, that the iteration procedure could achieve a very quick convergence without many iteration steps:

Table 47: Number of difference over limitation

Between iterations	Number of difference bigger than 0.01 mm	
	Left rail	Right rail
1 and 0	249	251
2 and 1	65	99
3 and 2	28	49
4 and 3	14	26
5 and 4	0	0
Total numbers	675	675

### 7.2.6. The exclusion of fish plated joints

It was easy to find from the Figure 19 that “valleys” could be found at the location of fish plated joints, where extraordinary higher rail deflections were measured. This was due to the lack of sufficient shear modulus of the rail. In other words, this could be understood as a reduced Young’s modulus of rail at the location of the fish plated joint.

Following this principle, the location of the fish plated joint was switched to another type of material in FEM model with reduced Young’s modulus (see Figure 56). The Young’s modulus would be predefined according to the measured deflection line.

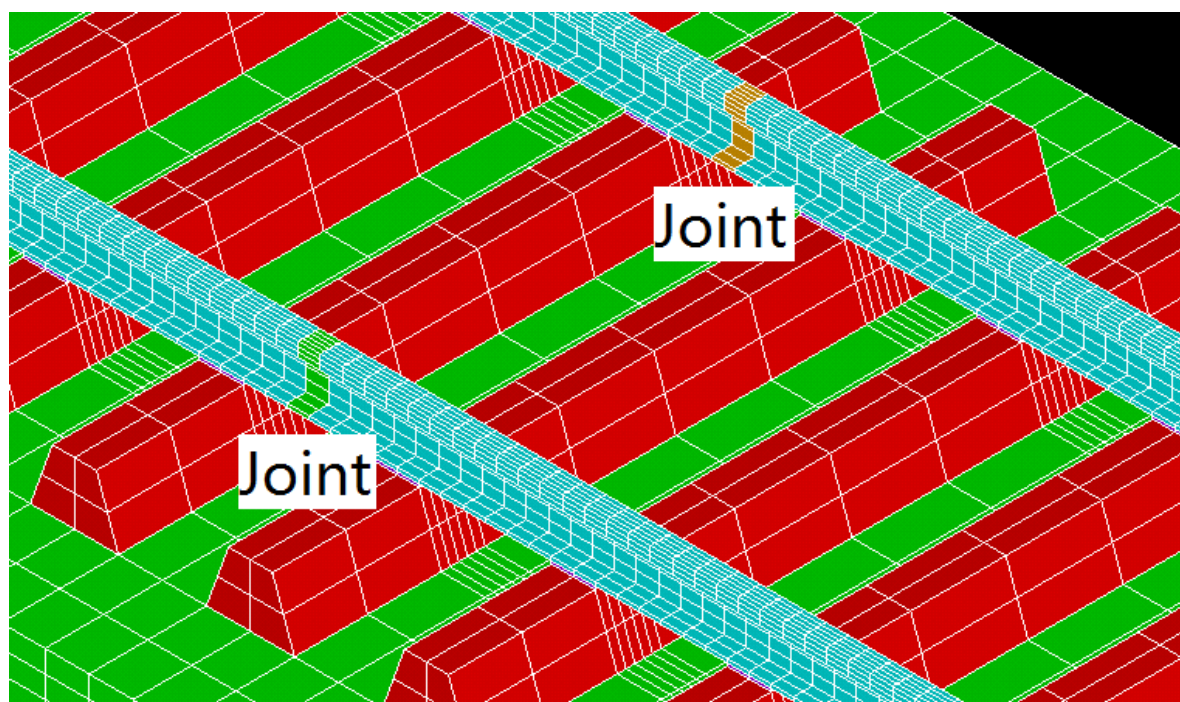


Figure 56 Modeling of fish plated joint (Joint as separate material)

Since those joints were only temporary solutions and would be replaced by continuous rail in normal operation, it was then possible to artificially “remove” those joints in the FEM model by simply setting the Young’s modulus of the joint material back to normal steel. The new result was shown in the following Figure 57:

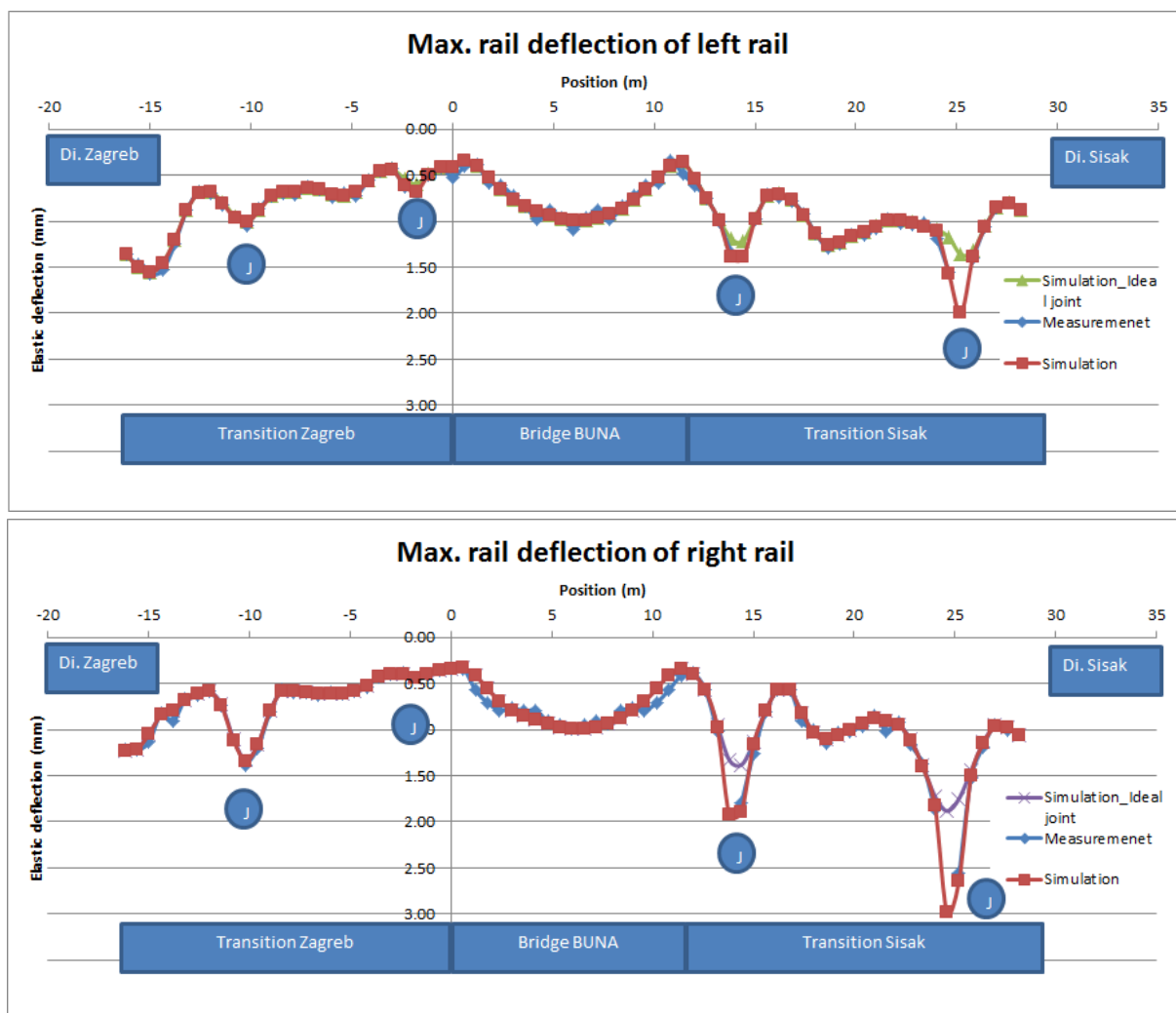


Figure 57 Simulation results after “removing” of the fish plated joints  
(measurement 2013)

It could be seen, that the rail deflection after “removing” the joint would be much smoother than before. It should anyway be noticed, that this “remove” was not supported by any measurement results and was only based on theoretical hypothesis.

## 7.2.7. The results and other comments

It was clear to see that when applying this method for the track section, five iteration steps could already give a converged result. Very good identification could be found between the measurement and simulation results. The following Table 48 and Figure 58 show the error analysis and the final result after the 5th iteration. It could be easily seen, that the error was very much reduced in comparison with the first result before iteration (shown in Table 45 and Figure 55).

Table 48: Error analysis after 5<sup>th</sup> iteration <sup>\*)</sup>

	RS i-8	RS i-7	RS i-6	RS i-5	RS i-4	RS i-3	RS i-2	RS i-1	RS i
	-4.8	-4.2	-3.6	-3	-2.4	-1.8	-1.2	-0.6	0
5A1	0.00	-0.03	0.01	0.04	0.07	0.08	-0.01	-0.06	0.00
5A3	-0.01	0.02	0.03	0.03	0.08	0.03	0.00	0.03	-0.02
5A5	0.02	0.02	0.02	0.08	0.06	0.06	0.09	0.04	0.01
5A7	0.01	0.00	0.06	0.05	0.11	0.19	0.16	0.11	0.08
5A9	0.00	0.03	0.04	0.10	0.20	0.23	0.23	0.11	0.04
5A11	0.01	0.02	0.05	0.11	0.12	0.17	0.10	0.00	0.00
5A13	0.01	0.01	0.03	0.01	0.07	0.07	0.10	0.00	-0.01
5A15	0.00	0.02	0.01	0.04	0.04	0.16	0.05	-0.06	0.01
5A17	0.01	0.00	0.03	0.04	0.10	0.10	-0.03	-0.11	0.01
5A19	0.01	0.02	0.01	0.06	0.08	0.02	-0.01	-0.03	-0.02

<sup>\*)</sup>: calculated by “Measurement – Simulation”

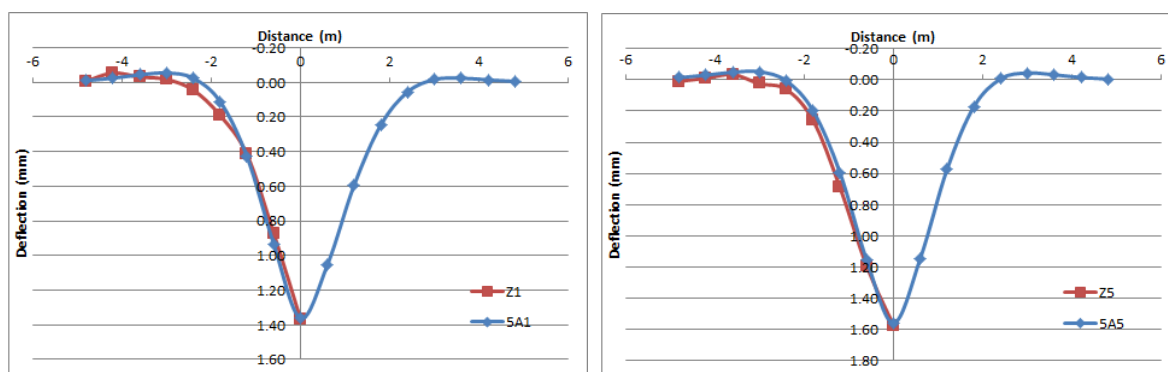


Figure 58 Interpolation and calculation result after 5<sup>th</sup> iteration

Following conclusions and perspectives could then be made:

- 
- The FEM program could very well rebuild the test section on behalf of elastic rail deflections;
  - A suitable iteration process for calibrating the elasticity under each rail seat was developed ;
  - The simulation result could provide a powerful evidence to point out some measurement errors on site;
  - The calibrated model could be used for further analysis needs.

#### **7.2.8. The adjustment to the new measurement results (April, 2014)**

The models could also be adjusted to the new measurement results in 2014. In order to better understand the change of elasticity during the operational runs for a half year, the Young's modulus of ballast layer would be newly set as variable for iterations and the Young's modulus of subgrade layer would be kept the calibrated values from the measurement results in 2013.



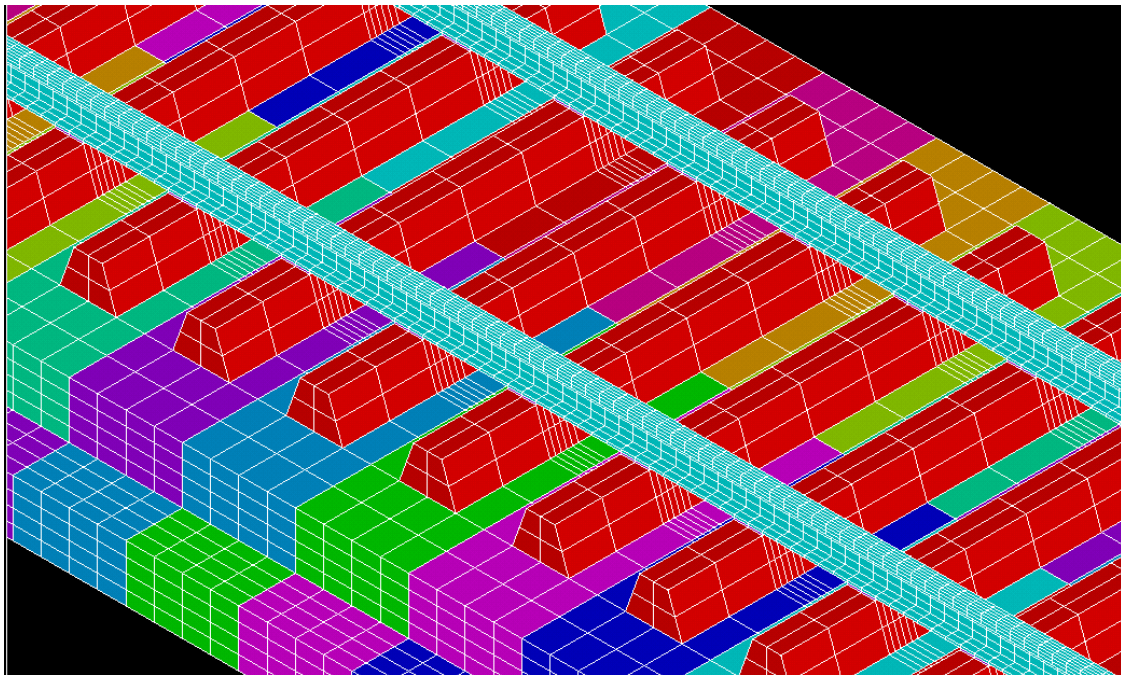


Figure 59 The new ANSYS model with variable ballast elasticity

The above Figure 59 shows the new model and the new calibrated maximum rail deflection. It should be pointed out that the individual value for ballast would not be identical to the real elasticity of the material, since the subgrade layer calibrated based on the measurement in 2013 had already included the difference in ballast elasticity from individual rail seats. Those values of ballast elasticity provide only the clues, how the overall elasticity of the rail seats changes after the half year operation. The overlapped results after simulation could be seen in Figure 60:

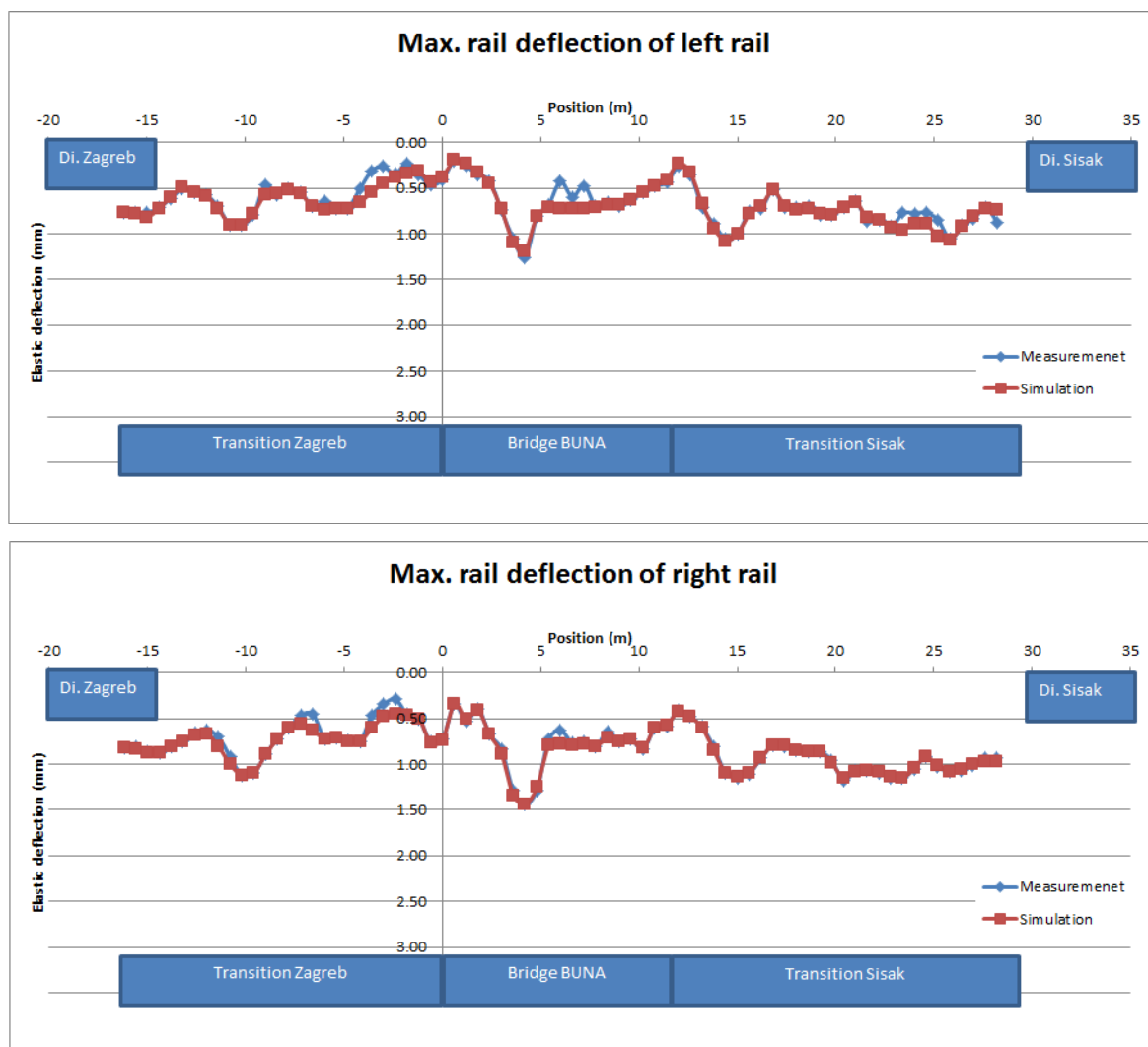


Figure 60 Identification between measurement and simulation results (according to measurement in 2014)

## 7.3.FEM analysis on determination of the dynamic wheel load under running trains (Cell 22)

### 7.3.1. Introduction and measurement result analysis

The calculation of dynamic wheel load was done based on the field measured dynamic strain and the calibrated FEM model described in section 7.2. It followed the principle that the induced dynamic strain was fully dependent on the transient dynamic wheel load on this location. This calculated the dynamic wheel load under both variation of elasticity and geometry.

### 7.3.2. Loading of the FEM model

The calculation was based on the FEM model illustrated in section 7.2. The smallest element distance in longitudinal direction was fixed to 75 mm. For adjusting those axle pairs which the axle spacing was not a multiple of 75 mm, a division of the load was performed. The principle is to simply divide the load to the both neighboring nodes (see Figure 61).

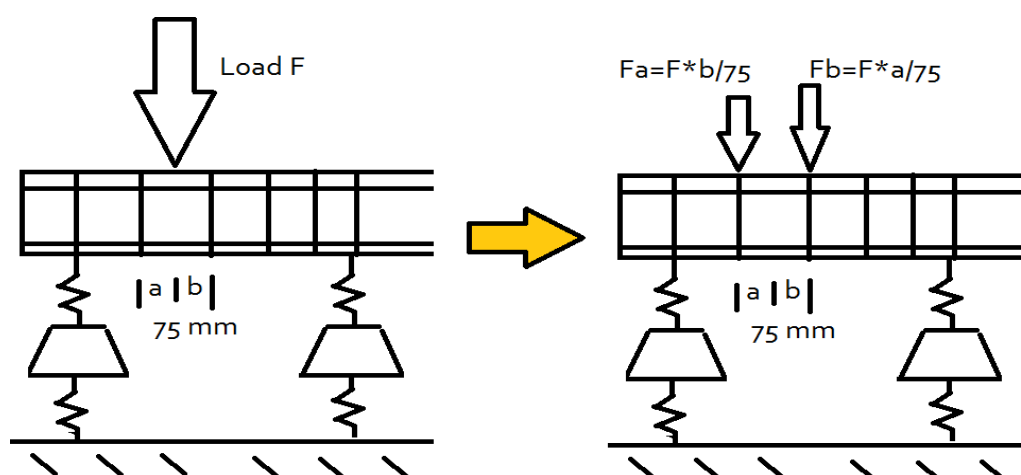


Figure 61 Application of wheel load in FEM

Since the design of the four axles of the middle wagon of the train set 6111 stays the same, a sample loading model of one of the both bogies was shown in Figure 62. The static load of each axle is around 17.0 t.

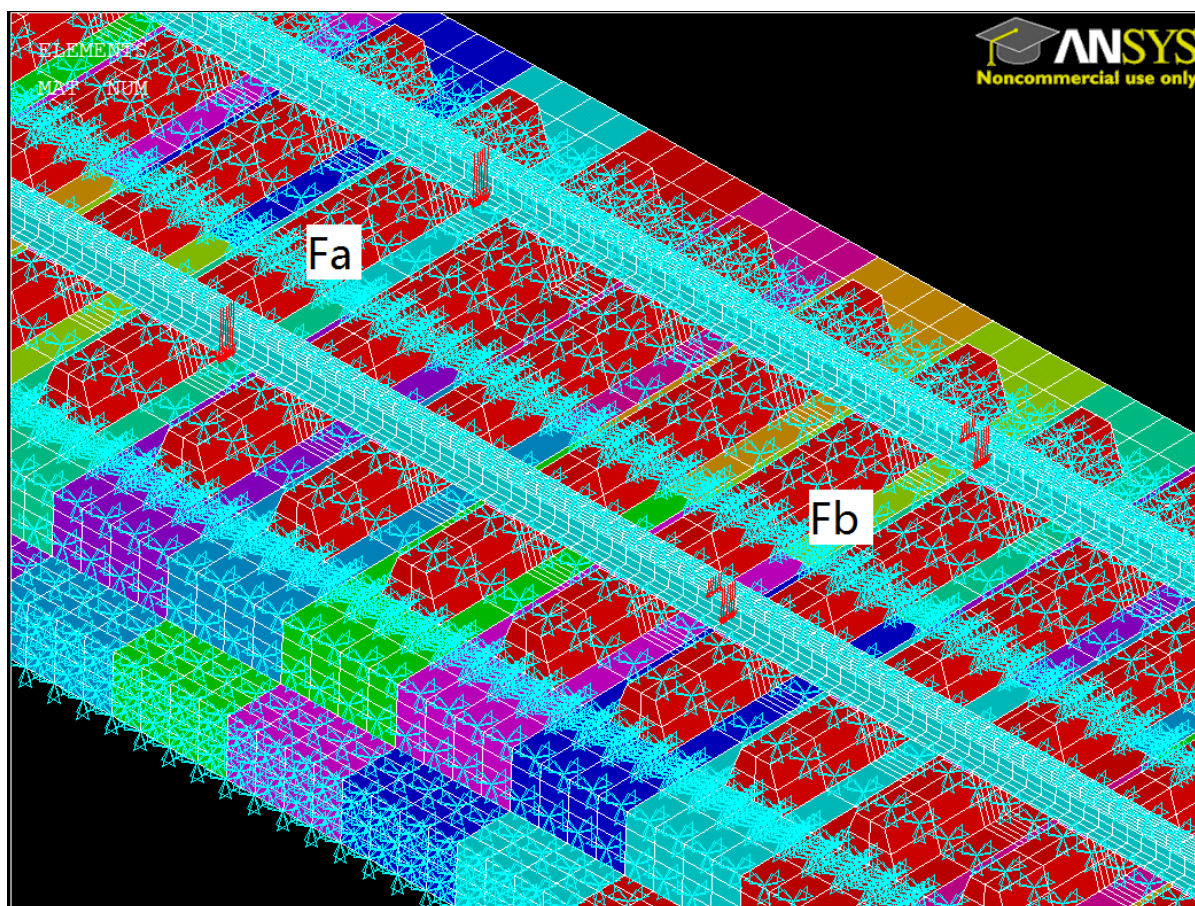


Figure 62 Sample loading model (front bogie of the middle wagon of train set 6111)

### 7.3.3. The modeling result and analysis – Test runs

The calculation of the dynamic wheel load was based on an iteration approach. The principle of the iteration method was already illustrated in section 7.2. The target was to find out the proper wheel load which could induce the same dynamic strain as measured in the field.

The calculation was done for all the measured test runs in 2014 (the results measured in 2013 were not calculated). The both axles of the load wagon were used for the analysis. Table 49 and Table 50 show the statistical results of the dynamic wheel load according to speed level.

Table 49: Statistical analysis of dynamic wheel load according to speed level  
(transition Zagreb, measurement 2014)

	Speed level (km/h)		
Average speed (km/h)	14	38	64
Number of measurements	6	4	3
Number of measured points	276	184	138
Max. dynamic wheel load (kN)	131.4	133.3	141.3
Average dynamic wheel load (kN)	102.1	101.1	109.4
Max. static wheel load (kN)	100	100	100
Standard deviation (kN)	12.23	12.65	14.09
Dynamic loading factor (%)	31.4	33.3	41.3

Table 50: Statistical analysis of dynamic wheel load according to speed level  
(transition Sisak, measurement 2014)

	Speed level (km/h)		
Average speed (km/h)	9	36	75
Number of measurements	8	4	3
Number of measured points	368	184	138
Max. dynamic wheel load (kN)	116.1	116.9	122.8
Average dynamic wheel load (kN)	91.0	93.6	94.3
Max. static wheel load (kN)	100	100	100
Standard deviation (kN)	10.96	10.24	17.80
Dynamic loading factor (%)	16.1	16.9	22.8



The term 'Dynamic loading factor' calculates the increased dynamic loading by dividing the maximum load into the static one. By referring to chapter 6.3 and figuring out, that the system elasticity shows variation at those locations where previously fish plated joint were installed, which leads clearly to a big increase in the dynamic loading at the same location as well. This increased dynamic load would counteractive make the deterioration of the track faster here than at other locations. Since there do not exist any sudden change in the design of the transition, it should be concluded that the increase of the dynamic loading is till now due to discontinuity of track superstructure elasticity.

#### 7.3.4. The modeling result and analysis – Train runs (train set 6111)

The calculation was done for all the runs of train set 6111 in 2014 (the results measured in 2013 were not calculated). The four axles of the middle wagon were used for the analysis due to heavier axle load. Table x shows the statistical results of the dynamic wheel load with a passage speed of  $120 \pm 5$  km/h. The Figure 63 shows the distribution of maximum, minimum, average and static wheel load along the bridge and transition area.

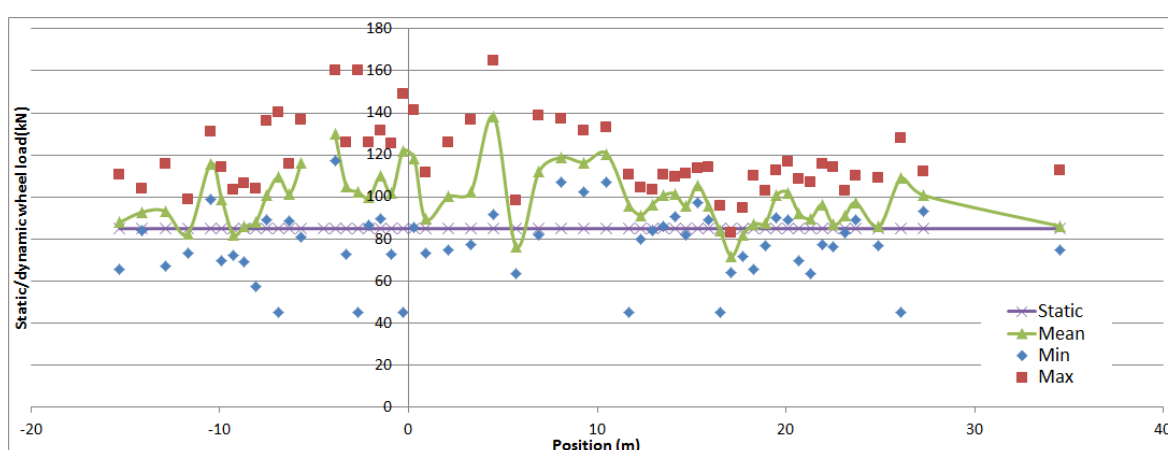


Figure 63 Distribution of static and measured dynamic wheel load  
(middle wagon of train set 6111, static wheel load of 85 kN)

The maximum measured axle wheel load reached 160 kN, meaning that in comparison to the static load of 85 kN, an increase of nearly 100% was possible. This should be considered from the combination of both track and vehicle sided imperfections (from vehicle side like flat spot in wheel, etc.). Since the effect due to vehicles would not be studied in the following MBS simulations, the simulated values could be smaller than the measured values shown above.

After the calibration, the wheel load  $F_a$  and  $F_b$  were applied with different values and the rail foot strain at the same location where the strain gauges were glued was determined. Figure 64 and Figure 65 show the overlap of the measurement and simulation curve when one of the axles was located at the transition in Sisak of  $x = 16.5$  m (just as example).

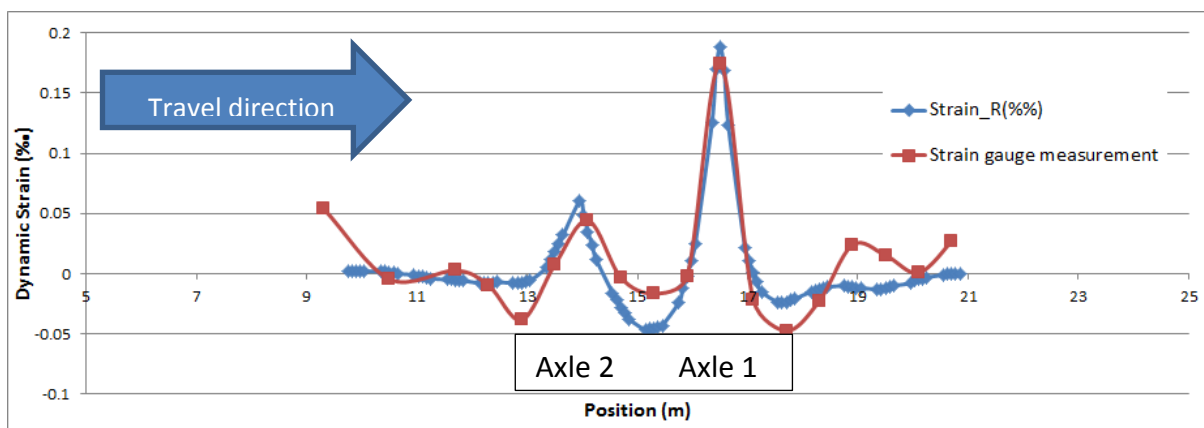


Figure 64 Measurement and simulation result (1<sup>st</sup> axle above strain gauge)

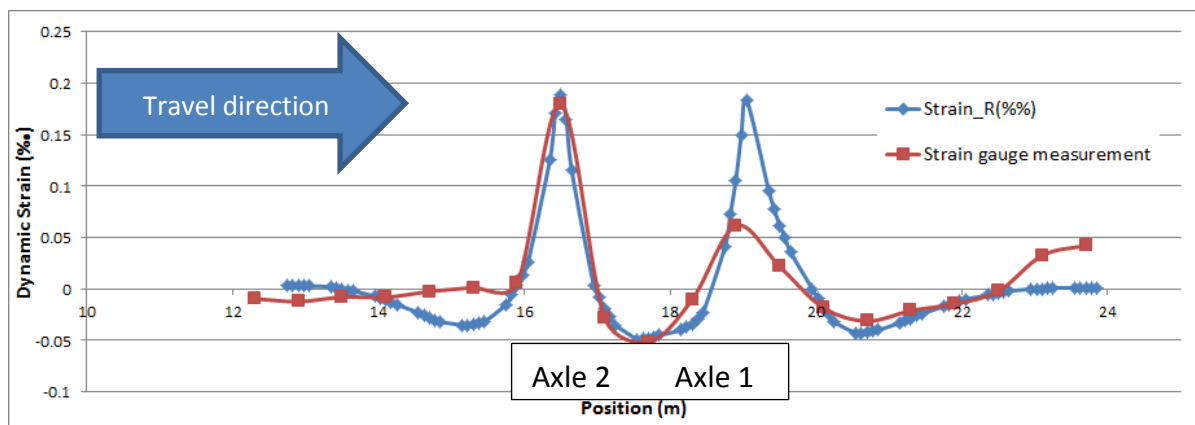


Figure 65 Measurement and simulation result (2<sup>nd</sup> axle above strain gauge)

It should be firstly pointed out, that due to the positioning of the neighboring axle not directly above one strain gauge, the measured value of the second axle could be significantly reduced. The passage with 120 km/h at this location caused a maximum dynamic load up to 100 kN, representing for a dynamic increase of around 17.6%. It should also not be neglected, that for the loading of the second axle, the dynamic load of the first axle was around 30 kN, meaning a weightlessness of 64.7% of this axle at the moment of the passage. When repeating this process under different speed levels or under different track qualities, correlations between the dynamic wheel loads and the respective parameters could be found.

## **7.4. MBS analysis on simulation of the dynamic wheel rail contact with pre-defined track excitations (Cell 31)**

### **7.4.1. Background and introduction**

Track sided excitation (normally in representation with track irregularities) is one of the most dominant factors influencing the dynamic vehicle-track interaction behavior. A train passage on irregular track would lead to variation of dynamic wheel load, which is the dominating the track deterioration rate. This variation was the consequences of train design, magnitude of track irregularity, train speed, etc. Therefore, a systematic numerical modeling (in this case MBS system) would be the best choice providing the overview of the actual travel behavior of the train.

The key element of the model is the wheel rail contact. The simulation of dynamic wheel rail contact in a MBS system needs inputs from both vehicle and track sides. The relative vehicle data would be typically the mass and suspension designs in the vertical direction, whereas the input from the track side would be merely track excitation (irregularity) exclusive with track elasticity inputs. The wheel and rail head profile would also be the determinant factor for the simulation.



### 7.4.2. Setup of track excitation

The software program for simulation was decided to be Simpack 8.904. The program provides various kinds of possibilities of inputting track irregularity as track sided excitations in three dimensions. For this research, the so called 'track-related' excitation variation would be used. Figure 66 shows how to define a 3D track excitation in Simpack which was separated into 4 independent subjects:

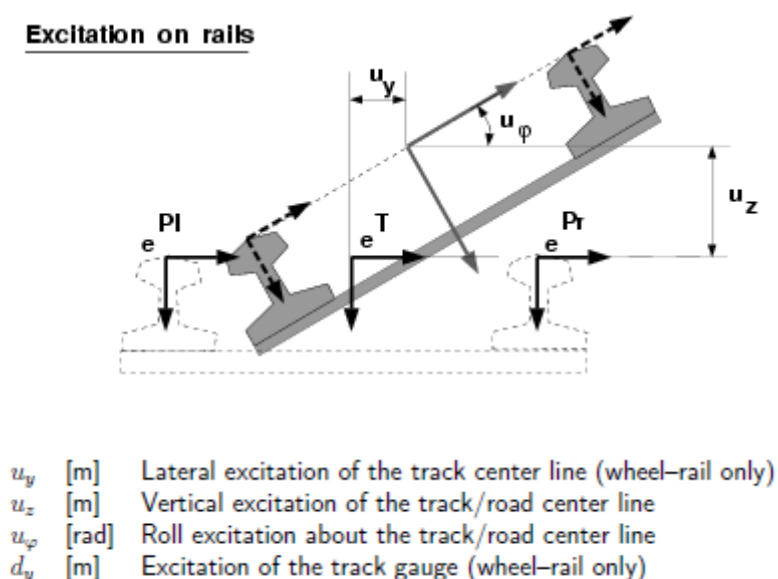


Figure 66 The definition of 3D track excitation in MBS system <sup>[22]</sup>

It should be pointed out, that the final shape of the track was the summary of all the four different subjects since it is easy to find out that they were orthogonal to each other. Especially for track gauge, the default gauge (e.g. 1435 mm) for the model would equal to 0 mm in gauge excitation and a plus value would represent for a narrowed gauge. See Figure 67 for the definition box in Simpack, the excitation type 09 allows the direct input from measurement results:

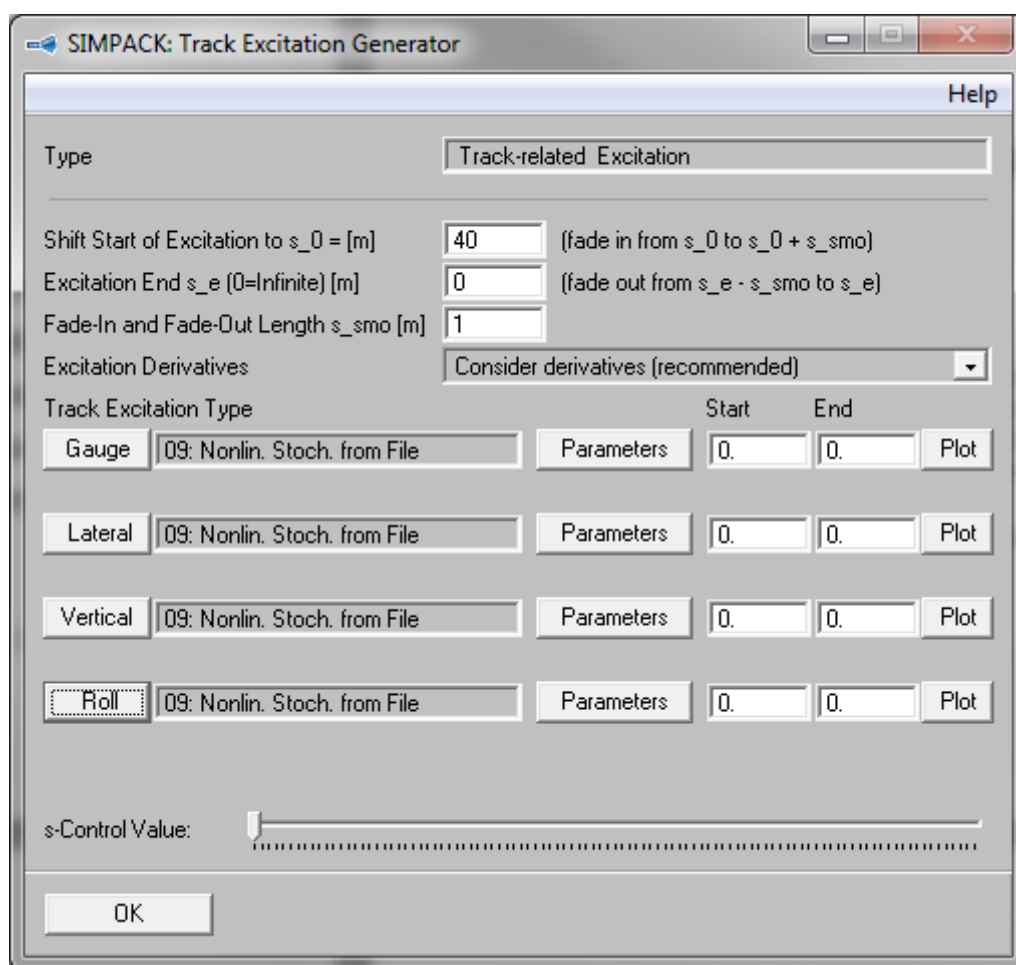


Figure 67 The definition of 3D track excitation in Simpack 8904

For simulation, the track geometry measurement results from 2014 (already shown in chapter 5.2) would be used as input. A filtering with maximum wave length of 50 m was applied to the measured raw data in order to prevent from aliasing effect.

### 7.4.3. Vehicle setup and parameters

A complex vehicle track model was built with the MBS software SIMPACK (see Figure 68). The train was equipped with 2 layers of suspensions namely the primary suspension between bogie frame and wheel sets as well as secondary suspension between vehicle body and bogie frame. For simplification reasons, only the heaviest

wagon of the train set 6111 (middle wagon) was built into the model. The axle load of the wagon was about 17.0 t (wheel load about 85 kN). Experience values for the suspension parameters were chosen.

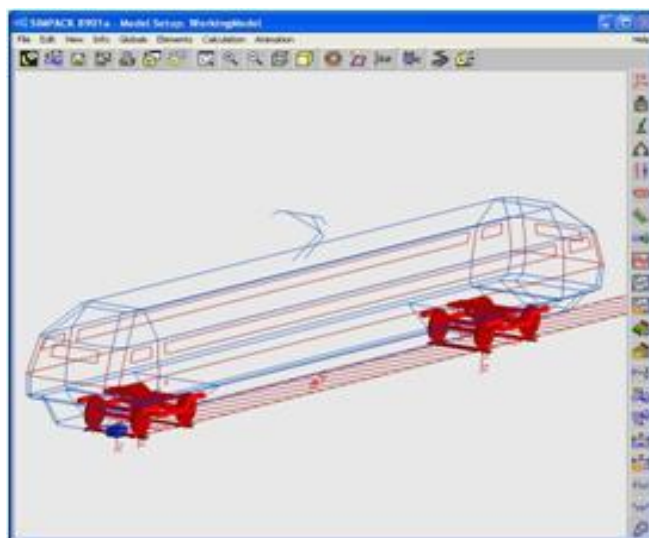


Figure 68 The vehicle model (middle wagon of train set 6111)

The measured track geometry would be input as track excitations for this model. The length of the measured excitation was 500 m. A maximum travel speed of 120 km/h would be given. It should be noticed that the original measurement data of strain gauges were initially applied the low pass filter of 500 Hz. The inclusion of a maximum filter frequency of 500 Hz ensured the data recording of every 7 cm (train speed of 120 km/h) and could be able to record the variance of the train load at the position. Therefore the sampling frequency for the simulation was fixed to 500 Hz.

It should be noticed, that the calculated dynamic wheel load was merely due to the effect of track irregularities, which in other words, meaning that no effect from track elasticity was included. This would lead to the fact, that the simulated dynamic wheel load would be different than what had been calculated in 7.3.3.

#### 7.4.4. The simulation results

The analysis of the measurement results would rely on selection of different type of filters. The initially applied filter of 500 Hz could record the transient distribution of the dynamic load, but due to restricted impact time, this short period peak load might not be critical for the general deterioration of the track. Therefore, for determining the maximum possible dynamic load, this method would be helpful.

For determining the dynamic load which was more determinant for the general deterioration rate of the track, the simulated dynamic wheel load should be filtered with a low pass filter of 20 Hz according to the European railway standard EN14363:2005 <sup>[23]</sup>. It should be figured out, that under this type of filtering, the excitation load due to roughness from wheel or rail would not be included since they would tend to excite the system by higher frequencies.

Figure 69 and Figure 70 show the variation of dynamic wheel load of the first axle (left and right wheel) along the bridge and transition. For easier understanding, the x-axis was switched to position of the track in meter with  $x = 0$  m representing for the bridge entrance on Zagreb side.

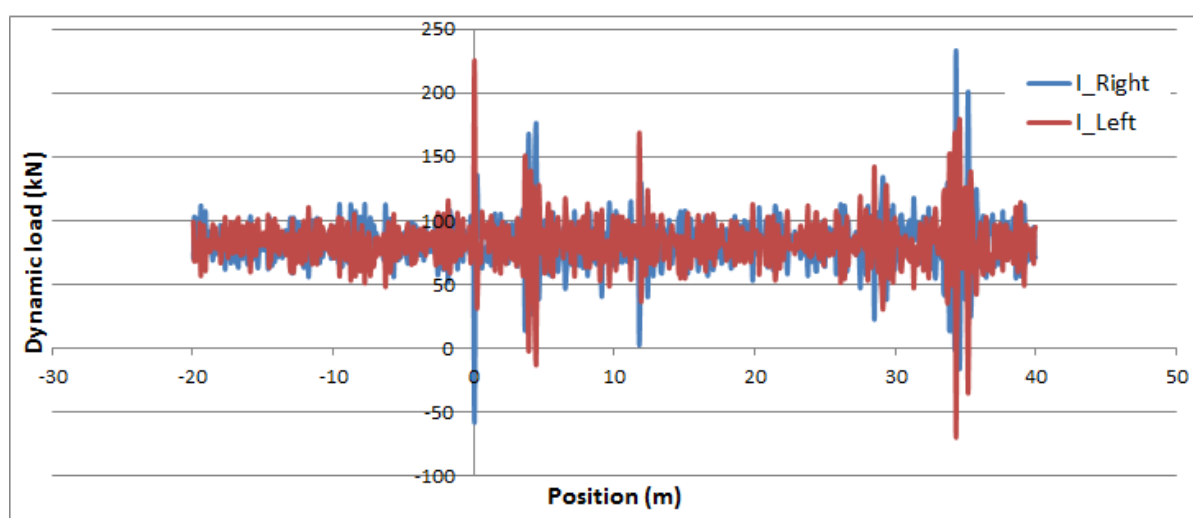


Figure 69 Dynamic wheel load under track irregularity ( $V = 120$  km/h,  $f_u = 500$  Hz)

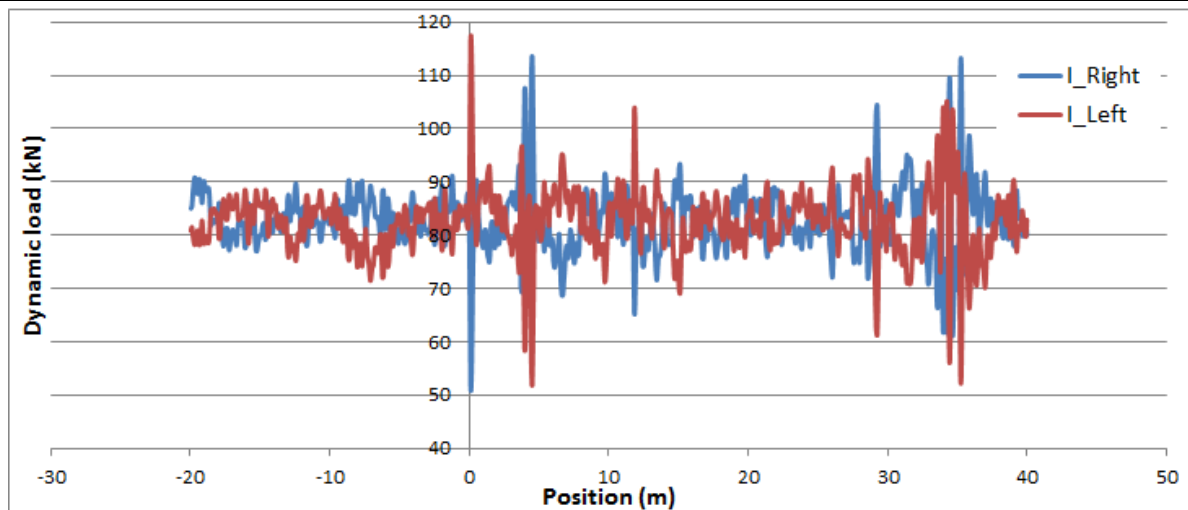


Figure 70 Dynamic wheel load under track irregularity ( $V = 120 \text{ km/h}$ ,  $f_u = 20 \text{ Hz}$ )

The simulation was also done with the vehicle speed of 95 km/h for visualization of the effect of travel speed. The graphical representation was shown in Figure 71 and Figure 72.

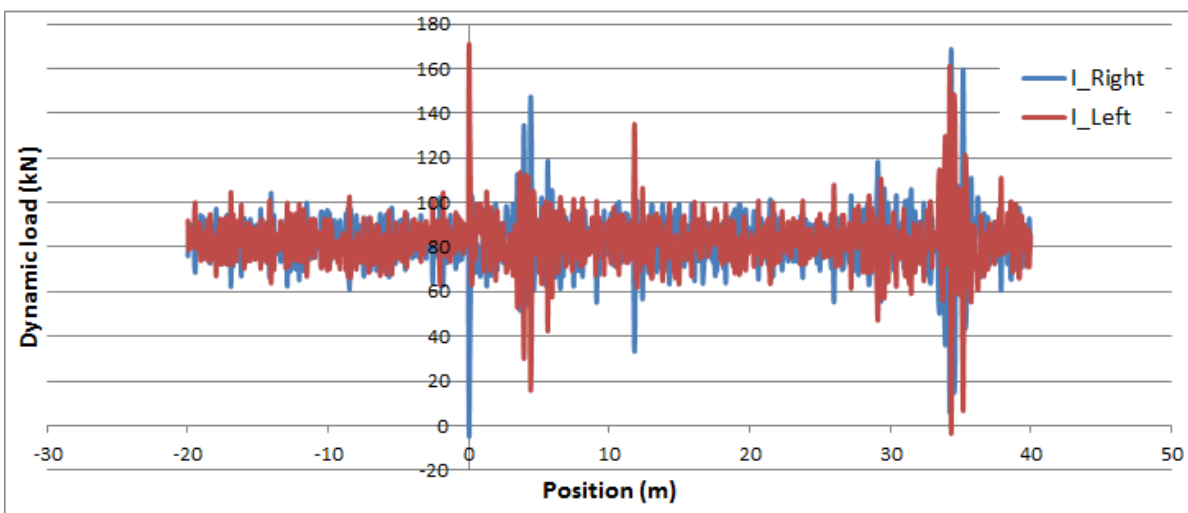


Figure 71 Dynamic wheel load under track irregularity ( $V = 95 \text{ km/h}$ ,  $f_u = 500 \text{ Hz}$ )

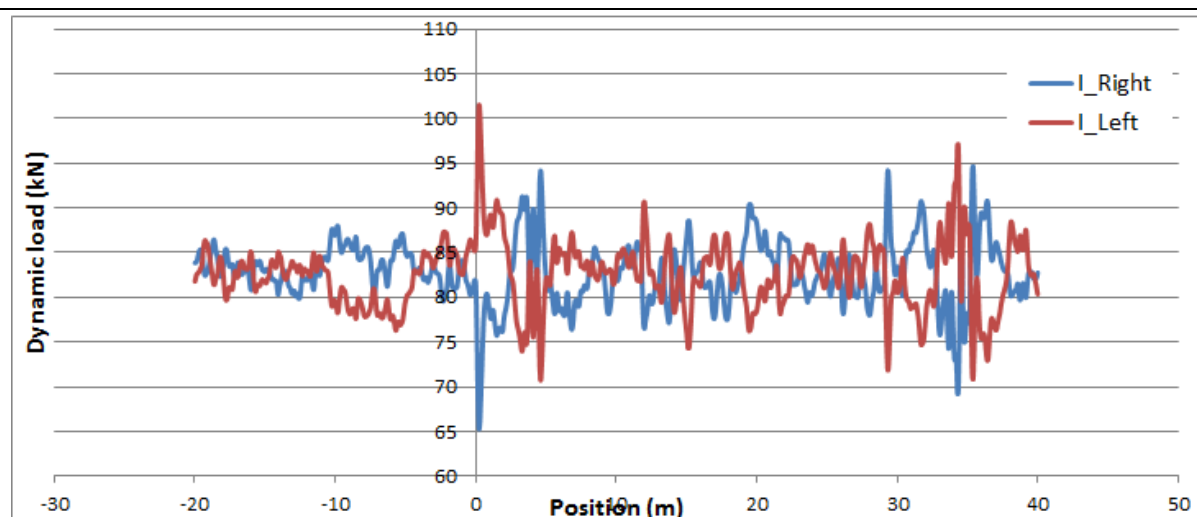


Figure 72 Dynamic wheel load under track irregularity ( $V = 95 \text{ km/h}$ ,  $f_u = 20 \text{ Hz}$ )

For a better illustration of the dynamic wheel load which was more useful of providing guideline for the track deterioration, the low pass filter of 20 Hz and a travel speed of 120 km/h would be included as the standard analysis method and the following simulation results would be all applied with this filter.

## 7.5. MBS analysis on simulation of the dynamic wheel rail contact with modal represented FEM input (Cell 32)

### 7.5.1. Background and introduction

The variation of track elasticity is also an important factor influencing the overall track dynamics. For sound track without special design specifications, the elasticity of the track would not change a lot in comparison with track irregularity characteristics and this part was usually left behind.

This should not be the case for this research, since the track elasticity due to the design of bridge and transitions would have significant impact on the overall travel behaviors. By repeated train load, those variations of track elasticity would have

counterproductive effect to the track geometry. In other words, the appearance of track irregularity was normally the consequence of discontinuity of track elasticity.

Generally, it is suggested to build up the track elasticity model in FEM system, since the materials of the single element could be given and the simulation of complex deflection behavior could be ensured. The disadvantage of the approach is the need of complex discretization of the geometry model into small and fine elements, due to which the model should normally orient itself in time-independent analysis.

As already illustrated in chapter 2, the co-simulation strategy would be used. The module included is the “FlexTrack” in Simpack. It utilizes information from both models in FEM and MBS and combines them together for solving the results. Since MBS was designed to accomplish time dependent simulations, the FEM model would be condensed and utilized as the prerequisite for the MBS model. This model condensation was achieved by the modal analysis approach <sup>[24]</sup>.

#### **7.5.2. Input of track elasticity characteristic by FEM model**

A simplified FEM model with regular volume elements was built up in ANSYS. The longitudinal grid spacing was set to 0.6 m which exactly met the actual sleeper spacing of the track. The elasticity modulus of the each independent grid was also set differently which could meet the design and measurement specifications. The following Figure 73 show the simplified model and the applied boundary conditions (different colors represent for different material input) and the adjusted deflection line under static loading.

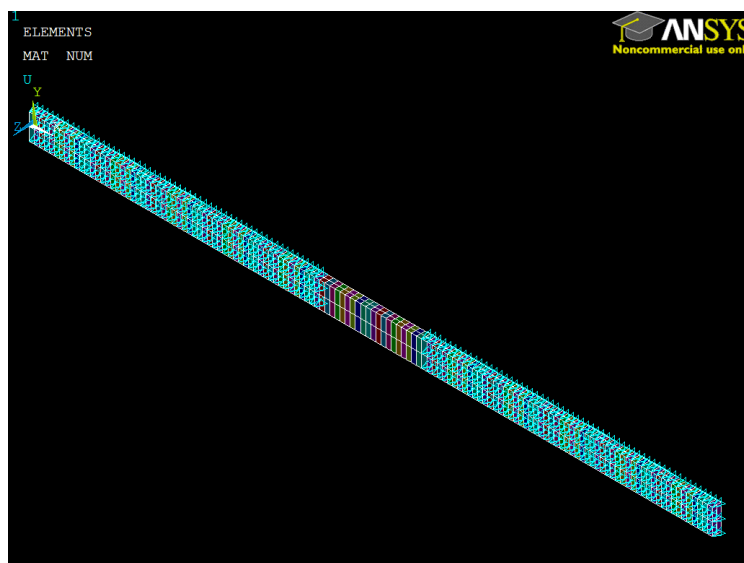


Figure 73 Simplified FEM model with individual elasticity modulus

The deflection behavior of the track was modeled firstly according to both the design specifications and measurement results. The formulation of the curve was already described in chapter 5.3. The deflection line in the bridge was calculated according to the design specification of the bridge (Deliverable 3.2 <sup>[15]</sup>). See Figure 74 and Table 51 for the input line of the static track deflection and the necessary model parameters.

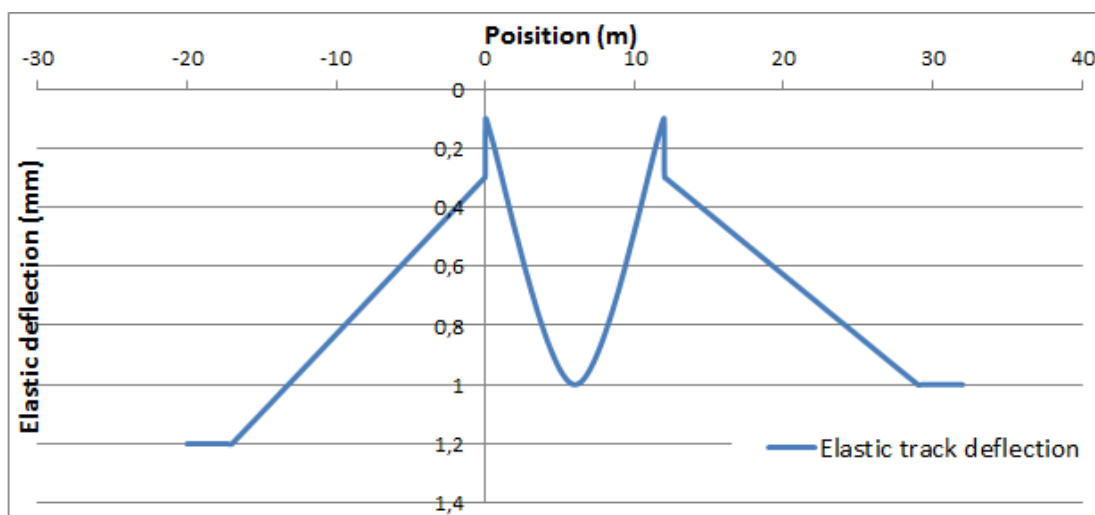


Figure 74 Calibrated elastic track deflection (single wheel load of 85 kN)

(x = 0 m represents for bridge entrance Zagreb)



Table 51: List of model parameters

	value
Length of transition	17.0 m
Length of bridge	12.0 m
Thickness of the structure	1.0 m
Width of the structure	3.0 m

In order to meet the needs of the FlexTrack calculation, all the nodes in the contact surface to the wheel were selected to be master nodes. The direction of interest would be only in vertical direction.

The modal analysis of the condensed model was done as the next step. From all the selected master nodes, only the eigenmodes on the center line of the surface area were calculated, due to the reason that the modes defining tilting and horizontal movement were not needed to be included in this research. The following Figure 75 and Figure 76 show some included eigenmodes.

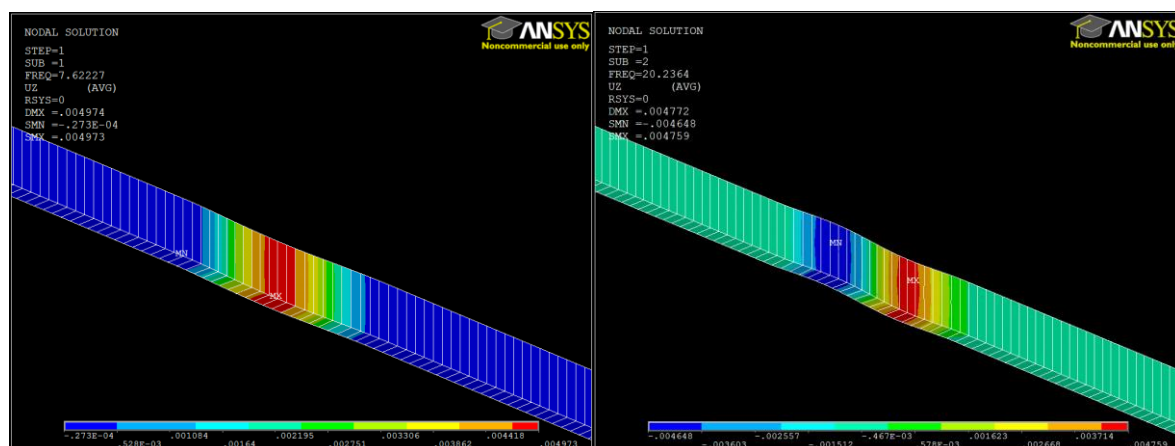


Figure 75 Eigenmodes 1 and 2 on bridge (zoom factor 50,  $f = 10.9$  and  $29.2$  Hz)

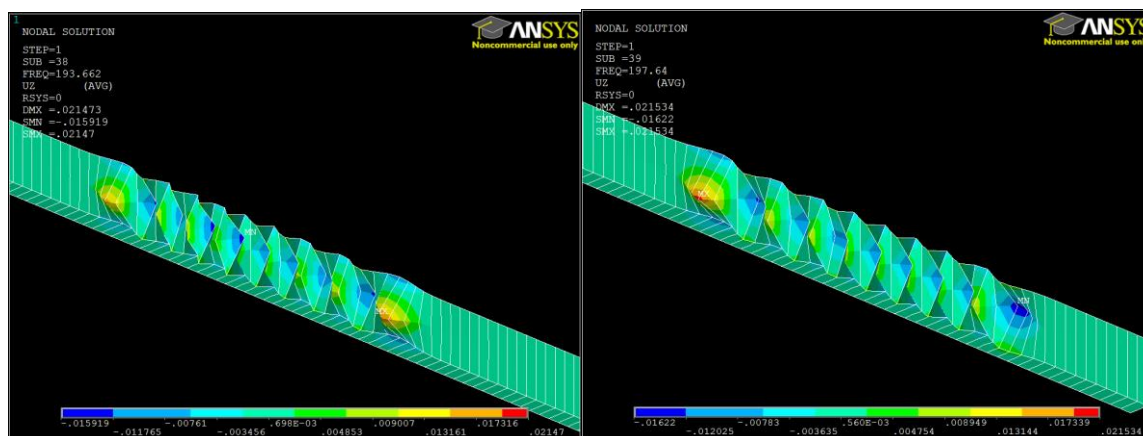


Figure 76 Eigenmodes 38 and 39 on transition Zagreb and Sisak

(zoom factor 50,  $f = 171.2$  and  $171.3$  Hz)

Due to the predefined design specification that a linear reduction of elastic track deflection should be achieved in both transitions, the representation of the transition should rely on many different modes which have different length of influence. The area with higher elastic deflections would need more eigenmodes and the area with smaller deflections need less eigenmodes. Therefore, the inclusion of eigenmodes should be quite a lot in order to cover the whole area of the bridge and transition. For importing into Simpack for the simulation with FlexTrack, 130 eigenmodes were included with a frequency variation from 8 and 500 Hz. This ensured the best rebuild of the elasticity behaviors in the whole measurement section.

### 7.5.3. Setup of model in Simpack and perform of simulation runs

The vehicle model was already built up in section 7.4. The speed of the vehicle was set to 120 km/h since it was the most frequent passage speed of the train in normal operations.

For setting up the elastic track within the FlexTrack module, the condensed model and the results of eigenmodes were read into the Simpack. An “fbi” file would be generated which contained all the information from FEM model. For a smooth

simulation, the communication step size should be adjusted to the highest included mode in the file. Various parameters could be adjusted within the FlexTrack definitions. General parameters would include the location to place the flexible track, the inclusion of eigenmodes and interaction nodes, the inclusion of model calculation direction, etc. The general view of the flexible track and the train was shown in Figure 77:

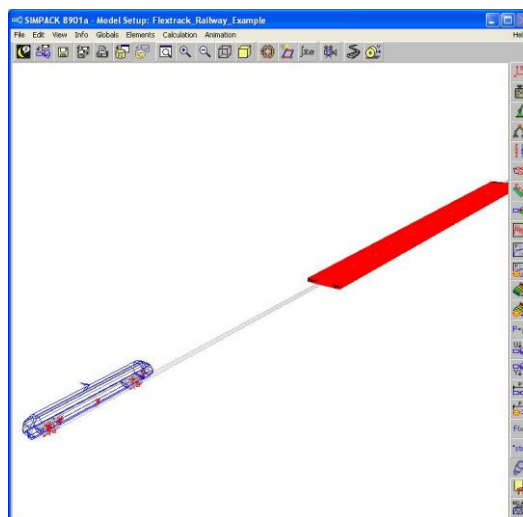


Figure 77 Simpack vehicle model with built-in flexible track structure

The output of the simulation run could include single deflection line at each predefined location, meaning a visualization of the deflection at single point during the train runs would be possible.

The simulation runs were performed in various ways. A quasi-static run with 1 m/s was firstly made for model calibration reasons. This was used to check whether there were already enough modes included for representation of the track elasticity characteristics. Afterwards, the simulation run was done for different speed levels with single elasticity input or both elasticity and irregularity inputs. The following Table 52 provided a more detailed list of information.

Table 52: Performed simulation runs

	Speed level	Track sided excitation
Quasi-static (calibration)	1 m/s	Only elasticity
Dynamic (calculation)	120 km/h	Elasticity & Irregularity

#### 7.5.4. Simulation results – quasi-static runs

The results under quasi-static run with 1 m/s was firstly shown in Figure 78. It displayed the elastic deflection curve of the passage of train under selected interview points in open track, transition and middle of the bridge. It was easy to conclude, that the included number of modes of 130 could be able to rebuild the track elasticity property in a very acceptable way. The deflection in the bridge was higher due to the overlap of both axles of the bogie.

The distribution of the dynamic load was not shown due to insignificant curve characteristic under 1 m/s.

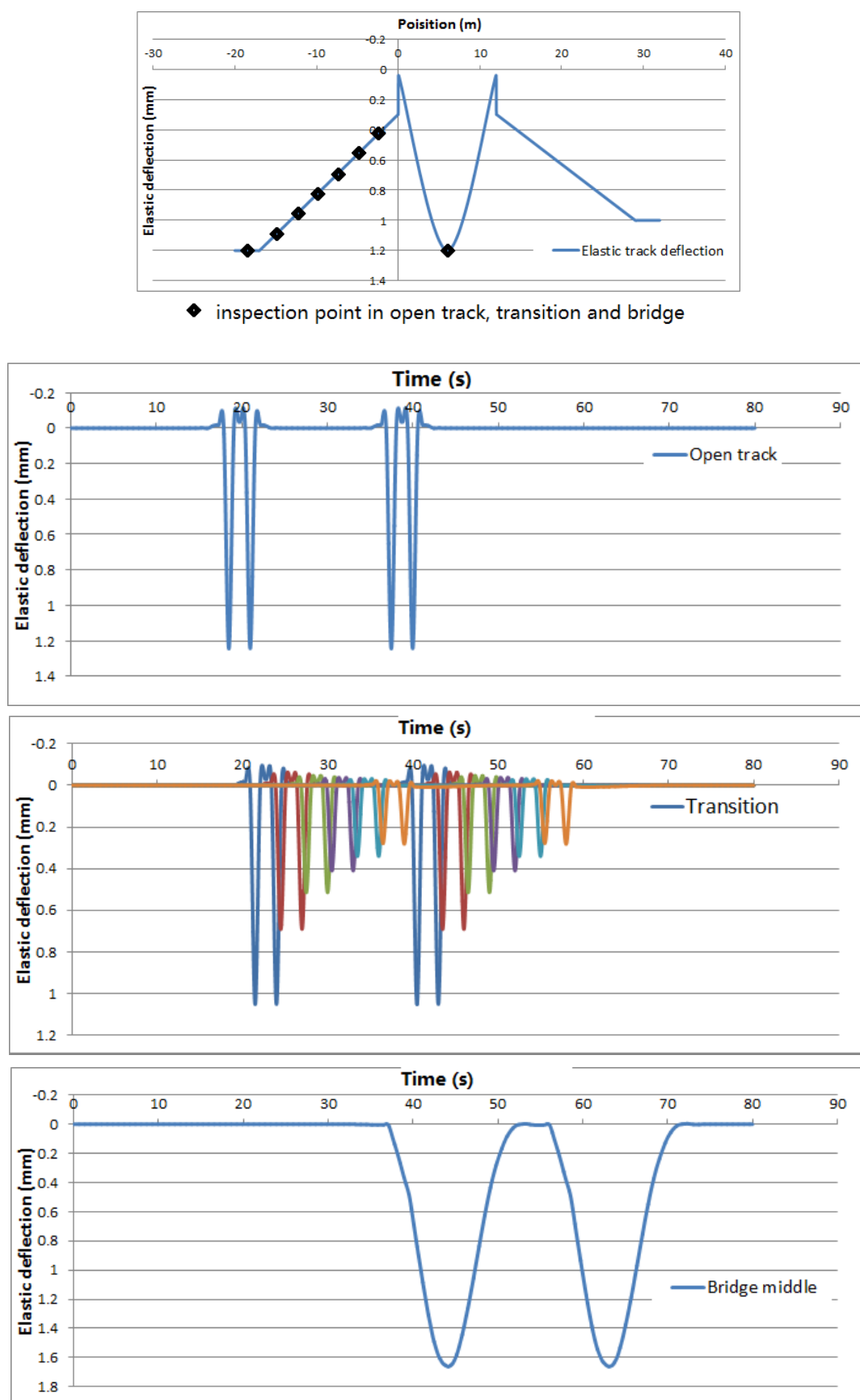


Figure 78 Elastic track deflection ( $V = 1$  m/s, quasi-static)

### 7.5.5. Simulation results – dynamic runs

After the step of model calibration, the flexible track input would be applied for train runs with higher speed. An important factor which should be considered was now the damping of the track. Since the FlexTrack module relied on the modal analysis of the flexible system with built in modal damping. The damping was now categorized as a number in percentage.

The selection of the modal damping should be dependent on the travel speed of the vehicle since the modal analysis could only provide a linear damping approach whereas the track damping in reality was found mostly to be nonlinear. It was defined under experience that a modal damping of about 5 % would be needed for the dynamic run with 120 km/h. The Figure 79 showed the distribution of the dynamic wheel load.

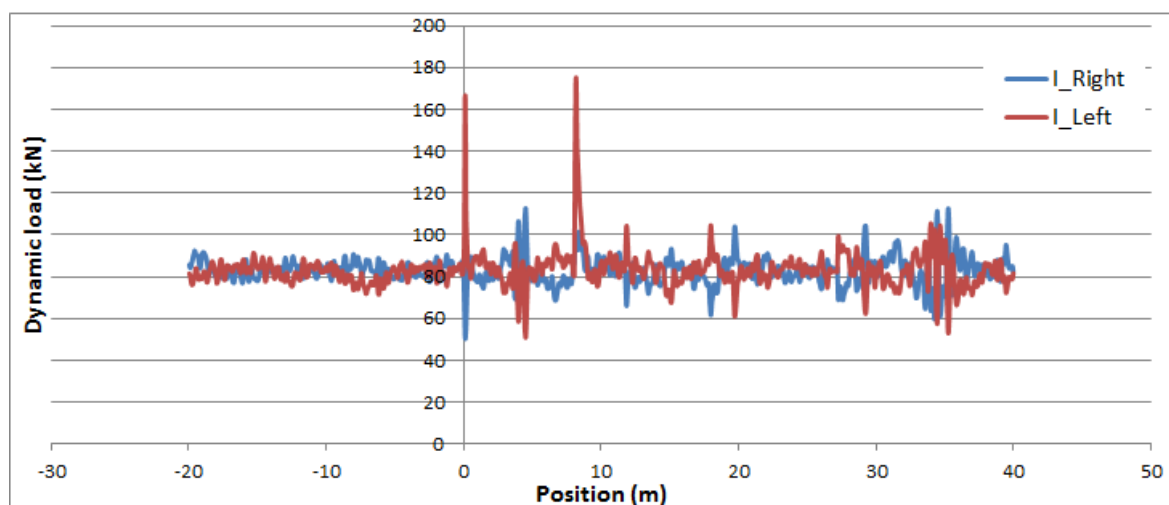


Figure 79 Dynamic wheel load under track elasticity and irregularity ( $V = 120$  km/h)

It was firstly intuitive to conclude the influence of the track elasticity of the dynamic wheel load by comparing the Figure 70 and Figure 79, with one only including track irregularity and the other one with both irregularity and design elasticity input. The Table 53 showed the statistical analysis of the measured dynamic load for both

scenarios. A comparison of the dynamic load at selected sensible locations was shown in Table 54.

Table 53: Statistical analysis of the simulation runs

	Only irregularity		Irregularity + Elasticity	
	Right wheel	Left wheel	Right wheel	Left wheel
Mean value (kN)	82.8	82.5	82.9	83.3
Standard deviation (kN)	5.63	5.89	6.97	9.03
Coefficient of variation (%)	6.8	7.1	8.4	10.8

Table 54: Comparison of maximum load at given location

	Only irregularity		Irregularity + Elasticity	
Location (m)	Max. dynamic load (kN)	Increase (%)	Max. dynamic load (kN)	Increase (%)
0	117	37.6	166	<b>95.3</b>
4	112	31.8	115	35.3
12	103	21.1	175	<b>105.9</b>
29	104	22.3	105	23.5

The values would be analyzed in two majors. Generally to see, the appearance of track elasticity variation would increase the variation of the dynamic wheel load. This increase would be dependent to the characteristic of the track elasticity and irregularity properties. For this test section with both transitions and bridge, an increase of the standard deviation of the dynamic wheel load for over 20 % could be seen.

The counteractive effect between track elasticity and irregularity could be quite clearly visualized from the above tables. It could be found out, that at those locations where a higher dynamic loading could be found under the “only irregularity” scenario, the additional inclusion of the track elasticity variation would always make the dynamic

loading higher. This was a strong evidence to conclude that the appearance of those track irregularities were due to the variation of track elasticity.

Table 55: Statistical analysis of dynamic wheel load

	Open track	Transition and bridge	Transition and bridge
	Only irregularity	Only irregularity	irregularity + design elasticity
Minimum (kN)	66	51	51
Maximum (kN)	101	115	175
Mean value (kN)	82	83	83
Standard deviation (kN)	4.54	5.76	7.32
Coefficient of variation (%)	5.5	6.97	8.8

The above Table 55 showed the statistical analysis of the dynamic loading in open track and bridge and transition areas. The evaluation of the structure could be done in the following two levels. In macroscopic level, since the quality of the included track irregularity in bridge and transitions was similar to the quality of it in open track, it could be seen as a normal operational qualification which could maintain the same quality level along the track. By inputting the design elasticity into the predefined irregular track in bridge and transitions, a higher standard deviation of the dynamic load could be seen, which concluded the fact that the track quality in bridge and transition was still found to be dominating the general maintenance process and more frequent maintenance in bridge and transition could be expected.

It should also be pointed out, that due to the installation of the bridge transition which already smoothed the track elasticity distribution in comparison to the conventional situation, the section would be found less critical than before and the overall design of the transitions could already fulfill the design specifications of extending the maintenance cycle due to sensible structures along a longer section.



The evaluation could be done in the microscopic level, meaning that inside the test area of bridge and transitions, some locations could still be found as significant till now. They were located at approximately  $x = 0, 4, 12$  and  $29$  m. At those locations mentioned above, there tends to exist a higher impact load which could transiently reach a value of more than  $100$  kN, meaning an increase of the axle of about  $25 - 30$  %.

Referring to the location information, it could be found out, that the  $x = 0$  and  $12$  m were exactly the both bridge entrances. It was clear to see that the discontinuity at the both locations in track elasticity would have enormous effect to the dynamic wheel load. The increase of the wheel load could transiently approach  $100$  % which should be certainly considered as decisive single failures. Under repeated loading, it could be always expected, that the track irregularity tends to increase quicker at here than at other locations. This explains the reason, why there exist by these two locations already a higher track irregularity and this should be taken as the fact that the distribution of elasticity was still not enough “smooth” at the bridge entrance and exit. By building in modern railway engineering materials like sub-ballast-mat in the bridge, the distribution of the dynamic loading could be significantly smoothed.

The higher impact load at  $x = 3$  m could be referred similarly from the distribution of the track elasticity. It could be concluded, that although the track irregularity was the direct consequence to the interruption, the real source was because of the discontinuity of the system elasticity at the location. The higher impact load at  $x = 29$  m should be seen as the intermediate point between transition and open track. These interruptions should be explained due to the construction work and was not related to the design itself. The both interruptions would normally appear in the form of a track under sleeper gap which could not provide enough ballast support at those locations.

---

## **7.6. Case study – Inclusion of sub-ballast-mat in the bridge section**

### **7.6.1. Background and introduction**

Due to stiff track support provided by the bridge structure, higher interaction forces could be expected along the bridge section. This was especially critical at the end of the bridge where normally much softer substructure elasticity could be expected.

Therefore, it was recommended to include modern railway construction materials for reducing the dynamic impact on the bridge and smoothing the variation of the track elasticity at both ends. This could be done by inputting sub-ballast-mat along the bridge section.

The task for modern sub-ballast-mat would be to increase load distribution by the track, reduce the vibration level and the ballast stress along the artificial structure by achieving a relative higher insertion loss of the vehicle sided emission, which was normally due to the dynamic wheel rail contact.

It is therefore suggested, that the sub-ballast-mat should be placed inside the bridge section in order to minimize the difference in structural elasticity between bridge and open track.

### **7.6.2. Determination of the bedding modulus of sub-ballast-mat**

Theoretic Finite-Element calculation was included for getting an overview of the eigen-parameters for the sub-ballast-mat. The determination of the parameter is dependent on the design of the section given by the Croatia Railway (HŽ) operators [17]. The design of the section is shown in Figure 80. The Table 56 shows the general design specifications for each model.



	Model 3
Mile pot	km 398+425 – km 398+800
Subgrade	Geotextile + Geogrid
Protective layer thickness	40 cm (2 x 20 cm)
Compression module (Surface subgrade)	$E_{v2,min} = 15 \text{ MN/m}^2$
Compression module (Surface protective layer)	$E_{v2,min} = 90 \text{ MN/m}^2$

Figure 81.

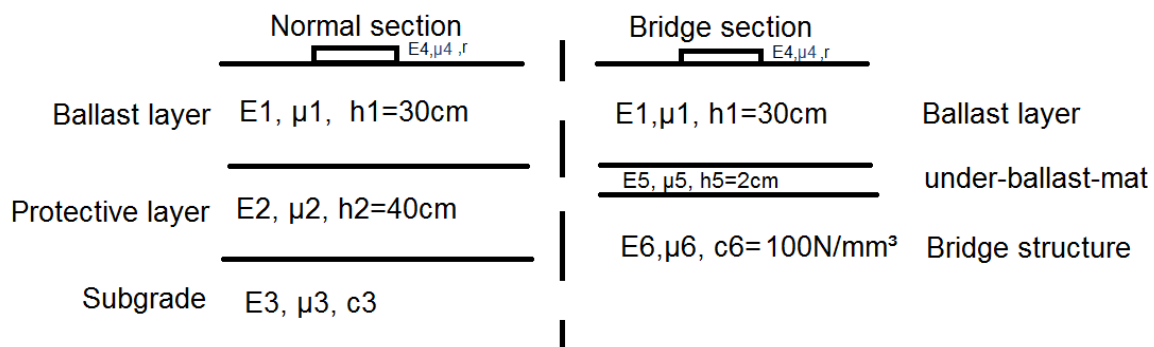


Figure 81: Structural design of the FEM model

The elasticity modulus was adjusted according to the design specifications.

The FEM model was showing in Figure 82. The form of the deflection was also given. It is clear to see that the load plate deforms uniformly ( $\sigma = 0.25$  MPa,  $r = 150$  mm). The results of the calculation were shown in Table 57.

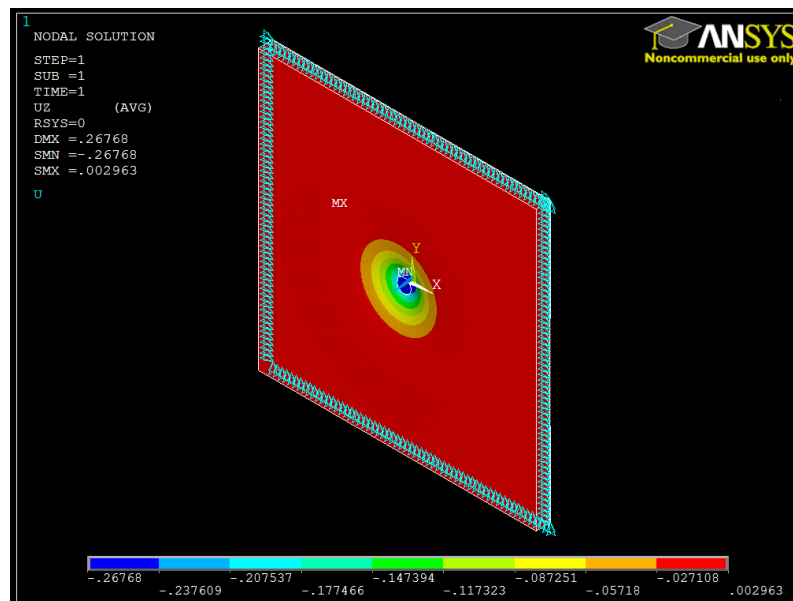


Figure 82: Sample FEM model and calculation results

Table 57: Calibrated parameters and simulation result

	Normal section (Model 3)	Bridge section
Layer 1	$E_1 = 400 \text{ MPa}^*)$ $\mu_1 = 0.30$	$E_1 = 400 \text{ MPa}^*)$ $\mu_1 = 0.30$
Layer 2	$E_2 = 100 \text{ MPa}$ $\mu_2 = 0.45$	$c_3 = 0.11 \text{ N/mm}^3$

Layer 3	$c_3 = 0.055 \text{ N/mm}^3$	$c_6 = 100 \text{ N/mm}^3$ **)
Load plate	$E_4 = 2.1\text{e}5 \text{ MPa}$	$\mu_4 = 0.30$
Deflection (mm)	0.268	

\*) : Experience values \*\*) : Rigid bridge structure

It could be seen, that a bedding modulus for the sub-ballast-mat of around  $0.11 \text{ N/mm}^3$  should be selected which could be best suitable of minimizing the variation of elastic deflection between bridge and open track. For categorization, this refers to a middle-rigid or rigid sub-ballast-mat with characteristic bedding modulus between  $0.10$  and  $0.15 \text{ N/mm}^3$ .

### 7.6.3. Simulation of the dynamic vehicle-track interaction with built-in sub-ballast-mat

This calibrated sub-ballast-mat would be built into the FlexTrack model described in section 7.5 for as a case study. The elasticity of the structure would be recalculated and the new distribution of the elastic system deflection could be seen in Figure 83:

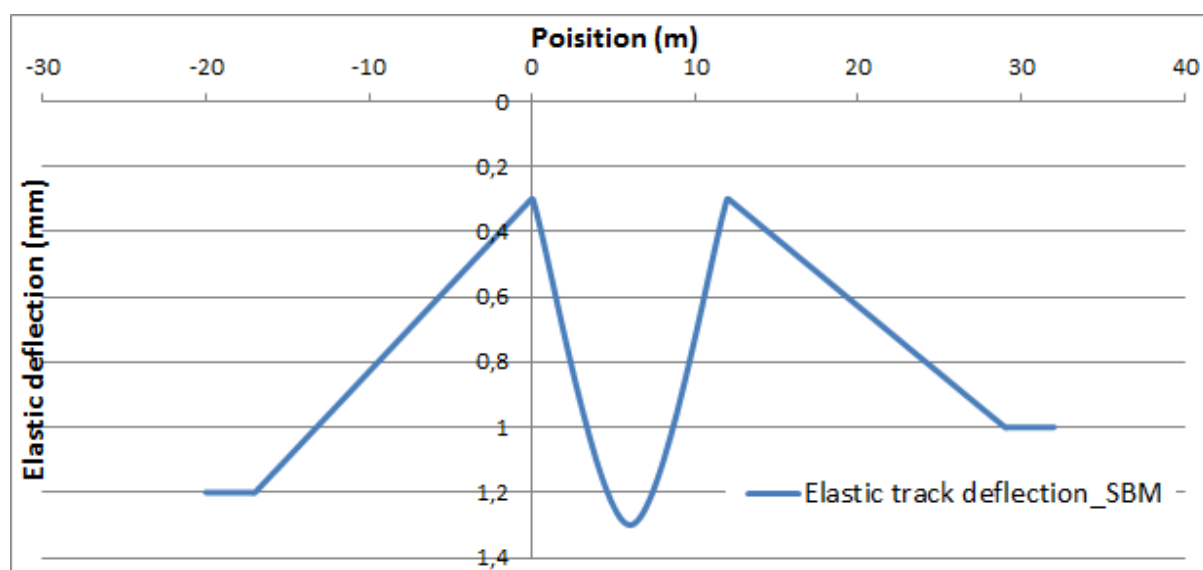


Figure 83: Elastic track deflection with built-in sub-ballast-mat in bridge

The only difference existing here would be the general increase of the elastic deflection inside the bridge of about 0.25 mm. This would be sufficient to fulfill the gap of track elasticity existed in the actual situation. After the imaginary “involve” of the sub-ballast-mat, no significant elasticity gap along the section could be seen.

#### 7.6.4. Simulation result of the dynamic runs

The simulation was again performed with the same vehicle described before. Notice that the only difference now would be the improved distribution of the track elasticity along the bridge. The Figure 82 and Table 58 showed the new distribution and the statistical analysis of the values. For comparison, the table has also included the calculated values from the previous sections.

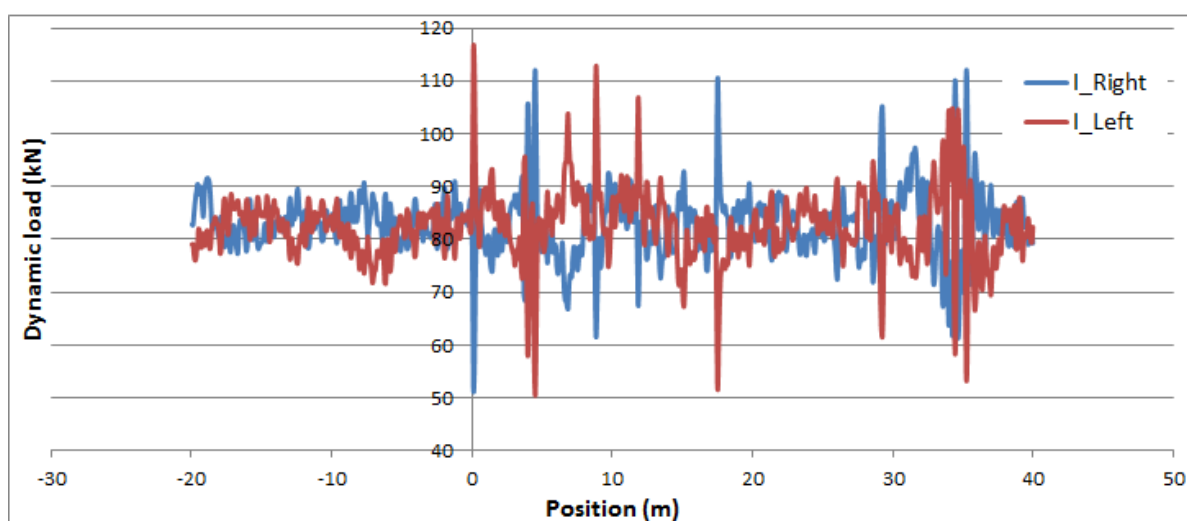


Figure 84: Sample FEM model and calculation results

Table 58: Statistical analysis of dynamic wheel load

	Open track	Transition and bridge	Transition and bridge	Transition and bridge
	Only irregularity	Only irregularity	irregularity + design elasticity	irregularity + design elasticity + Sub-ballast-mat
Minimum (kN)	66	51	51	51
Maximum (kN)	101	115	175	116
Mean value (kN)	82	83	83	83
Standard deviation (kN)	4.54	5.76	7.32	6.17
Coefficient of variation (%)	5.5	6.97	8.8	7.5

It could be seen from the above table and figure, that the maximum dynamic load at the entrance of the bridge was significantly reduced due to the appearance of sub-ballast-mat. The standard deviation of the dynamic load in bridge and transition would decrease for approximately 16 %, but this value was still higher than the value in open track. This could be explained by the actual inconvenient track irregularity situation along the bridge and section where those sections were already found to be critical by the simulation run only under track irregularity input. Therefore, it would be suggested, that the track sided work of smoothing the track irregularity level should also be performed by the installation of the sub-ballast-mat. This would provide the best quality in the bridge and transition area.

An evaluation of the track behavior in macroscopic level could be made. Since the quality of the included track irregularity in bridge and transitions was similar to the quality of it in open track, it could be seen as a normal operational qualification which could maintain the same quality level along the track. By determining this fact, it could be therefore concluded, that the smoothed section of track elasticity by building up bridge transition and sub-ballast-mat could not be classified as “significant” location along the line at the moment. This is equal to say, when referring to the whole line (like 50 km or longer), the section of bridge and transitions would not be found as

---

“sensible” location and the overall design of the transitions and sub-ballast-mat could fulfill the design specifications of smoothing the difference in track elasticity along the section.



## 8. Conclusion and recommendation

### 8.1. Overview of the research

Under the 7<sup>th</sup> Framework Program was the international research project *Smart Maintenance and Analysis of Rail Transport Infrastructure* (SMART Rail) since September, 2012 carried out, focusing on ensuring a safe, reliable and efficient operation of the aging European railway networks. The working package 3, *new rehabilitation technologies to extend service life of existing railway infrastructure*, oriented itself to take special care on the extension of the life cycle of existing and newly built “big structures” like bridge and tunnels, by smoothing the rigidity between those structures and open track with application of innovative transition zone carried out by the geotechnical specialists and modern railway super structure mats.

Higher excitation due to “spots” in track structure has counterproductive effect to the track quality itself, which increases the track deterioration rate and dominating the duration of track sided works. A deeper understanding of the train-track interaction as well as track-substructure interaction by varies kinds of field measurements and numerical simulations are the key for a systematic evaluation of the bridge transitions. The research presented in this report orients itself to the task 3.4, *Validation of the model*, which drove the effort on the evaluation of the innovative structure design by simulating this dynamic vehicle-track interaction, source of the track sided excitation, with modern numerical simulation methodologies including Finite-Element-Method (FEM) and Multi-Body-Simulation (MBS).

The overall work plan for the whole research work has included:

- Feasibility study (review of literature and methodologies, covered in Chapter 2);
- Design of field measurements at pilot section (covered in Chapter 3);
- Proceeding of three field measurements in 2013 and 2014 as well as the analysis and processing of the measurement data (covered in Chapters 4-6);

- Development of suitable simulation tools based on MBS in combination with FEM; Verification of the model with measurement results and model calculations (covered in Chapter 7);

## 8.2. Conclusions

Field measurements provide useful data as the input, whereas the simulation could help enlarge the sight of understanding the questions. The results shown provide the evidence that such simulation tools could be quite suitable to meet the respective requirements.

Developed by 2 Croatian partners in SMART Rail, Institute IGH d.d. and HŽ Infrastruktura d.o.o., the area before and after the bridge “Buna” on the railway line M104 Zagreb Main station- Sisak- Novska in the km 398+441 (near station Turopolje) has been chosen as the test area. Two different designs of bridge transition were realized with a length of 17 m. Following field measurements were performed according to the time scheme (see Table 36):

Table 59: Information on measurement sections

Number	Location	Max. allowable speed (km/h)	Rail status	Measurement done in
1	BUNA bridge, KM 398+441 (M104)	20	Temporary solution with fish plated joint	October, 2013
2	between Zagreb and Sisak, Croatia	140	Continuous Welded Rail (CWR)	April, 2014

Following activities were performed in the measurement section:

- 
- Track geometry (special focus on irregularities): A continuous 3D approach of the track irregularity was achieved during the field measurement including vertical, horizontal, gauge and rotation. A sufficient length of the sampling track was recorded in order to provide data input for MBS simulation.
  - Track elasticity (quasi-static loading): The Benkelman beam measurement is actually the best tool to determine track elasticity as well as changes in track elasticity (track quality) along the test section. It could record the (quasi-)static track elasticity (calculated from absolute track deflections) of given rail seats. The methodology was applied to more than 160 rail seats selected in open track, bridge and transition zone.
  - An innovative evaluation method was invented for determining the track quality according to design specifications. The method was applied to the measured values in both transitions and the bridge.
  - Calibration on static axle load (quasi-static and dynamic test runs): Test runs with speed level (between 5 and 80 km/h) were performed in order to conclude the dynamic effect due to travel speed. These results could also provide the information on the change of rail foot strain due to the variation of track elasticity as well.
  - Dynamic wheel load: Strain gauges are the most suitable measurement devices here as they provide quite accurate measurement data. Problem of discontinuous installation (at least every sleeper spacing) could be solved by installing more strain gauges along the line (through linear estimation method). Totally more than 80 strain gauges were installed in the measurement sections. The maximum measured speed of train passage is 120 km/h.

A better understanding of the influence of track geometry and track elasticity to the dynamic vehicle-track interaction could be achieved by application of modern numerical simulations. The selection the suitable numerical simulation methodologies relies on the specific target as well as the experiences from the previous works. Both Finite-Element-Method (FEM) and Multi-Body-Simulation (MBS) models were reviewed and their advantages as an auxiliary tool for the research work were also summarized. Table 38 shows the functionalities for both modeling strategies (listed according to the measurement items).

Table 60: Summarize of the functionalities of the numerical models

Measurement Item	Parameters measured	Data provision for numerical models	
Geometry	plastic track deformation	MBS (Input)	Alignment and track irregularity
Displacement (quasi-static)	Elastic track deformation	FEM (Input)	Structural design and track elasticity
Strain / stress	Dynamic rail foot strain	FEM + MBS (Output)	Dynamic wheel rail interaction

A summarization of the measured data shows the general track quality of the pilot section, divided into “open track”, “transition Zagreb”, “transition Sisak” and “bridge BUNA”. Table 61 collected all the important measurement results according to different measurement items. The term ‘Dynamic factor’ is by definition the division of the maximum measured stress into the average measured value.

Table 61: Summary of the important measurement results  
(measurement data from 2014)

<u>Vertical track geometry</u>					
	Open track Zagreb		Transition and bridge		Open track Sisak
Length of measurement (m)	218		50		230
Standard deviation	0.56 mm		0.54 mm		0.89 mm
<u>Track elasticity</u>					
<u>Benkelman beam (innovative evaluation method)</u>					
	Open track Zagreb	Transition Zagreb	Bridge	Transition Sisak	Open track Sisak
Length (m)	7	56	42	56	7
Standard deviation (mm)	0.16	0.18	0.24	0.18	0.13
<u>Test runs</u>					
<u>(average wheel load of 95 kN)</u>					
	Quasi-static run (V = 10 km/h)		Dynamic run (V = 64 / 75 km/h)		
	Transition Zagreb	Transition Sisak	Transition Zagreb	Transition Sisak	
Mean value (N/mm²)	41.3	42.6	44.6	44.3	
Standard deviation (N/mm²)	5.02	4.93	6.48	7.19	
Dynamic factor (%)	29.6	32.8	35.3	38.9	
<u>Train runs</u>					
<u>(middle wagon of train set 6111, wheel load 85 kN, V = 120 km/h)</u>					
	Transition Zagreb		Bridge	Transition Sisak	
Mean value (N/mm²)	41.8		40.0	43.6	
Standard deviation (N/mm²)	4.49		3.99	2.87	
Dynamic factor (%)	32.0		24.7	28.2	

From the table shown above and the in Chapter 7 described numerical models, following conclusions could be made:

- The track quality in bridge and transition is generally similar than in open track.

- 
- The variation of wheel rail contact load is comparable for both transitions under test runs.
  - A higher variation of dynamic wheel load could be found in transition Zagreb than in bridge and other transition.
  - The dynamic factor symbolizing the maximum possible induced wheel load is similar in both transitions and the bridge.
  - The similar measured average rail foot stress in test runs (quasi-static) and train runs (dynamic) for both transitions shows that the average wheel load of the middle wagon of train set 6111 under 120 km/h is close to 95 kN, with a general increase of wheel load for about 11.7 %.
  - The deterioration of the transition and bridge should also be monitored (not covered in this report).
  - It could be proved from the numerical modeling, that the most efficient solution would be the combination of the geotechnical works as transition and superstructure sided inclusion of innovative materials.
  - The inclusion of sub-ballast-mat could better smooth the track elasticity distribution.
  - It could be foreseen, that the inclusion of both solutions would significantly improve the life cycle of the system (sustainable solution).
  - Research on type of transition and the attached mat characteristic should be supported which focus on each specific cases (innovative solutions possible!)

### 8.3.Recommendations

After the evaluation of the behavior of the newly built transition zones, following recommendations would be made:

- Sub-ballast-mat should be built in the bridge area for better smoothing the distribution of track elasticity;
- The bedding modulus of the sub-ballast-mat should be between 0.10 and 0.15 N/mm<sup>3</sup>.

- 
- The design of bridge transition should also take care of the distribution of track elasticity (especially at the entrance of the bridge).
  - The deterioration of the track quality due to operational loading should be monitored.

---

## SOURCE OF REFERENCE

1. KAEWUNRUEN.S, REMENNIKOV.A.M. (2007), Response and Prediction of Dynamic Characteristics of Worn Rail Pads Under Static Preloads, University of Wollongong, Australia
2. ZIMMERMANN, H. (1888), Die Berechnung des Eisenbahnoberbaus, in German, Verlag von Ernst&Korn (Wihelm Ernst), Berlin, Germany.
3. VAN'T. ZAND. Ir. J. (1994), Assessment of dynamic characteristics of rail pads, Railway Engineering international edition Number 4
4. KUMARAN, G., MENON, D. and KRISHNAN, K. (2003), Dynamic Studies of Railtrack Sleepers in a Track Structure System, Journal of Sound and Vibration.
5. EN13481-2 (2002), Railway applications – Track – Performance requirements for fastening systems – Part 2: Fastening systems for concrete sleepers, European Committee for standardization
6. WOLTER, K., (2012), Rekonstruktion der originalen Gleislageabweichungen aus 3-Punkt-Signalen (Wandersehenmessverfahren) und Beurteilung hinsichtlich Amplitude, Fehlerwellenlänge sowie Fehlerform. In German. Berlin, Germany, 2012
7. OPPENHEIM, A.V, SCHAFER, R.W. (1999), Zeitdiskrete Signalverarbeitung, 3. Auflage. In German. Wien, Austria, 1999
8. DIRAC, P. (1958), The Principles of Quantum Mechanics (4<sup>th</sup> edition, 1958). Page 58. §15 The  $\delta$  function
9. DE MAN, A. P. (2002), DYNATRACK - A survey of dynamic railway track properties and their quality, PhD, Technical University Delft, DUP Science, Delft University Press, Netherlands
- 10.Intec GmbH (2008), SIMPACK Reference Guide, Page 19, SIMPACK Release 8.9, Wessling, Germany
- 11.ALBERS A. , HAEUSSLER P. (2005), Topology optimization of dynamic loaded parts using multibody simulation and durability analysis, University of Karlsruhe (TH), Karlsruhe, Germany
- 12.ANSYS, Inc. (1999), Theory reference, ANSYS release 5.6, 11th edition,
- 13.Intec GmbH (2008), SIMPACK Reference Guide, Page 17, SIMPACK Release 8.9, Wessling, Germany



14. Stefan Dietz, et.al (2001), Interaction of vehicles and flexible tracks by co-simulation of Multibody vehicle systems and finite element track models, Vehicle system dynamics
15. MILAKOVIĆ, D. (2014), Deliverable 3.2, SMART Rail. Zagreb, Croatia, 2014
16. Hrvatske željeznice, HŽ (not listed), Project documentation ŽP Greda-Turopolje-Knjiga (internal usage, not published), in Croatian. Zagreb, Croatia
17. Hrvatske željeznice, HŽ (not listed), Geotechnical documentation (internal usage, not published), in Croatian. Zagreb, Croatia
18. WEIDEMANN, C. (2003), Air-springs in Simpack, SIMPACK news, Wessling, Germany, 2003.
19. Vogel&Plötscher (2010), Production catalog, MessReg CLS. [www.vogelundploetscher.de](http://www.vogelundploetscher.de)
20. Hottinger Baldwin Messtechnik GmbH (2010), QuantumX MX840A – 8 – channel universal amplifier. <http://www.hbm.com>
21. LIU, J. (2007), Tragwirkung der elastische gelagerten Schiene unter exzentrischer vertikaler und horizontaler Belastung. Lehrstuhl und Prüfamnt für Verkehrswegebau der TU München. Diplomarbeit Nr. 805. In German. Munich, Germany. 2007.
22. Intec GmbH (2008), SIMPACK Track module, page 10.1-85, SIMPACK release 8.9, Wessling, Germany.
23. DIN EN 14363 (2005), Bahnanwendungen – Fahrtechnische Prüfung für die fahrtechnische Zulassung von Eisenbahnfahrzeugen – Prüfung des Fahrverhaltens und stationäre Versuche; Deutsche Fassung EN 14363:2005. In German. Berlin, Germany, 2005
24. Intec GmbH (2008), SIMPACK Track module, page 11.3-107, SIMPACK release 8.9, Wessling, Germany.

## List of Figures

Figure 1 Typical railway superstructure and elastic elements <sup>[01]</sup> .....	6
Figure 2 Typical deflection line calculated by Zimmermann Theory .....	7
Figure 3 Multi-elastic track model in vertical direction .....	8
Figure 4 Principle of LTI system .....	10
Figure 5 The calculation in frequency domain .....	11
Figure 6 Dirac delta function.....	12
Figure 7 Sample SIMPACK Model for railway vehicle <sup>[11]</sup> .....	17
Figure 8: Type of analysis available in ANSYS .....	22
Figure 9 Design of bridge transition Zagreb .....	23
Figure 10 Design of bridge transition Sisak .....	24
Figure 11 Interruption of the construction by application of intermediate bridge .....	24
Figure 12: Structural design of the section (open track) .....	27
Figure 13 Movable track recording wagon (Type CLS from company V&P) <sup>[13]</sup> .....	30
Figure 14 Benkelman beam for the measurement of track elastic deflection (photo from previous measurement event).....	32
Figure 15 Data amplifier QuantumX MX840A <sup>[14]</sup> .....	33
Figure 16 Installation of fish plated joint .....	36
Figure 17 Section plan and installation of test sensors (October, 2013) .....	44
Figure 18 three dimensional track geometry .....	46
Figure 19 Measured maximum rail deflection .....	48
Figure 20 Measured influence line (left rail seat -7).....	48
Figure 21 Difference of measurement data and reference line.....	51
Figure 22 Difference of measurement data and reference line.....	52
Figure 23 Sample strain gauge measurement result .....	54
Figure 24: Test section 1 – runs 1F1 and 1F3.....	56
Figure 25: Test section 2 – runs 2F3 and 2F6.....	56
Figure 26: standard deviation according to speed (both transitions) .....	59
Figure 27 Sample measurement of train set 6111 (middle car, V = 21.4 km/h). .....	61
Figure 28 Summary of all the passage of train set 6111 (middle wagon) .....	61
Figure 29: Distribution of the rail foot stress according to axle number .....	62
Figure 30 Section plan and installation of test sensors (April, 2014) .....	63
Figure 31 three dimensional track geometry (state 2014) .....	65
Figure 32 Measured maximum rail deflection.....	67
Figure 33 Difference of measurement data and reference line.....	69
Figure 34 Difference of measurement data and reference line.....	70
Figure 35 Sample strain gauge measurement result.....	72
Figure 36: Test section 1 – runs 1F4 and 1F13.....	75

Figure 37: Test section 2 – runs 2F3 and 2F14 .....	75
Figure 38: standard deviation according to speed (both transitions) .....	77
Figure 39 Sample measurement of train set 6111 (Right rail, $V = 121$ km/h) ....	79
Figure 40 Summary of all the passage of train set 6111 (middle wagon) .....	80
Figure 41: Coefficient of variation of train set 6111 .....	81
Figure 42: Summary of all the passage of train set 6112 (middle axles) .....	82
Figure 43: Coefficient of variation of train set 6112 (middle axles) .....	82
Figure 44: Summary of all the passage of locomotive 2062 .....	83
Figure 45: Coefficient of variation of locomotive 2062 .....	83
Figure 46 Comparison of track geometry (all area) .....	85
Figure 47 Comparison of track geometry (bridge and transition) .....	85
Figure 48 Measured maximum rail deflection .....	87
Figure 49: Transition Zagreb – standard deviation according to speed .....	88
Figure 50 General modeling process .....	91
Figure 51 Simplified rail model UIC60 <sup>[19]</sup> .....	92
Figure 52 Principle of the FEM model .....	93
Figure 53 Graphical representation of different elements in FEM model .....	94
Figure 54 The ANSYS model with 95 rail seats .....	96
Figure 55 Sample measurement and calculation result .....	98
Figure 56 Modeling of fish plated joint (Joint as separate material) .....	101
Figure 57 Simulation results after “removing” of the fish plated joints (measurement 2013) .....	102
Figure 58 Interpolation and calculation result after 5 <sup>th</sup> iteration .....	103
Figure 59 The new ANSYS model with variable ballast elasticity .....	105
Figure 60 Identification between measurement and simulation results (according to measurement in 2014) .....	106
Figure 61 Application of wheel load in FEM .....	107
Figure 62 Sample loading model (front bogie of the middle wagon of train set 6111) .....	108
Figure 63 Distribution of static and measured dynamic wheel load .....	110
Figure 64 Measurement and simulation result (1 <sup>st</sup> axle above strain gauge) ..	111
Figure 65 Measurement and simulation result (2 <sup>nd</sup> axle above strain gauge) ..	111
Figure 66 The definition of 3D track excitation in MBS system <sup>[13]</sup> .....	113
Figure 67 The definition of 3D track excitation in Simpack 8904 .....	114
Figure 68 The vehicle model (middle wagon of train set 6111) .....	115
Figure 69 Dynamic wheel load under track irregularity ( $V = 120$ km/h, $f_u = 500$ Hz) .....	116
Figure 70 Dynamic wheel load under track irregularity ( $V = 120$ km/h, $f_u = 20$ Hz) .....	117
Figure 71 Dynamic wheel load under track irregularity ( $V = 95$ km/h, $f_u = 500$ Hz) .....	117

---

Figure 72 Dynamic wheel load under track irregularity ( $V = 95$ km/h, $f_u = 20$ Hz)	118
Figure 73 Simplified FEM model with individual elasticity modulus	120
Figure 74 Calibrated elastic track deflection (single wheel load of 85 kN)	120
Figure 75 Eigenmodes 1 and 2 on bridge (zoom factor 50, $f = 10.9$ and $29.2$ Hz)	121
Figure 76 Eigenmodes 38 and 39 on transition Zagreb and Sisak	122
Figure 77 Simpack vehicle model with built-in flexible track structure	123
Figure 78 Elastic track deflection ( $V = 1$ m/s, quasi-static)	125
Figure 79 Dynamic wheel load under track elasticity and irregularity ( $V = 120$ km/h)	126
Figure 80: Structural design of the section (Model 3)	131
Figure 81: Structural design of the FEM model	131
Figure 82: Sample FEM model and calculation results	132
Figure 83: Elastic track deflection with built-in sub-ballast-mat in bridge	133
Figure 84: Sample FEM model and calculation results	134

## List of Tables

Table 1: Comparison of FEM and MBS approach .....	20
Table 2: Location of the interruption point of construction .....	25
Table 3: General information of track superstructure .....	25
Table 4: Design specifications .....	27
Table 5: Performance data of movable track geometry recording tool .....	30
Table 6: Allocation of strain gauges .....	34
Table 7: EMU series 6111, (HR- HŽ).....	37
Table 8: EMU series 6112, (HR- HŽ).....	38
Table 9: Locomotive series 1141, (HR- HŽ) .....	38
Table 10: Locomotive series 2062, (HR- HŽ) .....	39
Table 11: Summary of the general information along the bridge .....	40
Table 12: Summary of the design of measurement .....	41
Table 13: The measurement items and their functionalities for the numerical models.....	42
Table 14: Location of the interest points along the measurement of track geometry .....	45
Table 15: statistical analysis of vertical track geometry – open track and bridge .....	45
Table 16: Benkelman beam test – bridge and transition .....	47
Table 17: Information on selection of measurement points .....	49
Table 18: statistical analysis of rail seat deflection <sup>*)</sup> .....	50
Table 19: Statistical analysis according to new method .....	52
Table 20: Information on test runs – section 1 .....	53
Table 21: Sample evaluation of the rail foot stress .....	55
Table 22: Sample evaluation of the rail foot stress .....	55
Table 23: Statistical analysis of load wagon according to speed level (transition Zagreb).....	57
Table 24: Statistical analysis of load wagon according to speed level (transition Sisak) .....	57
Table 25: Comparison of both transitions .....	58
Table 26: Recorded train runs and time of passage .....	60
Table 27: Location of the interest points along the measurement of track geometry .....	64
Table 28: statistical analysis of vertical track geometry – open track and bridge .....	64
Table 29: Benkelman beam test – bridge and transition .....	67
Table 30: statistical analysis of rail seat deflection <sup>*)</sup> .....	68
Table 31: Statistical analysis according to new method .....	70

Table 32: Information on test runs – section 1 .....	71
Table 33: Sample evaluation of the rail foot stress (sensors on left rail, Section 1) .....	73
Table 34: Sample evaluation of the rail foot stress (sensors on right rail, Section 2) .....	74
Table 35: Statistical analysis of load wagon according to speed level .....	76
Table 36: Statistical analysis of load wagon according to speed level .....	76
Table 37: Comparison of both transitions .....	77
Table 38: Recorded train runs and time of passage .....	78
Table 39: statistical analysis of vertical track geometry – bridge .....	86
Table 40: Comparison of the test runs (transition Zagreb) .....	89
Table 41: Comparison of the test runs (transition Sisak) .....	89
Table 42: Parameters of the simplified rail model <sup>[19]</sup> .....	92
Table 43: Characteristic E and $\mu$ value for each section .....	95
Table 44: Characteristic E and $\mu$ value for open track and transition .....	97
Table 45: Error analysis after initial condition *) .....	98
Table 46: Boudary condition; Diff. Deflection [mm], Iteration 5 - 4.....	100
Table 47: Number of difference over limitation .....	100
Table 48: Error analysis after 5 <sup>th</sup> iteration *) .....	103
Table 49: Statistical analysis of dynamic wheel load according to speed level (transition Zagreb, measurement 2014) .....	109
Table 50: Statistical analysis of dynamic wheel load according to speed level (transition Sisak, measurement 2014).....	109
Table 51: List of model parameters .....	121
Table 52: Performed simulation runs.....	124
Table 53: Statistical analysis of the simulation runs .....	127
Table 54: Comparison of maximum load at given location .....	127
Table 55: Statistical analysis of dynamic wheel load .....	128
Table 56: Design specifications .....	131
Table 57: Calibrated parameters and simulation result .....	132
Table 58: Statistical analysis of dynamic wheel load .....	134
Table 59: Information on measurement sections.....	137
Table 60: The measurement items and their functionalities for the numerical models.....	140
Table 61: Summarize of the functionalities of the numerical models.....	139